University of Alberta

Tailoring the Chemistry of Gold Surfaces with Aryl Layers formed by the Electrochemical Reduction of Diazonium Cations.

by

Dwayne Michael Shewchuk

A thesis submitted to the Faculty of Graduate Studies and Research
in partial fulfillment of the requirements for the degree of

Doctor of Philosophy

Department of Chemistry

Fall 2010
Edmonton, Alberta

Examining Committee

Dr. Mark T. McDermott, Chemistry

Dr. D. Jed Harrison, Chemistry

Dr. Richard L. McCreery, Chemistry

Dr. Jonathan G. C. Veinot, Chemistry

Dr. Zhenghe Xu, Chemical and Materials Engineering

Dr. Daniel Bélanger, External Examiner, Department of Chemistry, University of Québec at Montréal

To my late mother Dianna

ABSTRACT

The electrochemical reduction of *para*-substituted aryldiazonium cations is a convenient method of introducing chemical functional groups to a surface. The number of conductive surfaces that have been used for this purpose is rapidly expanding. The body of work presented in this thesis will serve to further investigate this method as it applies to polycrystalline gold surfaces.

The stability of diazonium-derived nitroazobenzene (NAB) layers on Au was investigated by subjecting them to a variety of treatments including prolonged exposure to UV radiation, refluxing solvents, ultrasonication, chemical displacement by octadecanethiol (ODT), and the application of negative potentials to -1.5 V vs Ag/AgCl. Infrared reflection-absorption spectroscopy (IRRAS) and electrochemical blocking were used to make the assessments. The films are very resistant to ODT displacement reactions, moderately resistant to ultrasonication and refluxing; but not very resistant to the other treatments. In most cases, quantitative IRRAS measurements indicate that > 50 % of the layer resists the treatments. A direct, side-by-side comparison of the stability of nitrobenzene (NB) layers deposited electrochemically from nitrobenzene diazonium cations to self-assembled monolayers (SAMs) of mercaptonitrobenzene was made. Both types of layers are prone to removal by the various treatments. This is likely due to the presence of weakly bound, physisorbed material in addition to more strongly bound material. Immersion in an ODT solution results in complete displacement of the thiol derived nitrobenzene monolayer but does not completely displace the diazonium-derived layer.

Two-component, mixed molecular layers comprised of diazonium-derived NAB and dodecanethiolate (DDT) were prepared using a sequential deposition approach. The aryl component is first deposited electrochemically, followed by immersion in a solution of DDT. We will demonstrate that control over the composition of the layers can be achieved by manipulating the concentration of NAB diazonium cations at the electrochemical grafting step. The mixed layers were characterized by reflection-absorption spectroscopy, atomic force microscopy, electrochemical blocking, and x-ray photoelectron spectroscopy. The electron transfer kinetics of $Ru(NH_3)_6^{3+/2+}$ were examined at the mixed layer electrodes. The kinetics are highly dependent on the relative proportions of NAB and DDT present and the thickness of the NAB component.

The NAB:DDT mixed films were employed as the molecular layer in molecular electronics junctions. We examined the suitability of Al_2O_3/Au top contacts for these junctions. Junctions for which the molecular layer was mostly comprised of DDT showed an increased failure rate.

Acknowledgements

I had the pleasure of working with many talented individuals at the University of Alberta. I'd like to take this opportunity to thank those people that I interacted with on a more regular basis. Firstly, thanks to my supervisor, Mark McDermott, for your guidance and support throughout my Ph. D. program. Research can be frustrating at times and it helps when you have a supervisor that understands the necessity for a balance between patience and persistence.

I'd like to give a special thanks to Drs. John-Bruce Green, Jonathan Veinot, and Richard McCreery. John-Bruce and Jonathan served on my supervisory committee. It was an absolute pleasure discussing the status and direction of my project with these individuals. I'd like to thank John-Bruce for making that extra effort to make his equipment and expertise available to the McDermott group on a whim's notice. Likewise, Richard and his research team were a very accommodating bunch – thank you.

Thanks to the McDermott group members, both past and present. I'd like to give special thanks to my friends and colleagues: Brian Asher, Derek Bleackley, Victoria Cooper, Rongbing Du , Vishal Kanda, Lars Laurentius, Tiffany Meinzer, Francis Nsiah, Matt Ross, Bushra Sajed, Solomon Ssenyange, and Ni Yang. I have learned well the power of bringing good research together with good people.

Last, but certainly not least, I'd like to thank my family for making the extra effort to stay close despite the large geographical distances between us: my sister, Melanie; Mike; my cousins Darcey and Ryan; and my Aunty and Uncle, Sonya and Robert.

Table of Contents

List of Figures

List of Tables

List of Abbreviations

AFM	Atomic force microscopy
AU	Absorbance unit
CV	Cyclic voltammetry, cyclic voltammogram
DDT	Dodecanethiol
DEA	Diethylaniline
dNB	Diazonium-derived nitrobenzene
CME	Chemically modified electrode
CP	Carboxyphenyl
FT-IRRAS	Fourier-transform infrared reflection-absorption spectroscopy
HOPG	Highly oriented pyrolytic graphite
HRXPS	High resolution X-ray photoelectron spectroscopy
IRRAS	Infrared reflection-absorption spectroscopy
LBM	Langmuir-Blodgett monolayer
mAU	0.001 AU
MJ	Molecular junction
NAB	Nitroazobenzene
NAB:DDT	A mixed molecular layer comprised of NAB and DDT
NABDF	Nitroazobenzene diazonium salt
ODT	Octadecanethiol
oop	An out-of-plane vibrational motion
PPF	Pyrolyzed photoresist film
SAM	Self-assembled monolayer
SA	Spontaneous adsorption
SFM	Scanning force microscopy

SPM	Scanning probe microscopy
$TBABF_4$	Tetrabutylammonium tetrafluoroborate
tNB	Thiol-derived nitrobenzene
XPS	X-ray photoelectron spectroscopy

List of Symbols

E	An applied, electrochemical potential
$Fe(CN)_6^{3-/4-}$	Ferricyanide/ferrocyanide redox probe
Ag/AgCl	A reference electrode consisting of a silver wire coated with a layer of solid silver chloride. It is usually in an aqueous solution, saturated with KCl.
A_{1347}	The absorbance of the IR-active vibrational mode located at 1347 cm^{-1}
ΔE_p	$E_{p,a} - E_{p,c}$ measured from a cyclic voltammogram
$E_{p,a}$	The applied potential for which a peak in the anodic current occurs
$E_{p,c}$	The applied potential for which a peak in the cathodic current occurs
$k°$	Heterogeneous rate constant
$k_{app}°$	The apparent heterogeneous rate constant
$k_{Au}°$	Heterogeneous rate constant of an unmodified Au surface
$k°_{NAB(mono)}$	Heterogeneous rate constant for an Au surface modified with a monolayer of NAB
$I_{p,cath}$	Peak cathodic current
$I_{p,anod}$	Peak anodic current
$\nu_a(CH_2)$	Wavenumber position of the asymmetric methylene stretching vibration
$\nu_{a,NO2}$	Wavenumber position of the asymmetric nitro stretching vibration
$A_{s,NO2}$	Absorbance value of the symmetric nitro stretching vibration
% RSD	Relative standard deviation expressed as a percent
c_{NABDF}	Concentration of nitroazobenzene diazonium salt
δ	Thickness of the NAB film
θ_{NAB}	Fractional surface coverage of NAB molecules
q	Measured charge
q_o	Measured charge for an unmodified Au surface
$Ru(NH_3)_6^{3/2+}$	Hexamineruthenium(III)/(II) redox probe

d	Distance
β	Electron tunneling coefficient
J-V	Current density as a function of applied voltage bias
AlO_x	Aluminum oxyhydroxide *i.e.,* AlO(OH)
C	Capacitance, and a Coulomb (a unit of electrical charge)
$\nu_{a,NO2}$	Wavenumber position for the asymmetric nitro stretching vibration
$\nu_{s,NO2}$	Wavenumber position for the symmetric nitro stretching vibration

Chapter I

Introduction

1. General Introduction

The chemical alteration of the surface of a material, or simply surface modification, is both a clever strategy and a powerful tool. The premise behind the modification of a surface is to change its surface chemistry in a way that makes it more useful, while retaining its desirable, inherent, bulk properties. Painted surfaces, anti-reflective coatings on sunglasses, and non-stick cookware all demonstrate day-to-day examples of the usefulness of modified surfaces. Although the examples get more complex in the realm of surface science, the principle remains the same. In the context of contemporary research and development, applications to surface modification span several subjects, including chemical and wear resistant technologies,[1-3] adhesion,[4] sensors,[5, 6] biocompatibility,[7, 8] the fabrication of microelectronic circuitry,[9, 10] molecular electronics,[11-16] and separations.[17, 18]

Surface modification is a broad concept and to name every possible combination of material and modification strategy would result in an enormous list. More pertinent to this thesis is the modification of a small subset of this list, namely, electrode materials. In 1964, Boehm and coworkers first demonstrated that a graphitic carbon electrode surface could be thermally oxidized to produce a surface of carboxylic acid groups.[19] Recognizing the need to attach molecules to a surface by means other than mere

adsorption, Watkins and coworkers followed-up on this novel idea by subsequently attaching optically active amino acids to these surface carboxylic acid groups via amide linkages. They summarized their motivations to the publisher in one, brief statement, which reads: "Sir: Although electrode surfaces can be altered by adsorption it would be of interest to more drastically and permanently modify the surface by covalently binding molecules to it."[20] During the same timeframe, Lane and workers published the first account of chelated metal centers attached to platinum surfaces via Pt-C bonds with olefinic side chains.[21] They subsequently examined the electrochemical behavior of the tethered redox centers. From these two novel studies, the concept of a chemically modified electrode was born.

2. Chemically Modified Electrodes

Chemically modified electrodes (CMEs), so named by Murray and coworkers, are prepared by the chemical attachment of one or more layers of organic functional groups to the surface of an electrode.[22] This is usually done to give the electrode a desired property, for example, a surface charge or a specific chemical reactivity. As described above, this has classically been achieved by covalently linking small organic molecules to pre-existing surface functional groups. Modern definitions of CMEs have expanded to include themes for which the molecular moiety is attached to the surface by all types of adsorption *i.e.* both chemisorption and physisorption. Chemisorption entails a relatively strong interaction between the adsorbate and the surface. This includes both covalent and ionic interactions. Physisorption differs from chemisorption in that only weaker, Van Der Waals forces are typically involved. Although this seems counter-productive to the

original intentions of Watkins and coworkers, these new strategies have led to the development of some very useful interfaces. The rest of this chapter provides a review of the most widely used methodologies to produce CMEs. Due to the large number of existing strategies this list will, by no means, be exhaustive. Rather, it gives the reader a good sense of the strategies that are currently available.

a) Polymer-film CMEs

A variety of strategies have been used to coat electrodes with polymers. These include drop casting,[23] dip coating,[24] spin coating,[25] organosilane bonding,[26] electrochemical precipitation,[27] and plasma discharge polymerization.[28] Polymers are typically physisorbed to the electrode surface. In some cases, attachment is achieved by a covalent interaction. Some of the most widely studied polymer-film CMEs are described below.

Redox polymers contain an electroactive group in the repeat unit (*i.e.*, monomer). They represent an interesting class of polymer-film CMEs. The redox polymer, poly-o-aminophenol for example, is typically deposited electrochemically. Charge transport in redox polymer-film modified electrodes is thought to occur by an "electron hopping" mechanism where electrons hop between oxidized and reduced sites in the film.[29]

Electrically conducting polymers, otherwise known as "organic electrodes," have received considerable attention because of their potential applications in organic batteries, electrochromatic displays, and electrocatalysis. Electron transport in these polymers occurs by a band conduction mechanism similar to that of metals or semiconductors. The most widely used organic electrode, polypyrrole, is typically

deposited by electrochemical polymerization. It has been proposed that polymers like polypyrrole can be reversibly switched between conducting and insulating states by electrochemically converting them to an oxidized form on the electrode.[29]

Ion-exchange polymer films are also a subject of great interest. These films are characterized by having an exchangeable, ionic component in their structure. One of the most widely used ion-exchange polymers is Nafion®. Nafion®, a registered trademark of the DuPont company, is a tetrafluorethylene-based polymer with sulfonate, $-SO_3H$, groups incorporated into its structure. The protons on the sulfonate groups readily exchange with charged electroactive species in solution. This permits the uptake of ions into the polymer film.[30] It is typically spin coated or drop cast onto the electrode surface. Nafion® has also received considerable attention as a proton conductor in fuel cells due to its inherent thermal and mechanical stability.[31]

b) Organized Monolayers

Organized monolayers are characterized by an ordered array of surfactant molecules vertically (or near vertically), oriented at the electrode surface. There are two types of organized monolayers. These are Langmuir-Blodgett monolayers (LBMs) and self-assembled monolayers (SAMs).

i. *Langmuir-Blodgett Monolayers.* LBMs are prepared by the controlled transfer of a monolayer of surfactant molecules from an air-water interface to a solid material. The surfactant molecule typically has a polar head group and a hydrophobic tail structure. Classically, fatty acid salts are employed as the molecular unit. LBMs are often comprised of the same types of molecules found in living organisms (*e.g.*, phospholipids

and fatty acids) and therefore show great promise for modeling and understanding biological membranes.

Although LBMs were first reported in the 1930s, several aspects of their preparation have prevented their use in any modern, practical devices. First, LBMs require extremely meticulous preparation methodologies.[32] In addition, the films often lack reproducibility and typically contain many defect sites.[33] Another limitation of LBMs is the surfactant molecule is restricted to having no more than a single, polar functional group.[34] Finally, the interaction between the substrate and molecule is often weak and usually amounts to hydrogen bonding or Van Der Waals interactions. Consequently, LBMs often have poor thermal stability.[35] For these reasons, monolayer assemblies other than LBMs are usually considered for practical applications.

ii. *Self-Assembled Monolayers.* SAMs are typically comprised of surfactant molecules that spontaneously self-organize into compact, well-ordered molecular assemblies at a surface. They are renowned for the ease by which they are prepared, which usually amounts to immersing the surface of interest in a dilute solution containing the surfactant molecule. In some cases a gentle heating step is required to accelerate the self-assembly process.

Organothiolate SAMs

The most thoroughly characterized and widely used SAMs are organothiolate SAMs prepared by the spontaneous adsorption of organothiols or organo-dithiols to Au surfaces from dilute solutions in organic solvents (typically ethanol or hexanes). These

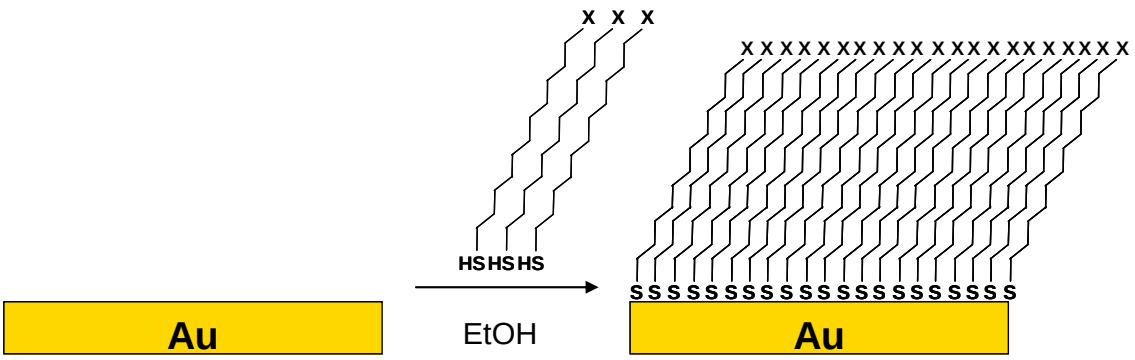

Figure 1.01. The formation of a SAM of a C_{12} ω-substituted alkanethiol at a Au surface.

SAMs provide a convenient way to produce a surface of chemical functional groups. Typically this requires the adsorption of a SAM of an ω-substituted alkanethiol of the form: $HS(CH_2)_yCH_2X$, where $0 \leq y \leq 21$, and X is a chemical functional group *e.g.*, CO_2H, NH_2, OH, etc.[36] X-ray photoelectron spectroscopy (XPS) studies have revealed the thiols adsorb to the Au surface as thiolates, RS^-, where R is the substituted alkyl-chain portion of the molecule.[37] Figure 1.01 illustrates the formation of a C_{12} ω-substituted alkanethiol SAM. The tail groups are oriented at 20-30°, with respect to the surface normal, to accommodate the spacing of the S atoms at the surface and tight packing of the chains.[36] The formation of a SAM from disulfides is similar, although the S-S bond dissociates upon adsorption.[38] The chemical equations that describe thiol SAM formation, for thiols and disulfides, are shown in Equations 1 and 2[36]:

$$Au + HS(CH_2)_yCH_2X \xrightarrow{-H_2,EtOH} Au - S^-CH_2(CH_2)_yCH_2X \quad [1]$$

$$2Au + [S(CH_2)_y CH_2 X]_2 \xrightarrow{-H_2, EtOH} 2Au - S^- CH_2(CH_2)_y CH_2 X \quad [2]$$

Gold is most often employed as the substrate for thiolate SAMs. The principle reason for this is that gold does not have a stable surface oxide (at standard temperature and pressure), which simplifies the substrate cleaning/preparation process. Other materials have successfully been employed as substrates for thiolate SAM formation. These include copper,[37] silver,[37, 39] platinum,[40] mercury,[41] iron[42] and gallium arsenide.[43] Thiolate SAMs formed on some of these other surfaces differ, considerably, in terms of their structure. For example, SAMs on Cu contain many defects and are not as compact as those formed on Au.[37] The usefulness of a thiolate SAMs is typically related to the compactness and crystallinity of the tail groups, though this certainly depends on the particular application. Highly compact SAMs that shield the substrate from the ambient or solution are usually sought. On Au, alkanethiolate SAMs for which $20 \geq y \geq 14$ tend to exhibit a high degree of crystallinity with respect to the alkyl chains, presumably due to higher inter-chain Van Der Waals forces.[44] Conversely, for $y \leq 8$ the alkyl chains tend to be more liquid-like and highly disordered.[44]

Formation of Au-thiolate SAMs occurs in two distinct steps. The initial step is a diffusion-controlled, Langmuir-adsorption process and is dependent on the thiol concentration. During this initial step, a less-organized, incomplete monolayer is formed on the order of minutes. The kinetics largely depend on the strength of the surface-head group interaction, and probably depend on the electron density around the sulfur atom.[45] The second step requires several hours and can be described as a surface crystallization

process where the alkyl chains reorganize into a well-ordered, compact, two-dimensional structure.

While the reported strength of the Au-S bond is quite high (*i.e.*, 30-40 kcal/mol), the exact nature of the interaction between the thiolate and the gold substrate is not fully understood.[38] It is argued the bond is ionic although, to our knowledge, no direct evidence to support the presence of oppositely charged ions at the surface (*e.g.*, Au^{+}) has been put forth. In addition, the fate of the hydrogen atoms has not been unveiled. Investigators have suggested that H atoms are produced and recombine rapidly at the surface. Molecular hydrogen gas, however, has not been detected while these SAMs are formed.[36]

Though thiolate SAMs provide a fast, convenient way of controlling the chemistry of these surfaces, they do not come without limitations. On Au, long-chain alkanethiols will displace shorter-chain thiols on the surface.[46] In addition, investigators have reported that thiolate SAMs start to show thermal instability at temperatures over 50° C.[47] It is generally accepted that formation of thiolate SAMs is governed by the thermodynamic principles of chemical equilibria and therefore the films are potentially less useful in non-equilibrium conditions. Thus, in situations where these limitations are a concern, other surface modification strategies may be more attractive.

Organosilicon SAMs

SAMs can also be prepared by covalently linking organosilicon molecules to hydroxide-terminated metal surfaces and metal oxide surfaces. The most widely used

organosilicon derivatives are alkylchlorosilanes and alkylalkoxysilanes. The organosilicon derivative is affixed to the metal surface by the formation of a M-O-Si linkage, where M is the metal atom. Interest in the modification of hydrated silica surfaces via Si-O-Si linkages began in the 1960s. Lee provided some of the first insights into the mechanistic details pertaining to the attachment chemistry.[48] Both trichlorosilanes and trialkoxysilanes are converted to silanetriols in the presence of trace amounts of moisture.[48] The silanetriol first adsorbs to the surface via hydrogen-bonding to the free OH's of the Si surface. In addition, the OH groups of neighbouring, adsorbed silanetriols hydrogen-bond to each other. Gentle heating then induces dehydration reactions that simultaneously cross-link neighbouring silanetriols via silyl ether linkages and covalently attach the polymer to the surface.[49] Figure 1.02 shows the surface polymerization reaction for silanetriols adsorbed to a hydrated silica surface. R is typically an ω-substituted alkyl chain, similar to those in ω-substituted alkanethiolate SAMs.

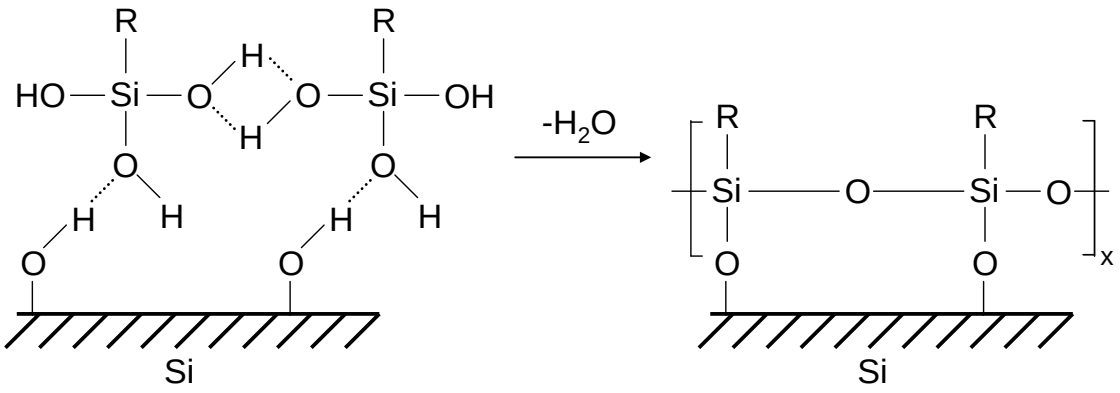

Figure 1.02. The surface polymerization reaction for organosilane derivatives adsorbed to a hydrated silica surface.

Organosilane SAMs have not been as extensively characterized as organothiolate SAMs. It is, however, known that densely-packed, true monolayers are formed and are generally devoid of surface imperfections.[49, 50] It has been proposed the alkyl chain portion of the organosilane is oriented at 10° from the surface normal.[50] Investigators have shown that island formation plays a key role in the growth of the monolayer structure.[51] In a recent study, it was shown that monolayer growth occurs in two, distinct steps.[52] In the first step a highly disordered, incomplete monolayer is formed with a large proportion of gauche defects in the alkyl chains. This is followed by a second, slower step where complete coverage is achieved and the alkyl chains adopt an ordered, all-trans configuration. Organosilane-derived SAMs are also known to be extremely moisture sensitive during both the preparation phases and after complete formation.

CMEs based on silane chemistry were first reported by Murray and coworkers. They demonstrated the covalent attachment of trialkoxyalkylamine-silane derivatives to SnO_2,[53, 54] TiO_2,[53, 54] glass,[53] glassy carbon,[53] RuO_2,[54, 55] and Pt/PtO.[54, 56] Their work also demonstrated organosilane derivatives can be used to anchor electroactive groups like the methylpyridinium ion to these surfaces. The surface-bound methylpyridinium ions can then be characterized using electrochemical methods such as cyclic voltammetry.

c) Aryl Layers Derived from Aryldiazonium Cations

The use of *para*-substituted aryldiazonium cations to modify surfaces began in 1992 when Pinson and coworkers modified a glassy carbon surface by electrochemically reducing 4-nitrobenzenediazonium cations in solution.[57] They proposed that this occurred via an aryl radical intermediate, similar to the mechanism by which aryl radicals

can be electrochemically generated from aryl halides and aryl sulfides.[58] It is now generally accepted that, once an aryl radical is generated in the diffusion layer of the electrode, it will covalently attach to the graphitic ring structure of the carbon electrode. This is known to be true for glassy carbon,[57, 59] carbon fiber composite materials,[60] highly oriented pyrolitic graphite (HOPG),[61, 62] and pyrolized photoresist films (PPF).[63, 64]

Films generated in this manner were once thought to be monolayers, although now it is well established that multilayered structures may be produced.[59, 62] It is hypothesized that aryl radicals attack the aryl groups that initially bind to the electrode, to form polyphenylene chains. The overall scheme for the modification of a surface by the electrochemical reduction of an aryldiazonium cation is depicted in Figure 1.03. Since there is flexibility in the choice of the R group, a surface of a variety of chemical functional groups can be created *e.g.,* R could be NH_2, CO_2H, OH, etc. This idea can be followed-up with classical organic transformation chemistries, and therefore has the potential to produce an enormous number of surface chemistries.

The number of literature reports showing that aryldiazonium cation reduction can be applied to substrates other than carbon is increasing rapidly. This strategy has now been applied to various metals (Co, Ni, Fe, Cu, Pt, Pd, Au),[65-72] Si,[67, 71, 73, 74] and GaAs.[67] For some of these newer substrates, the nature of the interaction between the surface and the aryl moiety has been determined. For Fe surfaces, there is direct evidence of an Fe-C bond.[68] On Cu surfaces, it has been shown attachment occurs via a Cu-O-C or a Cu-C bond, depending on the Cu surface preparation.[66] Although there is no unambiguous evidence for a Au-C bond on Au substrates, investigators have put forth some very compelling evidence that attachment can occur via azo linkages.[70, 75] The possibility that

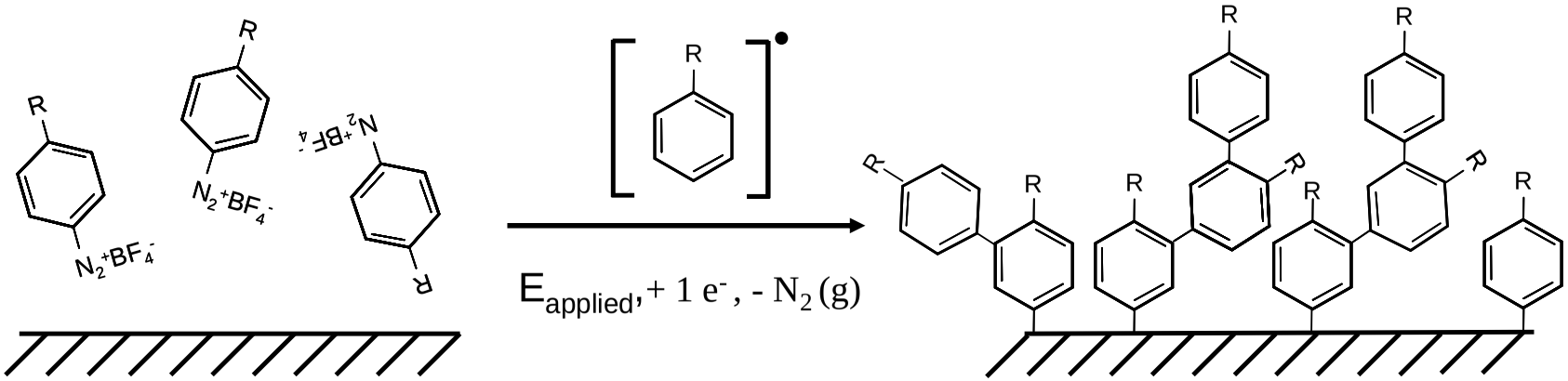

Figure 1.03. The electrochemical reduction of a para-sustituted aryldiazonium cation to produce a multilayer of aryl groups at a surface.

Au-C covalent bonds contribute to the attachment has not been ruled out.

Investigations of diazonium-derived aryl layers on Au were initiated by Vautrin-Ul and coworkers.[65] They studied nitrobenzene (NB) layers that were electrochemically grafted to Au. Following their derivatization procedures, the substrates were cleaned in an ultrasonic bath and transferred to a blank acetonitrile solution with supporting electrolyte. They demonstrated that Faradaic peaks from the electroactive nitro groups could still be observed using cyclic voltammetry. This result suggested that the layers were tightly bonded to the Au substrate.

Bélanger and coworkers recently carried out an in-depth study of diazonium-derived layers on Au.[70] By performing a coupled quartz-crystal microbalance/ chronoamperometry experiment, they observed that their electrochemical grafting procedures were inefficient. Only 35% of the radicals generated during the deposition attached to the surface. Despite this observation, aryl layers comprised of nitrobenzene (NB) and diethylaniline (DEA) groups provided a significant electrochemical barrier effect to $Fe(CN)_6^{3/4-}$. By contrast, carboxyphenyl (CP) layers did not provide a noticeable barrier effect. Further, the NB, DEA, and CP layers were not significantly perturbed by an ultrasonic rinsing treatment. This result demonstrated that there is a strong interaction between these layers and the Au substrate, but that the functional group on the phenyl ring does affect the overall layer structure. It was further demonstrated that NP, DEA, and CP films were much thicker than a monolayer, a similar result to what is observed for carbon substrates.[62]

The prospect that a Au-C bond could directly link the aryl groups to a Au surface provides the motivation to investigate the electrochemical reduction of aryldiazonium

cations as a viable means to modify Au surfaces. The disadvantages of the Au-thiolate interaction also contribute to the drive. Thiolates are prone to thermal desorption from Au surfaces. They are also prone to electrochemically induced desorption at potentials with absolute values greater than 800 mV *vs*. Ag/AgCl.[76] These limitations warrant the investigation of other strategies to chemically modify Au surfaces.

Research Objectives

At the time my thesis research began very little was known about diazonium-derived aryl layers on Au surfaces. As such, my objective was to investigate the structure and stability of these layers. It was my intention to examine the extent to which the deposited thickness of the layers can be controlled (and measured). Fourier-transform infrared reflection-absorption spectroscopy (FT-IRRAS) and electrochemical blocking methods served as the analytical tools to evaluate the thermal and mechanical stability of these layers. A direct, side-by-side comparison of the stability of aryl layers deposited electrochemically from diazonium salts to SAMs of the corresponding aromatic thiolate analogue was made. Efforts were focused on determining whether the strength of the interaction between Au and the diazonium-derived aryl groups supersedes that of the Au-thiolate bond.

It was also my intention to examine whether diazonium-derived aryl layers can cooperatively exist on the same gold surface as alkanethiolate molecules *i.e*., in a mixed-molecular layer setting. I will discuss the potential applications of this phenomenon. For example I observed how such structures behaved in molecular electronics devices. Some of the questions I will address are: Will the aryl groups show enhanced electrical

conduction when compared to the alkanethiolate molecules? Is it possible to observe localized differences in electrical conductivity in these layers? If so, can it be shown that this is due to different local film structures? The answers to these questions will be addressed herein.

References

1. Aktary, M.; McDermott, M. T.; MacAlpine, G. *Surface Engineering* **2002,** 18, (1), 70-74.

2. Aktary, M.; McDermott, M. T.; McAlpine, G. A. *Tribology Letters* **2002,** 12(3), 155-162.

3. Aktary, M.; McDermott, M. T.; Torkelson, J. *Wear* **2001,** 247(2), 172-179.

4. Swalen, J. D.; Allara, D. L.; Andrade, J. D.; Chandross, E. A.; Garoff, S.; Israelachvili, J.; Mccarthy, T. J.; Murray, R.; Pease, R. F.; Rabolt, J. F.; Wynne, K. J.; Yu, H. *Langmuir* **1987,** 3, (6), 932-950.

5. Cheng, M. L.; Yang, J. *Applied Spectroscopy* **2008,** 62, (1), 38-45.

6. Jonsson, G.; Gorton, L. *Biosensors* **1985,** 1, (4), 355-368.

7. Yeung, K. W. K.; Poon, R. W. Y.; Chu, P. K.; Chung, C. Y.; Liu, X. Y.; Lu, W. W.; Chan, D.; Chan, S. C. W.; Luk, K. D. K.; Cheung, K. M. C. *Journal of Biomedical Materials Research Part A* **2007,** 82A, (2), 403-414.

8. Ikada, Y. *Macromolecular Symposia* **1996,** 101, 455-462.

9. Chou, W. Y.; Mai, Y. S.; Cheng, H. L.; Yeh, C. Y.; Kuo, C. W.; Tang, F. C.; Shu, D. Y.; Yew, T. R.; Wen, T. C. *Organic Electronics* **2006,** 7, (6), 445-451.

10. Kim, J. M.; Lee, J. W.; Kim, J. K.; Ju, B. K.; Kim, J. S.; Lee, Y. H.; Oh, M. H. *Applied Physics Letters* **2004,** 85, (26), 6368-6370.

11. Weiss, E. A.; Chiechi, R. C.; Kaufman, G. K.; Kriebel, J. K.; Li, Z. F.; Duati, M.; Rampi, M. A.; Whitesides, G. M. *Journal of the American Chemical Society* **2007,** 129, (14), 4336-4349.

12. Bergren, A. J.; Harris, K. D.; Deng, F. J.; McCreery, R. L. *Journal of Physics-Condensed Matter* **2008,** 20, (37).

13. Reed, M. A.; Zhou, C.; Muller, C. J.; Burgin, T. P.; Tour, J. M. *Science* **1997,** 278, (5336), 252-254.

14. Bumm, L. A.; Arnold, J. J.; Cygan, M. T.; Dunbar, T. D.; Burgin, T. P.; Jones, L.; Allara, D. L.; Tour, J. M.; Weiss, P. S. *Science* **1996,** 271, (5256), 1705-1707.

15. Kelley, T. W.; Granstrom, E. L.; Frisbie, C. D. *Advanced Materials* **1999,** 11, (3), 261.

16. Mann, B.; Kuhn, H. *Journal of Applied Physics* **1971,** 42, (11), 4398.

17. Bilek, G.; Kremser, L.; Blaas, D.; Kenndler, E. *Electrophoresis* **2006,** 27, (20), 3999-4007.

18. Zlatkis, A.; Walker, J. Q. *Analytical Chemistry* **1963,** 35, (10), 1359.

19. Boehm, H. P.; Heck, W.; Sappok, R.; Diehl, E. *Angewandte Chemie-International Edition* **1964,** 3, (10), 669.

20. Watkins, B. F.; Behling, J. R.; Kariv, E.; Miller, L. L. *Journal of the American Chemical Society* **1975,** 97, (12), 3549-3550.

21. Lane, R. F.; Hubbard, A. T. *Journal of Physical Chemistry* **1973,** 77, (11), 1401-1410.

22. Murray, R. W. *Accounts of Chemical Research* **1980,** 13, (5), 135-141.

23. Rubinstein, I.; Bard, A. J. *Journal of the American Chemical Society* **1980,** 102, (21), 6641-6642.

24. Miller, L. L.; Vandemark, M. R. *Journal of the American Chemical Society* **1978,** 100, (2), 639-640.

25. Tachikawa, H.; Faulkner, L. R. *Journal of the American Chemical Society* **1978,** 100, (14), 4379-4385.

26. Itaya, K.; Bard, A. J. *Analytical Chemistry* **1978,** 50, (11), 1487-1489.

27. Merz, A.; Bard, A. J. *Journal of the American Chemical Society* **1978,** 100, (10), 3222-3223.

28. Nowak, R.; Schultz, F. A.; Umana, M.; Abruna, H.; Murray, R. W. *Journal of Electroanalytical Chemistry* **1978,** 94, (3), 219-225.

29. Komura, T.; Ito, Y.; Yamaguti, T.; Takahasi, K. *Electrochimica Acta* **1998,** 43, (7), 723-731.

30. White, H. S.; Leddy, J.; Bard, A. J. *Journal of the American Chemical Society* **1982,** 104, (18), 4811-4817.

31. Schmidt-Rohr, K.; Chen, Q. *Nature Materials* **2008,** 7, (1), 75-83.

32. Kuhn, H. *Thin Solid Films* **1983,** 99, (1-3), 1-16.

33. Zasadzinski, J. A.; Viswanathan, R.; Madsen, L.; Garnaes, J.; Schwartz, D. K. *Science* **1994,** 263, (5154), 1726-1733.

34. Nuzzo, R. G.; Allara, D. L. *J. Am. Chem. Soc.* **1983,** 105, (13), 4481-4483.

35. Cohen, S. R.; Naaman, R.; Sagiv, J. *Journal of Physical Chemistry* **1986,** 90, (14), 3054-3056.

36. Dubois, L. H.; Nuzzo, R. G. *Ann. Rev. Phys. Chem.* **1992,** 43, 437-463.

37. Laibinis, P. E.; Whitesides, G. M.; Allara, D. L.; Tao, Y. T.; Parikh, A. N.; Nuzzo, R. G. *Journal of the American Chemical Society* **1991,** 113, (19), 7152-7167.

38. Nuzzo, R. G.; Zegarski, B. R.; Dubois, L. H. *J. Am. Chem. Soc.* **1987,** 109, (3), 733-740.

39. Walczak, M. M.; Chung, C. K.; Stole, S. M.; Widrig, C. A.; Porter, M. D. *Journal of the American Chemical Society* **1991,** 113, (7), 2370-2378.

40. Shimazu, K.; Sato, Y.; Yagi, I.; Uosaki, K. *Bulletin of the Chemical Society of Japan* **1994,** 67, (3), 863-865.

41. Demoz, A.; Harrison, D. J. *Langmuir* **1993,** 9, (4), 1046-1050.

42. Volmer, M.; Stratmann, M.; Viefhaus, H. *Surface and Interface Analysis* **1990,** 16, (1-12), 278-282.

43. Sheen, C. W.; Shi, J. X.; Martensson, J.; Parikh, A. N.; Allara, D. L. *Journal of the American Chemical Society* **1992,** 114, (4), 1514-1515.

44. Porter, M. D.; Bright, T. B.; Allara, D. L.; Chidsey, C. E. D. *J. Am. Chem. Soc.* **1987,** 109, (12), 3559-3568.

45. Ulman, A. *Chemical Reviews* **1996,** 96, (4), 1533-1554.

46. Bain, C. D.; Troughton, E. B.; Tao, Y. T.; Evall, J.; Whitesides, G. M.; Nuzzo, R. G. *J. Am. Chem. Soc.* **1989,** 111, (1), 321-335.

47. Delamarche, E.; Michel, B.; Kang, H.; Gerber, C. *Langmuir* **1994,** 10, (11), 4103-4108.

48. Lee, L. H. *Journal of Colloid and Interface Science* **1968,** 27, (4), 751.

49. Sagiv, J. *Journal of the American Chemical Society* **1980,** 102, (1), 92-98.

50. Allara, D. L.; Parikh, A. N.; Rondelez, F. *Langmuir* **1995,** 11, (7), 2357-2360.

51. Wasserman, S. R.; Whitesides, G. M.; Tidswell, I. M.; Ocko, B. M.; Pershan, P. S.; Axe, J. D. *Journal of the American Chemical Society* **1989,** 111, (15), 5852-5861.

52. Liu, Y.; Wolf, L. K.; Messmer, M. C. *Langmuir* **2001,** 17, (14), 4329-4335.

53. Untereker, D. F.; Lennox, J. C.; Wier, L. M.; Moses, P. R.; Murray, R. W. *Journal of Electroanalytical Chemistry* **1977,** 81, (2), 309-318.

54. Moses, P. R.; Wier, L. M.; Lennox, J. C.; Finklea, H. O.; Lenhard, J. R.; Murray, R. W. *Analytical Chemistry* **1978,** 50, (4), 576-585.

55. Moses, P. R.; Murray, R. W. *Journal of Electroanalytical Chemistry* **1977,** 77, (3), 393-399.

56. Lenhard, J. R.; Murray, R. W. *Journal of Electroanalytical Chemistry* **1977,** 78, (1), 195-201.

57. Delamar, M.; Hitmi, R.; Pinson, J.; Saveant, J. M. *J. Am. Chem. Soc.* **1992,** 114, (14), 5883-5884.

58. Andrieux, C. P.; Pinson, J. *Journal of the American Chemical Society* **2003,** 125, (48), 14801-14806.

59. Kariuki, J. K.; McDermott, M. T. *Langmuir* **2001,** 17, (19), 5947-5951.

60. Delamar, M.; Desarmot, G.; Fagebaume, O.; Hitmi, R.; Pinson, J.; Saveant, J. M. *Carbon* **1997,** 35, (6), 801-807.

61. Liu, Y. C.; McCreery, R. L. *Journal of the American Chemical Society* **1995,** 117, (45), 11254-11259.

62. Kariuki, J. K.; McDermott, M. T. *Langmuir* **1999,** 15, (19), 6534-6540.

63. Ranganathan, S.; McCreery, R. L. *Anal. Chem.* **2001,** 73, (5), 893-900.

64. Brooksby, P. A.; Downard, A. J. *Langmuir* **2004,** 20, (12), 5038-5045.

65. Bernard, M. C.; Chausse, A.; Cabet-Deliry, E.; Chehimi, M. M.; Pinson, J.; Podvorica, F.; Vautrin-Ul, C. *Chem. Mater.* **2003,** 15, (18), 3450-3462.

66. Hurley, B. L.; McCreery, R. L. *J. Electochem. Soc.* **2004,** 151, (5), B252-B259.

67. Stewart, M. P.; Maya, F.; Kosynkin, D. V.; Dirk, S. M.; Stapleton, J. J.; McGuiness, C. L.; Allara, D. L.; Tour, J. M. *J. Am. Chem. Soc.* **2004,** 126, (1), 370-378.

68. Adenier, A.; Bernard, M. C.; Chehimi, M. M.; Cabet-Deliry, E.; Desbat, B.; Fagebaume, O.; Pinson, J.; Podvorica, F. *J. Am. Chem. Soc.* **2001,** 123, (19), 4541-4549.

69. Boukerma, K.; Chehimi, M. M.; Pinson, J.; Blomfield, C. *Langmuir* **2003,** 19, (15), 6333-6335.

70. Laforgue, A.; Addou, T.; Belanger, D. *Langmuir* **2005,** 21, (15), 6855-6865.

71. Combellas, C.; Kanoufi, F.; Pinson, J.; Podvorica, F. I. *J. Am. Chem. Soc.* **2008,** 130, (27), 8576-+.

72. Paulik, M. G.; Brooksby, P. A.; Abell, A. D.; Downard, A. J. *J. Phys Chem. C* **2007,** 111, (21), 7808-7815.

73. Allongue, P.; de Villeneuve, C. H.; Cherouvrier, G.; Cortes, R.; Bernard, M. C. *J. Electroanal. Chem.* **2003,** 550, 161-174.

74. deVilleneuve, C. H.; Pinson, J.; Bernard, M. C.; Allongue, P. *Journal of Physical Chemistry B* **1997,** 101, (14), 2415-2420.

75. Doppelt, P.; Hallais, G.; Pinson, J.; Podvorica, F.; Verneyre, S. *Chem. Mater.* **2007,** 19, 4570-4575.

76. Walczak, M. M.; Popenoe, D. D.; Deinhammer, R. S.; Lamp, B. D.; Chung, C. K.; Porter, M. D. *Langmuir* **1991,** 7, (11), 2687-2693.

Chapter II

Diazonium-Derived Nitroazobenzene Layers on Gold

1. Introduction

The electrochemical reduction of substituted aromatic diazonium salts is a versatile means to chemically alter the surface of an electrically conductive material such that a desired chemical functional group is exposed at the modified electrode surface. Versatility is imparted by the ease at which *para*-substituted aromatic diazonium salts, with virtually any reasonable substituent can be synthesized using classical synthetic procedures.[1] A wide range of aromatic amine precursors are available. This method is suitable for modifying a wide range of electrode materials, most notably carbon.[2-6] It is suited to applications that require a thin (~1-20 nm) molecular layer with a particular functional group exposed at the modified surface. Two areas of research where diazonium-derived organic layers have shown great promise are biosensing,[7-9] and molecular electronics.[10,11]

Pinson and coworkers first demonstrated the aryl substituent of a *para*-substituted aromatic diazonium salt can readily be attached to the surface of glassy carbon through electrochemical induction.[3] The continued investigations by Pinson and other investigators have revealed much information about layers created by this method. For carbon substrates, it is known that the films are quite stable towards long-term exposure

to ambient conditions and ultrasonication in several organic solvents.[12] This led to the notion that a carbon-carbon bond is formed between the aryl group and the electrode.

In the last decade materials other than carbon have been investigated as plausible substrates for this modification scheme including metals[12-17] and semiconductors.[14,18-22] With these new substrates, details of the attachment chemistry between the layer and the substrate are actively being investigated. For metallic substrates investigators have reported evidence that a metal-C bond is responsible for fixation of the layer to the substrate.[15,16] McCreery and coworkers have shown that metal oxides play a key role in the attachment.[17] Bélanger and coworkers have provided compelling evidence that in addition to a metal-C bond, azo-linkages also play a role in the attachment.[15] It is postulated that azo-linkages could serve as a direct link to the substrate or they could provide a means of linking additional aryl groups to an already existing layer, forming a multilayered film structure. It is equally possible that both of these scenarios coexist.

Despite numerous studies, a complete understanding of the strength and nature of the attachment of the layer to the substrate has yet to be unveiled. This is especially true for metallic substrates. While metal-carbon bonds are known for metals in coordination compounds, the existence of covalent bonds between carbon and a metal surface is less established.[23,24] It therefore follows that more research is necessary to better address the attachment chemistry that is involved for diazonium derived layers on metals.

The aim of this chapter is to provide a preliminary assessment of organic films deposited on polycrystalline gold electrodes by the electrochemical reduction of nitroazobenzene diazonium cations. The grafting of NAB substituents to gold without electrochemical induction was also explored in parallel.[25] This can be considered an

analogy to self-assembled thiolate monolayers on gold.[26,27] A key subject will be the stability of the layer-substrate interaction for NAB layers deposited using these methods.

The strength of the interaction between the diazonium-derived layers and the gold will be explored primarily by subjecting modified electrodes to two separate treatments. These two treatments are thorough sonication in organic solvents and lengthy immersion into a dilute solution of a long-chain aliphatic thiol. The ability of the NAB films to endure other treatments such as exposure to intense heating, intense UV irradiation, and resistance to electrochemical desorption will also be investigated. The techniques of infrared reflection-absorption spectroscopy (IRRAS) and electrochemical blocking will be employed before and after each treatment and a subsequent comparison of the results will be made to quantitatively assess the effect on the NAB layer.

2. Experimental

Preparation of Gold Substrates. Gold was deposited onto glass microscope slides via thermal evaporation using 99.99% Au shot (Goodfellow). The final thickness of the gold layer was 100 nm for all substrates in this study. A 6 nm layer of Cr was used in between the glass and gold film to enhance adhesion. All glass substrates and glassware in this study were cleaned using hot piranha solution (1:4 30% H_2O_2:H_2SO_4) followed by thorough rinsing with deionized (18 MΩ)/filtered H_2O (NANOpure™ water purification system, Barnstead International, Dubuque, Iowa). Substrates were blown dry using Ar gas. [*Warning: Piranha solution should be handled with extreme care; it is a strong oxidant and reacts violently with many organic materials. It also presents an explosion danger. All work should be performed under a fume hood*.]

Electrochemical Deposition of the Aryl Films. 4-nitroazobenzenediazonium tetrafluoroborate (NABDF) was synthesized according to procedures published by Starkey.[1] Tetrabutylammonium tetrafluoroborate ($TBABF_4$) (≥99%) was used as received (Sigma-Aldrich Canada Ltd., Oakville, Ontario). Spectroscopic grade acetonitrile was also used as received (Caledon Laboratories Ltd., Georgetown, Ontario). Prior to surface modification, all gold substrates were subjected to a 10 min cleaning in a Model 42 UVO® commercial ozone cleaner (Jelight Company, Inc., Irvine California). Following the ozone cleaning, the substrates were stirred in anhydrous ethanol (Commercial Alcohols Inc., Brampton, Ontario) for 10 min. Electrochemical grafting of the aryl layers to the gold substrates was achieved by cyclic voltammetry using a software controlled Model AFCBP1 bipotentiostat (Pine Instrument Company, Grove City, Pennsylvania). For all non-aqueous electrochemistry the reference electrode consisted of a silver wire submerged in a 200 mM $AgNO_3$ solution in acetonitrile with 0.1 M $TBABF_4$. A platinum wire/platinum mesh assembly with adequate surface area served as a counter electrode. All electrochemical depositions were carried out by sweeping the potential from +300 mV to -900 mV at a sweep rate of 200 mV/s, and a diazonium salt concentration of 1 mM in acetonitrile with 0.1 M $TBABF_4$. Diazonium salt solutions were deaerated for 10 min with Ar gas prior to all depositions. Following the modification, samples were thoroughly rinsed with acetonitrile, blown dry with a gentle stream of Ar gas, and used immediately with minimum exposure to the ambient.

IRRAS. IRRAS spectra were collected using an ATI Mattson Infinity Series Fourier transform infrared (FTIR) spectrometer equipped with a liquid nitrogen cooled mercury-cadmium telluride (MCT) detector. The p-polarized IR beam was incident on the gold

surface at an angle of 80° with respect to the surface normal. A total of 1500 scans were averaged for each experiment at a resolution of 4 cm^{-1}. The interferograms were Fourier transformed using triangular apodization. A gold slide modified with a SAM of $CD_3(CD_2)_{16}CD_2$-SH was used as a reference.

Electrochemical Blocking Studies. Ferrocene (≥98%) (Sigma-Aldrich Canada Ltd., Oakville, Ontario) was used as received. Solutions were deaerated for 10 min with Ar. A 3-necked inverted electrochemical cell was clamped to a modified/unmodified electrode surface with a solvent resistant, Viton o-ring (6 mm diameter) in between to define the electrode area of 0.28 cm^2. Potentials were measured with respect to an Ag wire submerged in a 200 mM solution of $AgNO_3$ in acetonitrile.

Ultrasonication Procedure. Modified electrodes were placed in a sealed glass jar containing the appropriate organic solvent. A Model 275D TRU-SWEEP™ Ultrasonicator (Rose Scientific Ltd., Edmonton, Alberta) operated at the maximum setting was used to ultrasonicate all samples. Samples were sonicated in acetonitrile and then acetone (HPLC grade, ≥99%) (Sigma-Aldrich Canada Ltd., Oakville, Ontario) for 15 min each. The bath temperature was maintained at room temperature with the addition of ice for the duration of the procedure.

ODT Displacement Reactions. Octadecanethiol (ODT, 98%) was used as received (Sigma-Aldrich Canada Ltd.). Cleaned gold substrates were immersed in a 1 mM ODT solution in ethanol. All solutions were deaerated with Ar gas for 10 min prior to the self-assembly process.

UV Irradiation Procedure. Modified electrodes were placed under a standard UV-lamp used for visualizing spots on thin-layer chromatography plates for one hour.

Reductive Desorption Procedure. Potassium Chloride (≥99%) and potassium hydroxide (>99 %) (Fisher Scientific International, Hampton, New Hampshire) were used as received. All aqueous solutions were prepared by dilution with 18 MΩ deionized H_2O, and bubbled with Ar for 10 min prior to the analysis. The potential was cycled between 0 mV and 1500 mV at a sweep rate of 25 mV/s. Potentials were measured with respect to an Ag/AgCl (saturated KCl) reference electrode using the same counter electrode described above.

3. Results and Discussion

3.1 Investigation of Layer Deposition Parameters

The purpose of this section is to establish a relationship between the choice of deposition parameters and the amount and quality of layer deposited. Nitroazobenzene diazonium fluoborate (NABDF) was employed because the resulting surface-bonded nitroazobenzene groups produce strong absorptions in the mid-IR region This allows for quantitative detection using FT-IRRAS. Three sets of deposition conditions were chosen for an initial study: 1 mM NABDF and 2 voltammetric cycles, 1 mM NABDF and 15 voltammetric cycles, and immersion in 1 mM NABDF for 24 hours. For the electrodes derivatized electrochemically, the naming convention used throughout this chapter will be “X-cycle”, where X denotes the number of voltammetric cycles used in the deposition process. For example a “2-cycle” electrode is one in which 2 complete potential scans from +300 mV to -900 mV, at 200 mV/s, were applied using cyclic voltammetry. The

final condition involving simple immersion into the deposition solution will be referred to as a spontaneously adsorbed (SA) approach to film deposition throughout this thesis, since no external externally applied potentials were used.

The sets of cyclic voltammograms for typical 2-cycle and 15-cycle depositions of NAB to the surface of a gold electrode are shown in Figures 2.01 and 2.02, respectively. For both of these conditions the first two cycles are nearly identical, as expected. The cathodic peak centered at -0.1 V is associated with the production of NAB radicals in accordance with the currently accepted mechanism. Based on four independent measurements the average magnitude of this peak during the first deposition cycle is -2400 ± 200 μA. Following the first cycle, the wave is diminished to an undetectable level which suggests that the electrode is coated with a sufficient layer to inhibit further diazonium cation reduction.

Careful inspection reveals that the reduction wave is unsymmetrical. This could be due to the presence of a weak shoulder at potentials more negative of the -0.1 V peak. The observation of two peaks in the voltammogram has previously been reported for the deposition of nitrobenzene groups to glassy carbon electrodes using an *in-situ* method.[28] Similar observations were made by Downard using glassy carbon substrates.[29] The origins of this second peak are unknown, although it has been suggested that it could be associated with the reduction of the radical itself.[30]

At more negative potentials (~ -0.8 V) a sharp rise in the current is observed. This current rapidly decreases with each additional cycle. We suspected that this is due to a solvent-related process. However, the blank trace in Figure 2.01 (0.1 M $TBABF_4$ in acetonitrile) provides evidence contrary to this argument. In a separate report by Pinson it

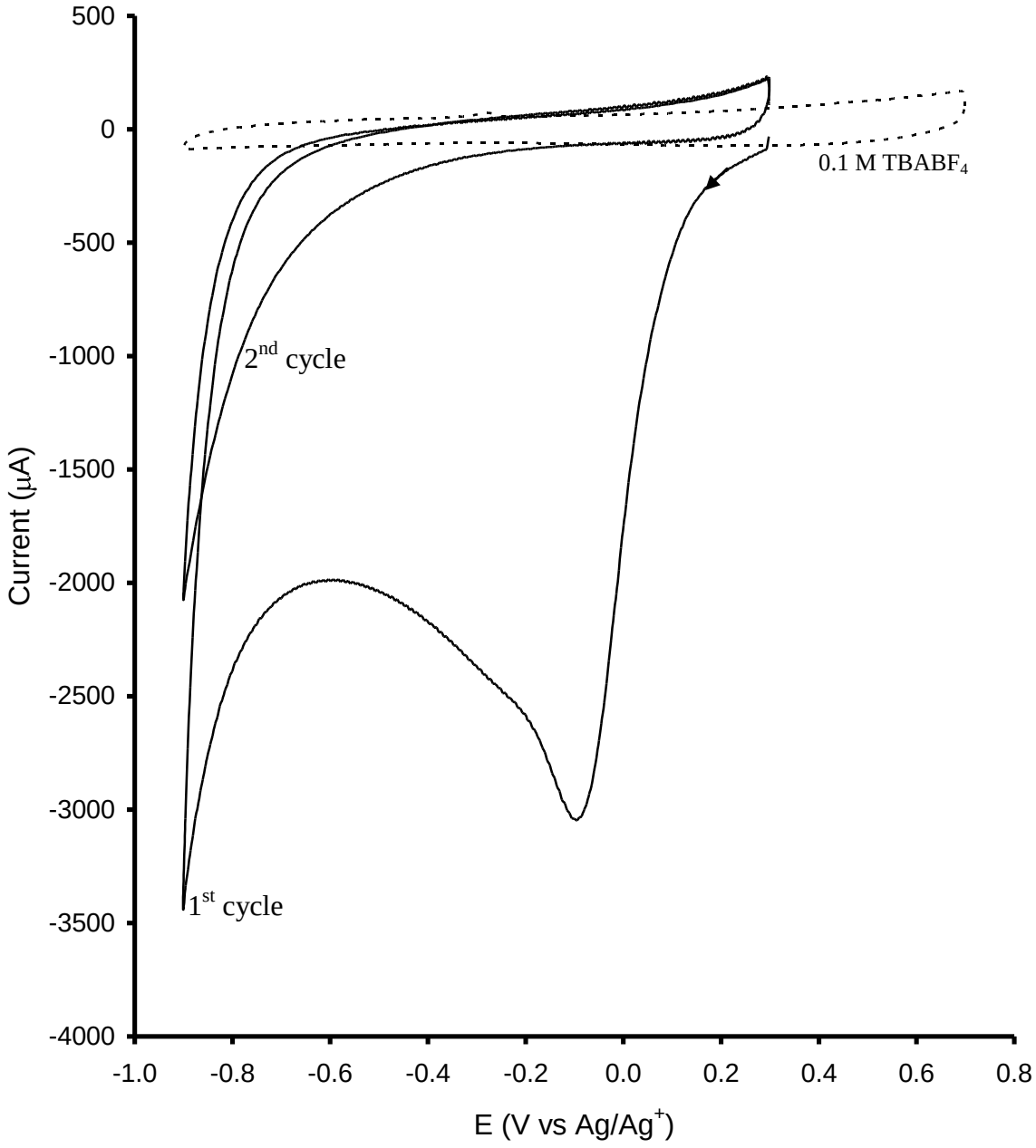

Figure 2.01. Cyclic voltammogram for a 2-cycle deposition of nitroazobenzene groups to a gold electrode from 1 mM NABDF in acetonitrile with 0.1 M $TBABF_4$ supporting electrolyte. Scan rate: 200 mV/s.

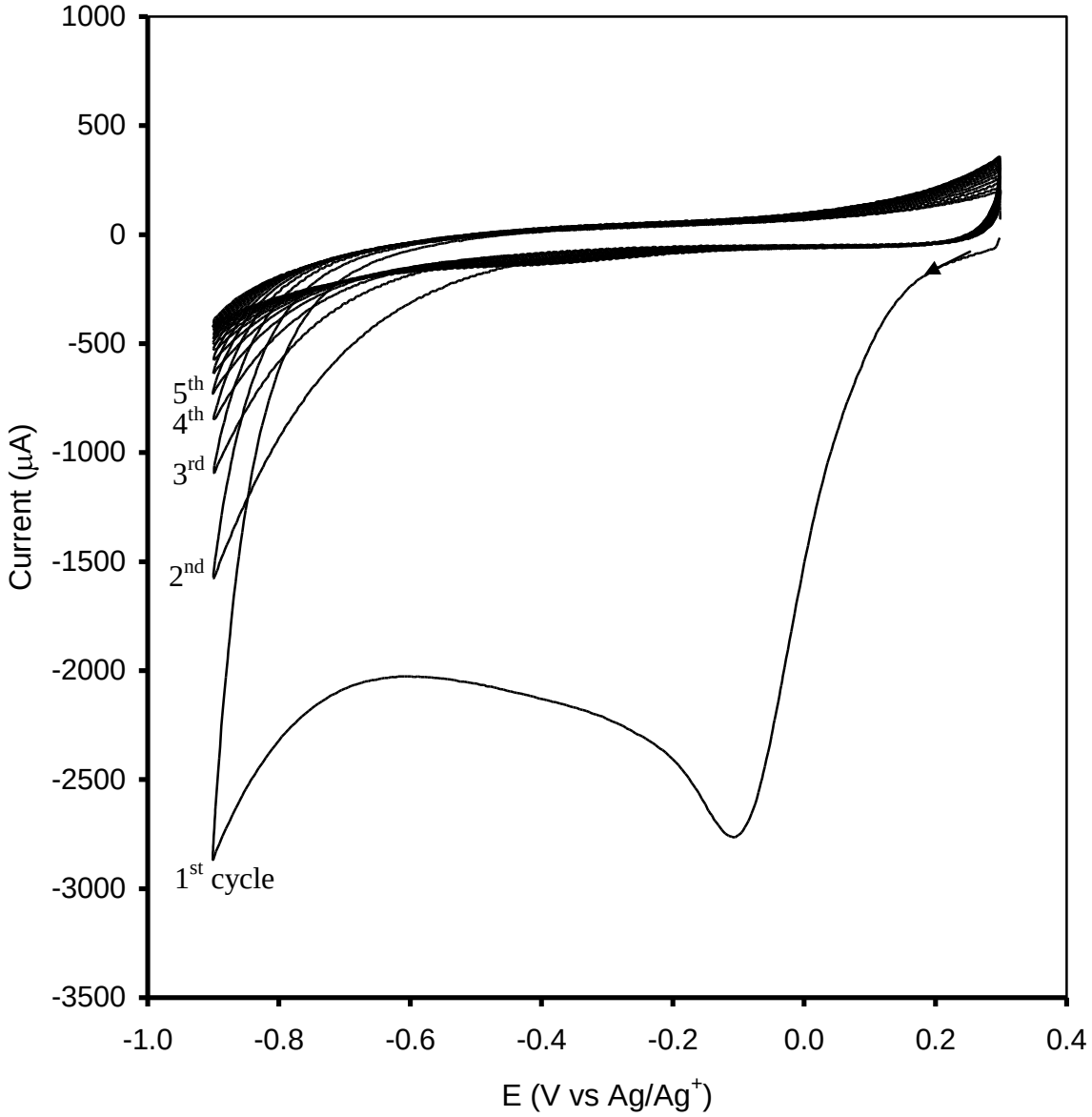

Figure 2.02. Cyclic voltammogram for a 15-cycle deposition of nitroazobenzene groups to a gold electrode from 1 mM NABDF in acetonitrile with 0.1 M $TBABF_4$ supporting electrolyte. Scan rate: 200 mV/s

was suggested that a similar peak was produced from the reduction of nitrobenzene to its radical anion when nitrobenzene groups were grafted to carbon fibers in aprotic media.[31]By analogy this peak could be due to the reduction of nitroazobenzene to a nitroazobenzene radical anion.

3.2 Quantification of the NAB Layers by IRRAS

IRRAS was employed to investigate the structure of the NAB layers spectroscopically. The fingerprint region of the IRRAS spectrum for gold electrodes modified using three different conditions is depicted in Figure 2.03. A 15-cycle deposition produces the highest band intensities, 2 cycles produces an intermediate value and the SA method produces the lowest values. Since IRRAS is an absorption technique, the NAB band intensities should be directly proportional to the amount of NAB groups on the gold surface. In addition, the IRRAS selection rules for thin films at metal surfaces dictate that only vibrations for which a component of the transition dipole moment is oriented perpendicular to the gold surface will produce an appreciable signal.[32] Thus, changes in band intensities as a function of the deposition conditions can be attributed to two effects, namely: differences in amount of NAB deposited and an orientation effect. However, based on work that will be presented in Chapter 3 of this thesis, we believe that orientation effects are minimal for diazonium-derived NAB layers. We will assume that changes to the band intensities are solely due to changes in the amount of NAB groups bound to the gold surface.

A summary of the band positions, their respective assignments and average observed intensities is provided in Table 2.01. As a general comment, the IR spectra of most organic molecules that contain a nitro group is dominated by a strong symmetric nitro stretch at ~1350 cm^{-1} and a strong asymmetric nitro stretch between ~1500 and 1550 cm^{-1}. The bands at 1347 cm^{-1} and 1525 cm^{-1} are therefore assigned to these vibrations, respectively, because they display the highest intensity. The band at 1525 cm^{-1} also displays a shoulder at a slightly lower wavenumber. This shoulder is assigned to stretching of the aromatic C-C bonds of the ring structures. We make this assignment because typical aromatic compounds exhibit a pair of stretches at ~1600 cm^{-1} and ~1500 cm^{-1} and therefore the shoulder, together with the peak observed at 1600 cm^{-1}, is likely a member of the pair.

The bands at 1141 cm^{-1} and 1109 cm^{-1} are assigned to the phenyl-NN and phenyl NO_2 stretches (respectively) and have been previously discussed in the literature.[33] The peak at 1457 cm^{-1} is assigned to the N=N azo stretch. Finally the band observed at 861 cm^{-1} is assigned to the out-of-plane (oop) aromatic C-H bending vibration.

The absorbance of the symmetric nitro stretch at 1347 cm^{-1}, A_{1347}, was used as a diagnostic to assess the relative amounts of film deposited. Its presence is unquestionably associated with the presence of the nitroazobenzene groups on the surface. This band was also chosen because it is the most intense band in all three of the spectra, allowing for good statistical treatment in terms of signal-to-noise (S/N) ratios. The results show that ~33 % of the nitroazobenzene groups affixed to the surface during a 2-cycle deposition are affixed by mere immersion in the deposition solution for 24 hours, all other things being equal. This would suggest that grafting by electrochemical induction is a more

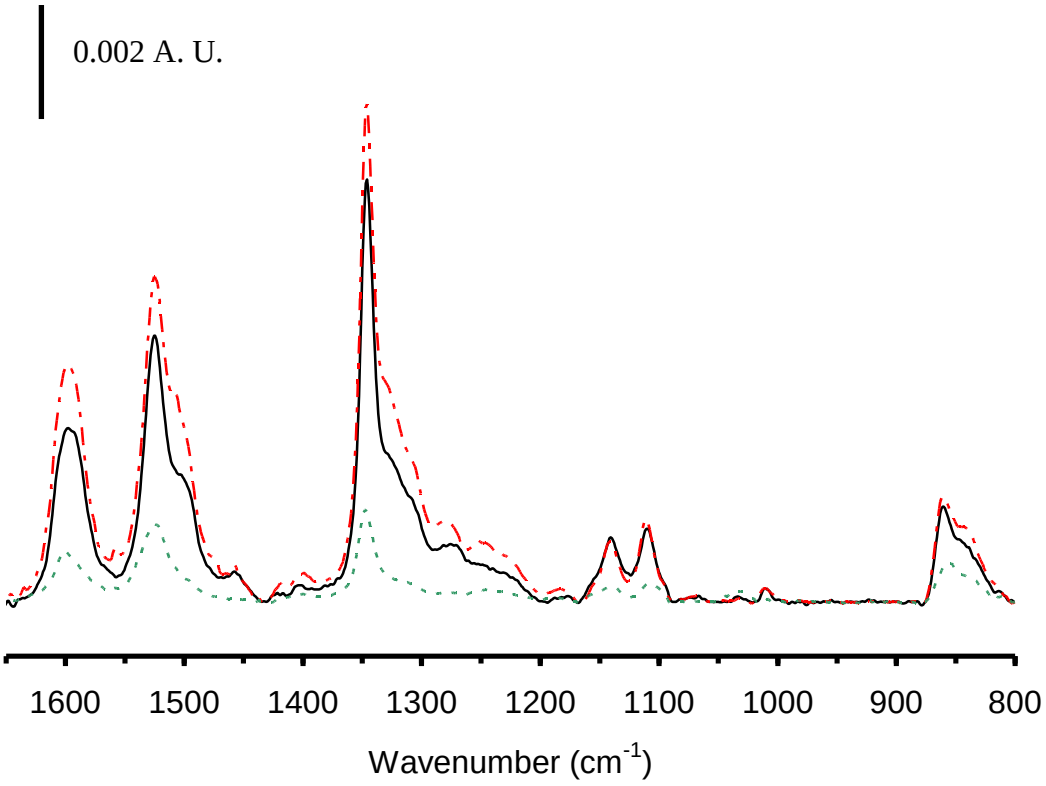

Figure 2.03. IRRAS spectra for nitroazobenzene layers attached to gold using a 2 (solid), 15 (dot-dash) cycle deposition via cyclic voltammetry and by immersion in a 1 mM NAB solution with 0.1 M $TBABF_4$ supporting electrolyte for 24 hours (dash).

position (cm^{-1})	absorbance (10^{-3} AU)	assignment
	2-cycle[a]	
1600	3 ± 0.3	C=C aromatic ring stretch
1525	4.7 ± 0.3	asymmetric NO_2 stretch ($v_{a,NO2}$)
1457	0.4 ± 0.2	N=N stretch
1347	7.3 ± 0.6	symmetric NO_2 stretch ($v_{s,NO2}$)
1141	1.1 ± 0.3	phenyl-NN stretch
1109	1.2 ± 0.3	phenyl-NO_2 stretch
861	1.6 ± 0.2	C-H oop deformation
	15-cycle[a]	
1600	4.3 ± 0.1	C=C aromatic ring stretch
1525	5.9 ± 0.1	asymmetric NO_2 stretch ($v_{a,NO2}$)
1457	0.5 ± 0.2	N=N stretch
1347	9.0 ± 0.3	symmetric NO_2 stretch ($v_{s,NO2}$)
1141	1.1 ± 0.004	phenyl-NN stretch
1109	1.5 ± 0.001	phenyl-NO_2 stretch
861	1.9 ± 0.1	C-H oop deformation
	SA[b]	
1600	1.3 ± 0.1	C=C aromatic ring stretch
1525	1.9 ± 0.1	asymmetric NO_2 stretch ($v_{a,NO2}$)
1457	negligible	N=N stretch
1347	2.4 ± 1.1	symmetric NO_2 stretch ($v_{s,NO2}$)

[a]Statistics are based on 2 independent measurements. [b]Statistics are based on 3 independent measurements.

Table 2.01. Average peak intensities and assigned identities for the IRRAS spectra of gold electrodes modified with NAB groups using different deposition conditions.

efficient process since significantly more material can be attached in the time required to perform cyclic voltammetry (in this case 24 seconds) than the 24 hours used in the self-assembled sample.

For a 15-cycle deposition, A_{1347} increases by 24 %, when compared to a 2-cycle deposition. Our interpretation of this result is that 24 % more material is deposited. This suggests that the amount of material deposited does not scale linearly with the number of cycles used. Further, the data suggest that the bulk of the material is deposited during the first two cycles of a multi-cycle deposition. An average A_{1347} value of 7.3 mAU is obtained following a 2-cycle deposition alone, while A_{1347} increases by only 1.7 mAU after 13 additional deposition cycles. It is also reasonable to conclude that the bulk of the material is deposited during the first cycle alone since this is the only cycle for which Faradaic current at -0.1 V is observed.

3.3 Effect of the Deposition Method on Film Structure

Considering the IRRAS selection rule, we felt that an analysis of certain band intensity ratios would provide additional information on the structure of the films. To elaborate, the relative intensities of certain bands produced from the bound NAB groups will be highly dependent on the structure of the network of interlinked NAB groups themselves. A film that is characterized by many randomly oriented NAB groups will likely produce an IRRAS spectrum that is considerably different from that produced by a

film with a more ordered, regular structure. The absorbance ratio of the symmetric nitro stretch to the asymmetric stretch, A_{1347} / A_{1525}, is perhaps the most appropriate value to discuss. These two are the most intense bands and the vibrational modes that they represent are relatively simple with only three atoms involved. A table summarizing this ratio, for the three deposition conditions explored, is presented in Table 2.02.

The average A_{1347} / A_{1525} values for electrodes modified using 2-cycle and 15-cycle depositions are 1.57and 1.51, respectively. Our interpretation of this result is that the films likely have a similar structure. In contrast, the average A_{1347} / A_{1525} ratio for the electrodes modified using a SA approach is significantly lower (1.25) which suggests this film has a different structure than the films prepared electrochemically. The A_{1347} / A_{1525} ratio was also measured for a pure NABDF powder sample and was found to be 1.45. Based on this data, we surmise that the films prepared electrochemically contain more structural similarities to NABDF powder. Powdered samples will likely have molecules

Sample	**A_{1347} / A_{1525}**
NABDF Powder[a]	1.45
NAB-Au (2-cycle)	1.57 ± 0.01
NAB-Au (15-cycle)	1.51 ± 0.02
NAB-Au (SA)	1.25 ± 0.06

[a] Collected for freshly synthesized NABDF using an FTIR microscope setup.

Table 2.02. The average ratio of the intensities of the symmetric and asymmetric nitro stretch peaks for gold electrodes modified with NAB using a 2-cycle and 15-cycle electrochemical deposition, and with no electrochemical induction. The results are averages of two independent measurements.

with random orientations since individual powder granules are not confined to a specific orientation. Thus an A_{1347} / A_{1525} value of 1.45 should be representative for a sample containing NAB groups that exist in random orientations. The data therefore suggests that the electrochemically deposited NAB films are composed of NAB groups that are more randomly oriented, a configuration that is expected to prevail in highly branched, multilayered structure.

Based on the collective results of this section and the previous (Section 3.2), we suspect that grafting with electrochemical induction favors a film structure that is multilayered, with the NAB groups randomly oriented in space. We also strongly suspect that grafting without electrochemical induction results in a film that is a monolayer in thickness. It is, however, very difficult to make the latter statement with confidence, because it is just as likely that a "less-extended" multilayer is produced. We will present a more thorough investigation of film thickness as a function of deposition conditions, using scanning probe microscopy, in Chapter IV of this thesis.

3.4 Assessment of Layer Quality Using an Electrochemical Redox Probe

A thin film deposited at an electrode surface can serve as a barrier to electron transfer to and from the underlying electrode. A film that is compact and devoid of imperfections will exhibit a greater barrier effect than one that contains "pinhole" defects. Chidsey *et al.* demonstrated this concept using SAMs of thiolate adsorbates prepared at gold electrodes.[27] SAMs that adopted a closely packed, well-ordered structure impeded

electron transfer to $Fe(CN)_6^{3-}$ in solution. Monolayers that took on a much more loosely packed, disordered structure permitted electron transfer $Fe(CN)_6^{3-}$. Ferrocene was chosen as a redox probe, in the present study, to assess the barrier properties of the NAB-modified electrodes using cyclic voltammetry.

Ferrocene was chosen because it is a simple, 1 e^-, outersphere redox species. It is soluble in acetonitrile and thus quite compatible with the deposition solutions used to prepare the modified electrodes. Additionally, ferrocene exhibits quasi-reversible behavior at polycrystalline gold electrodes. The relationship between the quantity ΔE_p, the voltage difference between the cathodic and anodic peaks of a cyclic voltammogram, and the heterogeneous electron transfer rate of the electrode, k°, is well documented.[34] Similar principles are used in the present study to establish a relationship between experimentally measured ΔE_p values and through-film, apparent electron transfer rates, $k°_{app}$'s, of NAB modified electrodes. Small ΔE_p values or values closer to those measured for a bare, unmodified gold electrode are associated with higher $k°_{app}$'s, and very efficient electron transfer. They imply a less compact, less insulating film. Conversely, large ΔE_p values imply a more compact film that shields the underlying gold electrode from exchanging electrons with ferrocene in solution.

Figure 2.04 contains a representative set of cyclic voltammograms, in 1 mM ferrocene, at unmodified and NAB modified gold electrodes. The ΔE_p values from these voltammograms are tabulated in Table 2.03. All comparisons are made to the observed ΔE_p for an unmodified Au electrode (280 mV). For the electrode modified via spontaneous adsorption, a slight increase in ΔE_p to 293 mV is observed. There is a slight suppression of both the cathodic and anodic peak currents, $I_{p,cath}$ and $I_{p,anod}$, respectively.

Sample	ΔE_p (mV)
Bare Au	280
NAB-Au (2-cycle)	700
NAB-Au (15-cycle)	immeasureable
NAB-Au (SA)	293

Table 2.03. The measured ΔE_p values of ferrocene using gold electrodes modified with NAB using a 2-cycle and 15-cycle electrochemical deposition, and via spontaneous adsorption.

Conversely, the electrodes modified with NAB electrochemically produce larger ΔE_p values. A 2-cycle electrochemical deposition results in an increase of ΔE_p to 700 mV. The $k°_{app}$ of this electrode is much lower than k° of an unmodified electrode. In addition, $I_{p,cath}$ and $I_{p,anod}$ are significantly reduced. This is indicative of a high surface density of NAB groups. Similarly, a 15-cycle deposition results in a ΔE_p value that is essentially immeasurable. $I_{p,cath}$ and $I_{p,anod}$ are reduced to very small values. These results show that NAB films deposited electrochemically block electron transfer to and from ferrocene more efficiently than the NAB films prepared by SA methods.

To help understand these results, an analogy is drawn to SAMs of aromatic thiolates on gold. Investigators have reported that monolayers prepared using thiophenol, *p*-biphenyl mercaptan and *p*-terphenyl mercaptan do not completely block electron transfer to $Fe(CN)_6^{4-/3-}$. [35] Based on these results, we believe that even a 2-cycle deposition produces an NAB film that is thicker than a monolayer of NAB groups. The results in Section 2.2 indicate that the amount of material deposited during a 15-cycle deposition is not much greater compared to the amount deposited during a 2-cycle deposition (*i.e.*, ~24 % more). Thus, the data in Figure 2.04 suggests that a 25 % increase

in the amount of material results in a film that blocks electron transfer to ferrocene much more efficiently. We hypothesize that this is because a 15-cycle deposition promotes films that support a more extended, multilayered structure. Current transfer to/from ferrocene likely only occurs at "pinhole" regions (microelectrodes) in these extended films. The sigmoidal shape of the CV supports this hypothesis.

The results for the NAB films prepared by SA are similar to the results reported for monolayers of aromatic thiolates on gold. For these films, it is possible that the layer is not as compact in some regions or contains many imperfections. In such a case, it is not expected that the films will block electron transfer very efficiently. The SA films could also be a monolayer thick.

3.5 Resistance of the NAB Films Towards Harsh Mechanical Treatment

The stability of the NAB layers was assessed by subjecting the derivatized electrodes to a thorough rinse in an ultrasonication bath. A 15 minute ultasonication was performed sequentially in acetone and acetonitrile, to ensure the maximum amount of material would be removed. IRRAS spectra and cyclic voltammograms in ferrocene were collected before and after the ultrasonication. IRRAS spectra for ultrasonicated electrodes modified using 2-cycles are shown in Figure 2.05 and are representative for the results of the other electrodes. Cyclic voltammograms of the ultrasonicated electrodes measured in the presence of ferrocene are presented in Figure 2.06. An overall summary of the results for all modified electrodes is presented in Table 2.04.

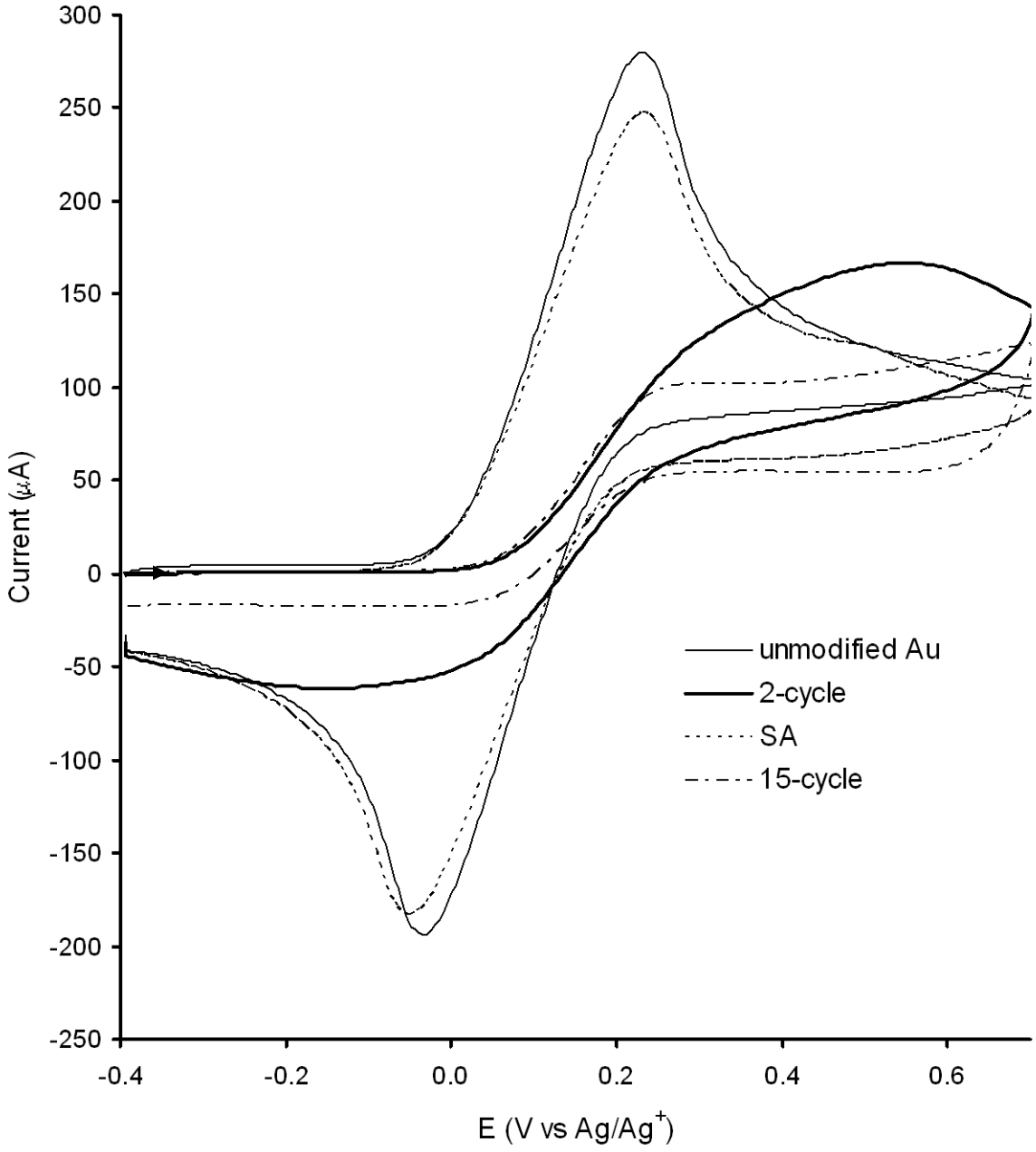

Figure 2.04. Cyclic voltammograms for NAB-modified gold electrodes in a 1 mM solution of ferrocene in acetonitrile with 0.1 M $TBABF_4$ supporting electrolyte. The scan rate is 100 mV/s.

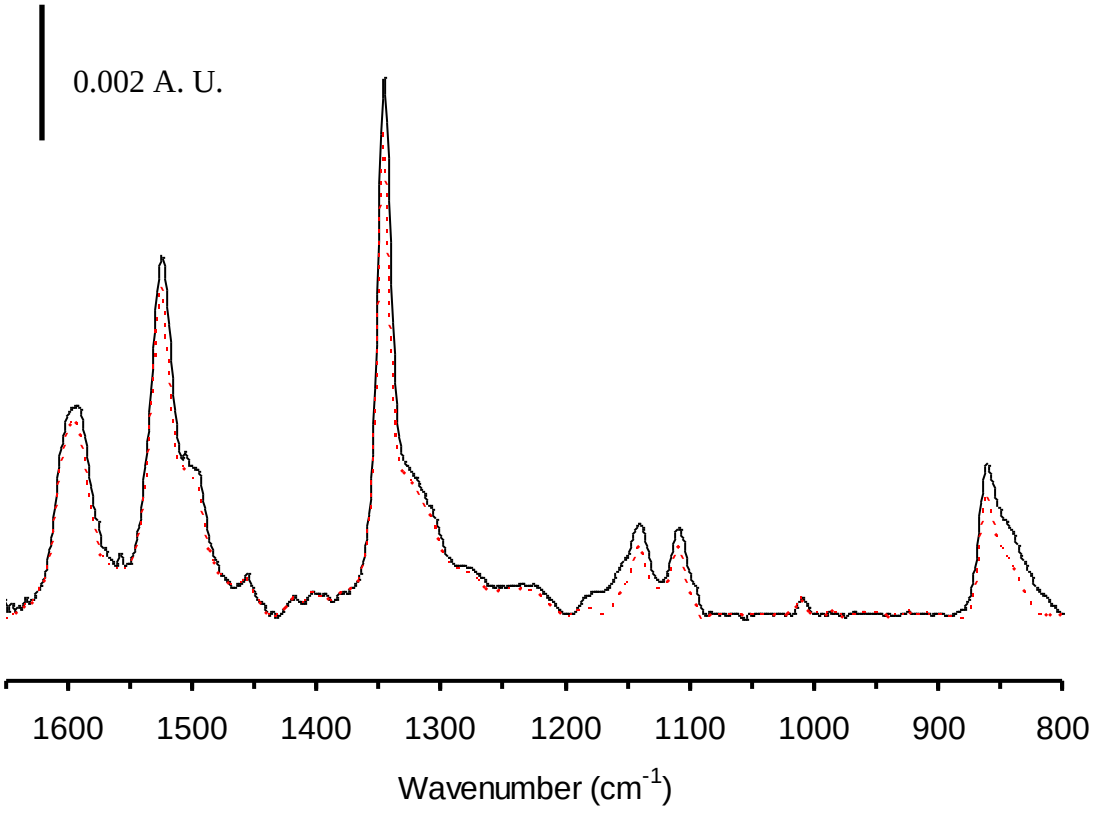

Figure 2.05. IRRAS spectra for nitroazobenzene layers attached to gold using a 2-cycle deposition before (solid) and after (dashed) ultrasonic cleaning in acetone and acetonitrile.

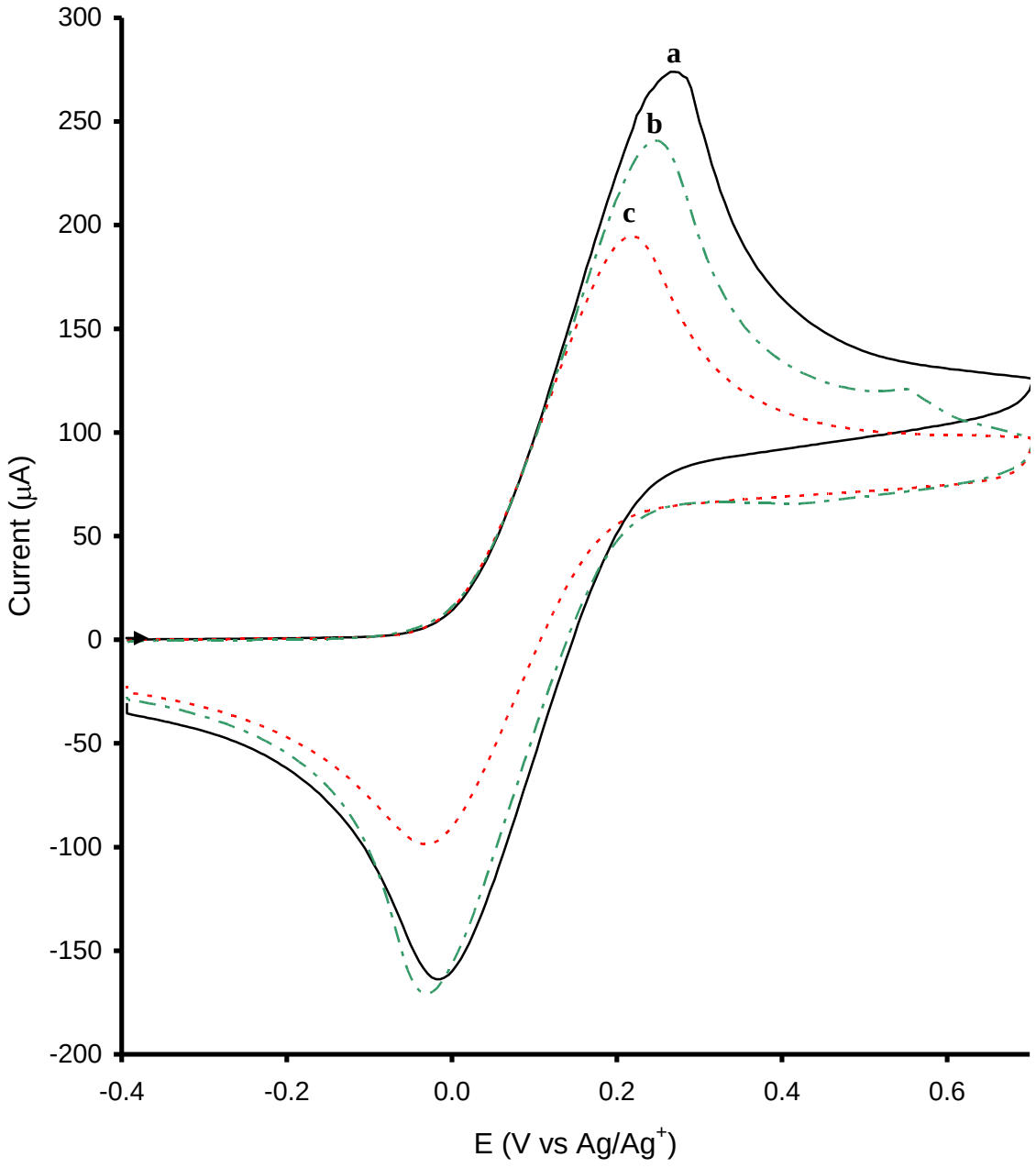

Figure 2.06. Cyclic voltammograms for ultrasonicated, NAB-modified gold electrodes in a 1 mM ferrocene in acetonitrile with 0.1 M $TBABF_4$ supporting electrolyte. The NAB was deposited using **a)** 2 cycles, **b)** 15 cycles **c)** without any externally applied potentials (spontaneous adsorption). The scan rate is 100 mV/s.

For electrodes modified with a 2-cycle deposition the IRRAS results indicate that approximately 10% of the layer is removed by ultrasonic rinsing. We attribute this to the loss of material that is weakly bound to the substrate. By contrast, approximately 90% of the layer resisted the ultrasonic rinsing. This suggests that most of the material is quite strongly bound to the gold substrate. In addition, the observed ΔE_p value of the sonicated film is significantly reduced from 700 mV to 289 mV, almost to that of an unmodified Au electrode. From this result it is apparent that the blocking capability of the films is significantly reduced after the weakly bound material is removed by ultrasonication.

Films prepared using a 15-cycle deposition display similar results, with 12 % of the material removed via ultrasonication. This result suggests that some weakly-bound material is also present when the number of deposition cycles is increased. The ΔE_p value of the 15-cyle electrode changes from an initially immeasurable value to 253 mV, a result that is comparable to that seen for the 2-cycle electrode. Thus, the blocking ability of the 15-cycle film is perturbed by the ultrasonication rinsing.

The NAB films prepared by SA display the largest change with respect to the amount of material lost during ultrasonication (29 %). In addition to this the films display similar ΔE_p values before and after sonication (293 mV and 288 mV, respectively). The results imply that these films exhibit poor blocking ability initially. In this context, the relatively large amount of material lost from the ultrasonication is insignificant. It is therefore evident that electrodes modified using a SA approach exhibit more loosely bound material than the electrodes modified with electrochemical induction.

The material that does not resist ultrasonic rinsing could be attributed to residual compounds that resist the routine, post-deposition rinsing step. For example it has been

postulated that two generated aryl radicals can couple to form stable dimeric structures in the deposition solution.[15,20,36] These stable organic compounds could subsequently intercalate into the intact layer without actually forming a strong interaction with the substrate. Additionally, such structures may simply physisorb to the gold surface preventing further attachment of NAB groups.

	A_{1347} (A. U.)			ΔE_p (mV)	
	before	after	% loss	before	after
NAB-Au (2 cycles)	0.0078	0.0071	8	700	289
NAB-Au (15 cycles)	0.0090	0.0079	12	immeasureable	253
NAB-Au (SA)	0.0024	0.0017	29	293	288
unmodified Au				280	

Table 2.04. Summary of the IRRAS and electrochemical blocking data for gold electrodes modified with NAB using different deposition conditions before and after ultrasonication. The IRRAS results are averages of two independent measurements.

3.6 Resistance to Displacement via Long-Chain, Alkanethiolates

Long chain, aliphatic thiols, $CH_3(CH_2)_nSH$ ($n \geq 10$), readily self-assemble at gold surfaces from dilute ethanolic solutions to produce stable, densely packed monolayers of adsorbed thiolate structures.[27,37] It is known that short-chain thiolates ($n < 10$) can be displaced by long-chain thiolates.[37] In addition, the formation of thiolate SAMs is governed by the thermodynamic principles of equilibria.[37,38] The stability of the NAB films in the current study can therefore be tested by exposing NAB-modified electrodes to a dilute solution of a long-chain aliphatic thiol for lengthy period of time. By examining whether the NAB groups are displaced by octadecanethiol (ODT) it is possible

to determine whether the interaction responsible for the binding of the NAB groups to the gold is a thermodynamically labile interaction, or is much stronger.

Similar to the previous section, the intensity of the symmetric NO_2 band serves as a measure of the amount of material lost during the displacement process. Results are tabulated in Table 2.05. Also included in Table 2.05, is the wavenumber position of the asymmetric CH_2 stretch mode, $\upsilon_a(CH_2)$, of the alkyl chain portion of the bound thiolate structures. This value serves as a useful diagnostic measurement, as described below. Additionally, IRRAS spectra before and after ODT displacement for a 2-cycle NAB-modified electrode are included in Figure 2.07 and are representative of the entire data set.

	A_{1347} (A. U.)			
	before	after	% loss	$\upsilon_a(CH_2)$ (cm^{-1})
NAB-Au (2 cycles)	0.0069	0.0059	14	2921
NAB-Au (15 cycles)	0.0092	0.0091	1	2921
NAB-Au (SA)	0.0024	0.0021	11	2919
ODT monolayer				2918

Table 2.05. Changes in the intensity of the symmetric NO_2 band for gold electrodes modified with NAB using different deposition conditions before and after immersion in ODT for 24 hours. The results are averages of two independent measurements.

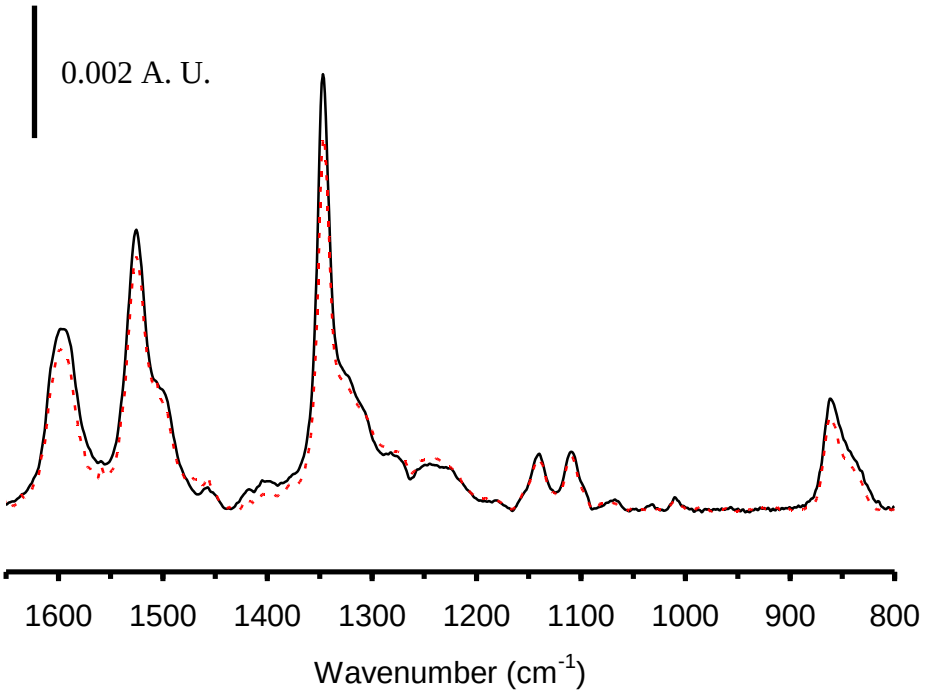

Figure 2.07. IRRAS spectra for nitroazobenzene layers attached to gold using a 2-cycle deposition before (solid) and after (dashed) immersion in 1 mM ODT in ethanol for 24 hr.

The data in Table 2.05 shows that, for all of the modified electrodes, most of the NAB layer remains intact following immersion in ODT for 24 hours. The 2-cycle and SA electrodes experience the largest change, with ~10 % of the material lost in both cases. The electrode modified with 15 cycles shows the largest resistance to displacement, with an observed net change of 1 %. Recall that, for the 15-cycle electrode, more NAB groups are present on the surface initially. This result could be the result of a thicker NAB layer, which reduces the ability of ODT to permeate the film to reach the underlying electrode. In contrast to the ultrasonication results, the electrodes modified with NAB without electrochemical induction display good resistance to displacement by the C_{18} thiolate.

This could mean that the interaction between the SA film and electrode is stronger than a mere physisorption.

The region of the IRRAS spectrum where alkane-type CH stretching occurs also provides useful information. The appearance of C-H stretching bands confirms the presence of adsorbed ODT, presumably as a result of the displacement of some of the NAB groups. Figure 2.08 contains IRRAS spectra of the various substrates in the C-H stretching region. Previous investigations have shown that for SAMs derived from alkanethiols on gold, $\upsilon_a(CH_2)$ is sensitive to the structure adopted by the alkyl chain portion of the monolayer.[27] A $\upsilon_a(CH_2)$ value at 2918 cm^{-1} implies that the alkyl chains are densely packed in an all-trans conformation similar to crystalline polyethylene.[39] Values at higher wavenumbers are indicative of a more disordered, liquid-like arrangement of the alkyl chains. In the case of the SA NAB film, $\upsilon_a(CH_2)$ for the displacing ODT takes on a value of 2919 cm^{-1} which is indicative of a crystalline structure. The observed $\upsilon_a(CH_2)$ value for both the 2-cycle and 15-cycle electrodes is 2921 cm^{-1}. This suggests that, for thiolates that cooperatively exist with NAB films deposited electrochemically, the alkyl-chains take on a more liquid-like structure. A possible explanation for this is that electrochemically deposited NAB films are more compact and only permit binding of thiolates into sparsely distributed defect sites. In contrast, the less compact NAB films deposited via self-assembly permit thiolates to fill-in larger, unmodified regions of the electrode. This is consistent with the electrochemical blocking results presented in Figure 2.04. The large peak intensities observed for the 15-cycle NAB layer could be the result of an orientation effect, whereby the thiolates are held in a position that allows better coupling between dipole transitions involved with the CH stretches and the electric

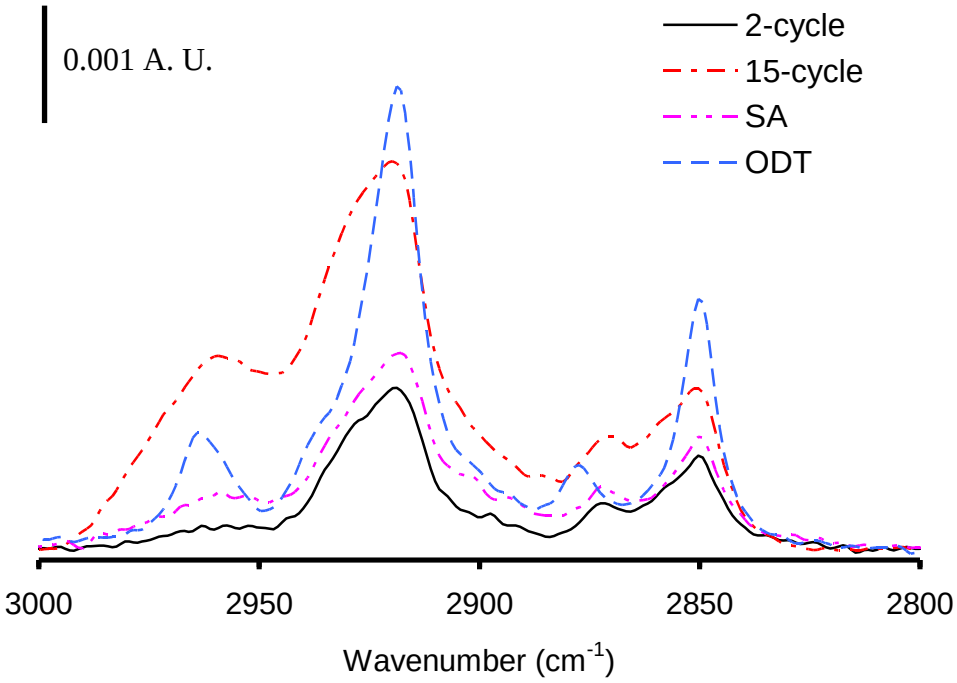

Figure 2.08. IRRAS spectra in the CH stretch region for NAB-modified gold electrodes immersed in an 1 mM ODT solution for 24 hours. The CH stretch region of a SAM of ODT is also shown for comparison.

field component that is normal to the surface.

3.7 Resistance of the NAB Films to Other Treatments

Three other treatments were employed to test the stability of the NAB films. They were: a 1 hour exposure to UV radiation, refluxing in boiling acetonitrile (80 °C) for 1 hour, and cycling an externally applied potential between 0 mV and -1500 mV (vs Ag/AgCl, $KCl_{Sat.}$) *i.e.* to induce reductive desorption. For these experiments only a 2-cycle electrode was investigated. As with the previous sections A_{1347} values measured before and after each treatment are presented. In addition, cyclic voltammetry in 1 mM ferrocene was employed to assess the post-treatment blocking capabilities of the films. The A_{1347} and ΔE_p values are collectively summarized in Table 2.06.

Treatment	A_{1347} (A. U.)			ΔE_p (mV)	
	before	after	% loss	before	after
Reductive Desorption	0.0071	0.0028[a]	61	700[b]	134
UV Irradiation	0.0063	0.0015	76	700[b]	245
Refluxing at 80 °C	0.0062	0.0049	20	700[b]	233
unmodified Au				253	

Table 2.06. Summary of the IRRAS and electrochemical blocking data for 2-cycle NAB-modified electrodes subjected to various treatments. [a]result after 1 complete cycle. [b]value taken from Table 2.03.

I. Refluxing.

When compared to both the ultrasonication and ODT displacement results, the treatments in this study yield a greater effect with respect to the observed change in A_{1347}. The refluxing treatment produced the smallest effect, with only a 20 % decreases in A_{1347}. Assuming this corresponds to a 20 % loss in the amount of NAB at the surface, 80 % of the layer is still intact following the lengthy refluxing. The purpose of performing this measurement was to make a comparison with the thermal stability of SAMs of alkanethiolates on gold, which reportedly is not very good.[37] SAMs of alkanethiolates, although very stable to the ambient, desorb very readily in organic solvents at temperatures over 70 °C. Thus, contrary to alkanethiolates, the NAB films display good overall stability towards refluxing conditions.

With respect to the electrochemical blocking measurement, ΔE_p decreased from 700 mV to 233 mV after refluxing. The barrier properties of the NAB film are therefore lost following the reflux treatment.

II. UV Exposure.

The results in Table 2.06 show that A_{1347} decreases by 80 % after irradiation with UV light. This treatment produced the largest change in A_{1347}. After UV irradiation, the ΔE_p measured from the ferrocene voltammetry is 245 mV. This value is very similar to the value for an unmodified gold electrode, which is not unexpected considering the large change to A_{1347}.

The photooxidative removal of thiolates, RS^-, where R is either an alkane chain or and aromatic group, from a gold surface with UV radiation is well documented.[40,41] The process involves the photooxidation of the thiolate to the corresponding sulfonate.

Sulfonates exhibit a much weaker interaction with the gold surface and are subsequently removed by rinsing with water. Although it is highly speculative at this time, we surmise that, by analogy, the aryl groups of the NAB films are photoxidized to compounds that contain a carbonyl functional group, namely, ether, epoxide, aldehyde, or carboxylate functional groups. A recent study has shown that the surface of single-walled carbon nanotubes (SWNTs) can be photooxidized to these compounds with UV radiation in vacuum.[42]

III. Reductive Desorption.

Alkanethiolates can be electrochemically desorbed from gold substrates in alkaline, aqueous solutions via a 1 e^- reduction of the Au-thiolate moiety.[43] A similar methodology was employed in the current study to determine whether NAB groups could be removed electrochemically, by applying relatively large, negative potentials. A total of 10 voltammetric sweeps from 0 mV to -1500 mV were applied to an electrode derivatized with NAB. In Table 2.06 observe that A_{1347} decreases by 61 % following a single sweep to -1500 mV. IRRAS spectra before and after the application of 1 and 10 voltammetric cycles are presented in Figure 2.09. The applied potentials significantly change the intensity ratios of the NAB bands. This implies that, in addition to the removal of material, the NAB film structure changes significantly. Further, a ΔE_p of 134 mV is measured from the CV in ferrocene. Collectively, these results indicate that large amounts of the film are removed by this procedure, and large regions of bare gold surface are produced.

The CVs obtained during the reductive desorption procedure are presented in Figure 2.10. For the first sweep, the observed electrochemical response is characterized

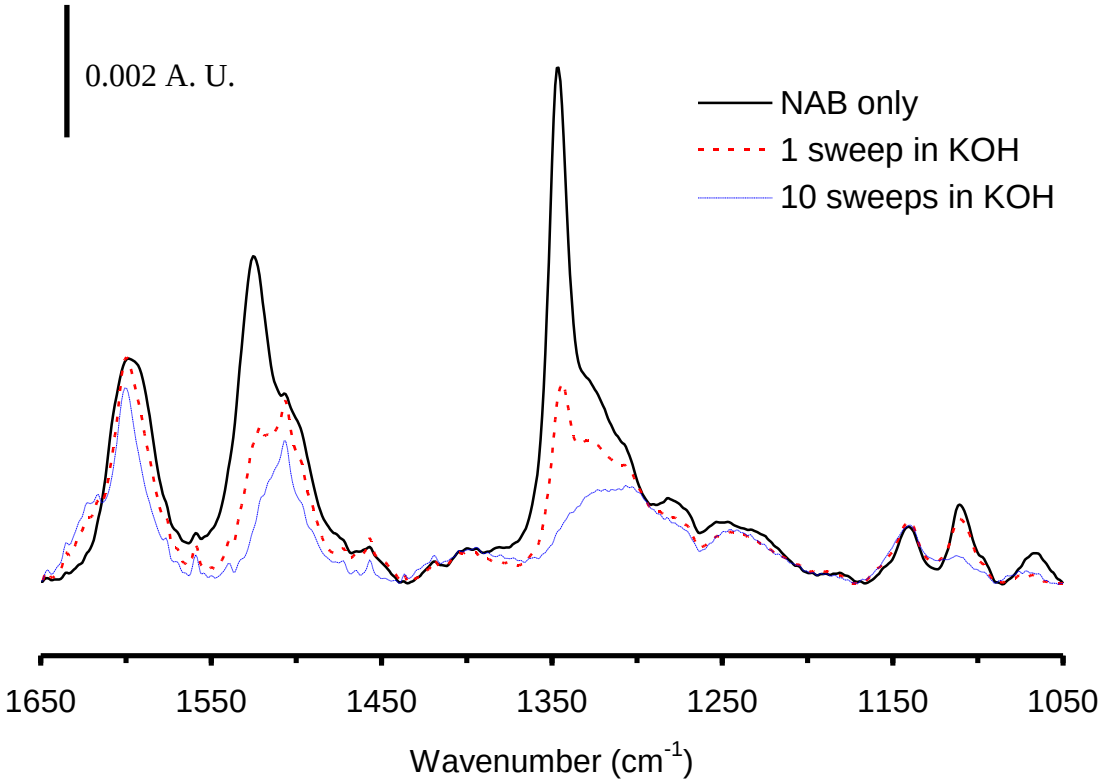

Figure 2.09. IRRAS spectra for an NAB-modified gold electrode before and after the potential was cycled between 0 and -1500 mV in 0.5 M KOH(aq). The same electrode was used in all three spectra.

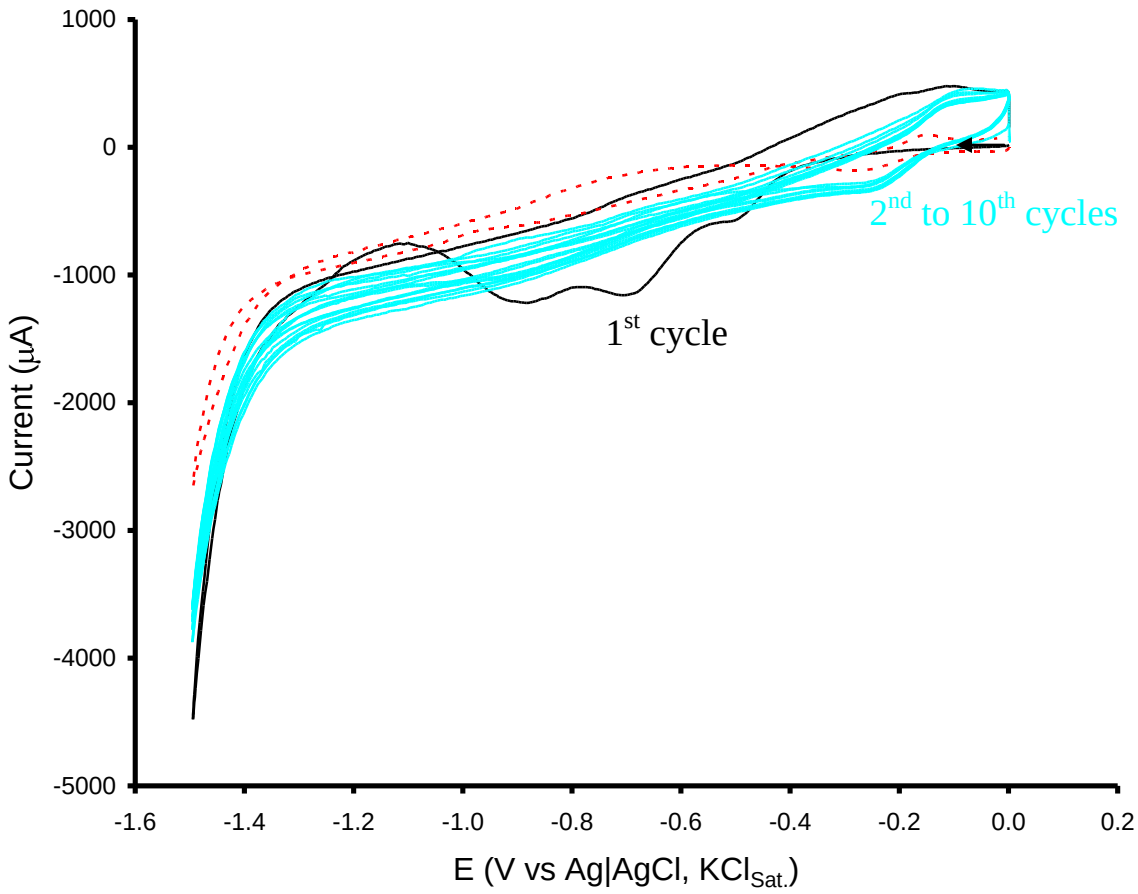

Figure 2.10. Cyclic voltammograms from 0 to -1500 mV for an NAB-modified gold electrode in 0.5 M KOH(aq). The dotted trace is the same experiment but for an unmodified gold electrode. The sweep rate was 25 mV/s.

by three cathodic peaks at -500 mV, -700 mV and -900 mV. The current densities of these peaks are 25, 50, and 40 $\mu A/cm^2$, respectively. No detectable Faradaic current is observed during the reverse scan towards positive potentials. By contrast, for alkanethiolates on gold, reductive desorption is characterized by the appearance of a cathodic peak, the position of which is dependent on the chain length of the R-group; and an anodic peak on the reverse scan. Walczak *et. al.* observed peak current densities of approximately 218 $\mu A/cm^2$ during the reductive desorption of C_{12} alkanethiolate monolayer from a gold surface.[43] Since the current densities are similar, it is possible that a 1 e^- reduction of the aryl moieties occurs, which results in the subsequent removal from the surface. The multiple peaks could correspond to the removal of differently sized fragments of the NAB film, each requiring a specific electrode potential energy for desorption.

4. Conclusions

Films comprised of NAB groups were grafted to evaporated, polycrystalline gold electrodes with and without electrochemical induction. The amount of NAB groups grafted, and the quality of the film, is dependent on the method chosen. For electrochemically deposited NAB films, the number of voltammetric cycles during the deposition can be used to control the amount of NAB grafted and quality of the film.

The electrochemically deposited films are better at blocking electron transfer to ferrocene and are more tightly bound to the gold than films deposited by spontaneous

adsorption. We hypothesize that this is because they are thicker, more compact and characterized by fewer defect sites and pinhole regions.

NAB layers electrochemically grafted to gold are prone to desorption by UV radiation, by externally applied negative potentials; and to some degree, refluxing in organic solvents. Regardless of the deposition method, the NAB films are very resistant to chemical displacement by ODT. None of the treatments used in this study were able to remove the NAB layers completely. In most cases the majority (>50%) of the film resisted the treatments.

References:

(1) Dunker, M. F. W.; Starkey, E. B.; Jenkins, G. L. *Journal of the American Chemical Society* **1936**, *58*, 2308-2309.

(2) Downard, A. J.; Prince, M. J. *Langmuir* **2001**, *17*, 5581-5586.

(3) Delamar, M.; Hitmi, R.; Pinson, J.; Saveant, J. M. *J. Am. Chem. Soc.* **1992**, *114*, 5883-5884.

(4) Saby, C.; Ortiz, B.; Champagne, G. Y.; Belanger, D. *Langmuir* **1997**, *13*, 6805-6813.

(5) Liu, Y. C.; McCreery, R. L. *Journal of the American Chemical Society* **1995**, *117*, 11254-11259.

(6) Kariuki, J. K.; McDermott, M. T. *Langmuir* **1999**, *15*, 6534-6540.

(7) Harper, J. C.; Polsky, R.; Dirk, S. M.; Wheeler, D. R.; Brozik, S. M. *Electroanal.* **2007**, *19*, 1268-1274.

(8) Corgier, B. P.; Li, F.; Blum, L. J.; Marquette, C. A. *Langmuir* **2007**, *23*, 8619-8623.

(9) Liu, G. Z.; Gooding, J. J. *Langmuir* **2006**, *22*, 7421-7430.

(10) Tian, H.; Bergren, A. J.; McCreery, R. L. *Applied Spectroscopy* **2007**, *61*, 1246-1253.

(11) Fave, C.; Leroux, Y.; Trippe, G.; Randriamahazaka, H.; Noel, V.; Lacroix, J. C. *Journal of the American Chemical Society* **2007**, *129*, 1890.

(12) Bernard, M. C.; Chausse, A.; Cabet-Deliry, E.; Chehimi, M. M.; Pinson, J.; Podvorica, F.; Vautrin-Ul, C. *Chem. Mater.* **2003**, *15*, 3450-3462.

(13) Adenier, A.; Bernard, M. C.; Chehimi, M. M.; Cabet-Deliry, E.; Desbat, B.; Fagebaume, O.; Pinson, J.; Podvorica, F. *J. Am. Chem. Soc.* **2001**, *123*, 4541-4549.

(14) Stewart, M. P.; Maya, F.; Kosynkin, D. V.; Dirk, S. M.; Stapleton, J. J.; McGuiness, C. L.; Allara, D. L.; Tour, J. M. *J. Am. Chem. Soc.* **2004**, *126*, 370-378.

(15) Laforgue, A.; Addou, T.; Belanger, D. *Langmuir* **2005**, *21*, 6855-6865.

(16) Boukerma, K.; Chehimi, M. M.; Pinson, J.; Blomfield, C. *Langmuir* **2003**, *19*, 6333-6335.

(17) Hurley, B. L.; McCreery, R. L. *J. Electochem. Soc.* **2004**, *151*, B252-B259.

(18) deVilleneuve, C. H.; Pinson, J.; Bernard, M. C.; Allongue, P. *Journal of Physical Chemistry B* **1997**, *101*, 2415-2420.

(19) Combellas, C.; Kanoufi, F.; Pinson, J.; Podvorica, F. I. *J. Am. Chem. Soc.* **2008**, *130*, 8576.

(20) Allongue, P.; de Villeneuve, C. H.; Cherouvrier, G.; Cortes, R.; Bernard, M. C. *J. Electroanal. Chem.* **2003**, *550*, 161-174.

(21) Allongue, P.; de Villeneuve, C. H.; Pinson, J.; Ozanam, F.; Chazalviel, J. N.; Wallart, X. *Electrochimica Acta* **1998**, *43*, 2791-2798.

(22) Allongue, P.; de Villeneuve, C. H.; Pinson, J. *Electrochimica Acta* **2000**, *45*, 3241-3248.

(23) Simoes, J. A. M.; Beauchamp, J. L. *Chemical Reviews* **1990**, *90*, 629-688.

(24) Vicente, J.; Arcas, A.; Mora, M.; Solans, X.; Fontaltaba, M. *Journal of Organometallic Chemistry* **1986**, *309*, 369-378.

(25) Adenier, A.; Cabet-Deliry, E.; Chausse, A.; Griveau, S.; Mercier, F.; Pinson, J.; Vautrin-Ul, C. *Chem Mater.* **2005**, *17*, 491-501.

(26) Nuzzo, R. G.; Zegarski, B. R.; Dubois, L. H. *J. Am. Chem. Soc.* **1987**, *109*, 733-740.

(27) Porter, M. D.; Bright, T. B.; Allara, D. L.; Chidsey, C. E. D. *J. Am. Chem. Soc.* **1987**, *109*, 3559-3568.

(28) Baranton, S.; Belanger, D. *Journal of Physical Chemistry B* **2005**, *109*, 24401-24410.

(29) Brooksby, P. A.; Downard, A. J. *Langmuir* **2004**, *20*, 5038-5045.

(30) Andrieux, C. P.; Pinson, J. *Journal of the American Chemical Society* **2003**, *125*, 14801-14806.

(31) Delamar, M.; Desarmot, G.; Fagebaume, O.; Hitmi, R.; Pinson, J.; Saveant, J. M. *Carbon* **1997**, *35*, 801-807.

(32) Greenler, R. G. *Journal of Chemical Physics* **1966**, *44*, 310.

(33) Itoh, T.; McCreery, R. L. *Journal of the American Chemical Society* **2002**, *124*, 10894-10902.

(34) Nicholson, R. S. *Analytical Chemistry* **1965**, *37*, 1351-&.

(35) Sabatani, E.; Cohenboulakia, J.; Bruening, M.; Rubinstein, I. *Langmuir* **1993**, *9*, 2974-2981.

(36) Reshetnyak, O. V.; Kozlovs'ka, Z. E.; Koval'chuk, E. P.; Obushak, M. D.; Rak, J.; Blazejowski, J. *Electrochemistry Communications* **2001**, *3*, 1-5.

(37) Bain, C. D.; Troughton, E. B.; Tao, Y. T.; Evall, J.; Whitesides, G. M.; Nuzzo, R. G. *J. Am. Chem. Soc.* **1989**, *111*, 321-335.

(38) Laibinis, P. E.; Nuzzo, R. G.; Whitesides, G. M. *J. Phys. Chem.* **1992**, *96*, 5097-5105.

(39) Snyder, R. G.; Strauss, H. L.; Elliger, C. A. *Journal of Physical Chemistry* **1982**, *86*, 5145-5150.

(40) Tarlov, M. J.; Burgess, D. R. F.; Gillen, G. *Journal of the American Chemical Society* **1993**, *115*, 5305-5306.

(41) Huang, J. Y.; Hemminger, J. C. *Journal of the American Chemical Society* **1993**, *115*, 3342-3343.

(42) Oliveira, L.; Debies, T.; Takacs, G. A. In *Nanotubes, Nanowires, Nanobelts and Nanocoils - Promise, Expectations and Status*; Bandaru, P. R., Grego, S., Kinloch, I., Eds.; Materials Research Society: Warrendale, 2009; Vol. 1142, p 99-104.

(43) Walczak, M. M.; Popenoe, D. D.; Deinhammer, R. S.; Lamp, B. D.; Chung, C. K.; Porter, M. D. *Langmuir* **1991**, *7*, 2687-2693.

Chapter III

Comparison of Diazonium Salt Derived and Thiol Derived Nitrobenzene Layers on Gold*

1. Introduction

Chapter II provided us with useful insights with respect to the structure and stability of diazonium-derived aryl layers at polycrystalline gold surfaces. This chapter expands on this subject providing a direct comparison of the structure and stability of nitrobenzene films derived from diazonium salts with monolayers formed from the corresponding thiol.

The modification of graphitic carbon with aryl groups derived from diazonium salts has become a widely used method to tailor the surface chemistry of this electrochemically useful material.[1-6] The primary advantage of this method is that a covalent bond is formed between the carbon surface and the aryl group, resulting in a tightly bound organic layer. In addition, functionalized diazonium salts are easily prepared from a wide range of commercially available aromatic amines. These films are generally deposited electrochemically and the grafting mechanism is well understood.[1] Briefly, diazonium salts are electrochemically reduced in an appropriate organic solvent

* A form of this chapter has been published in *Langmuir*, **2009**, 25(8), 4556-4563

(usually acetonitrile) at relatively low potentials to produce aryl radicals in the diffusion layer near the electrode surface. Since these radicals are generated in close proximity to the electrode, they react with the surface forming a carbon-carbon bond. The highly reactive radicals produced during this process can also form bonds with aryl groups already attached to the surface, frequently resulting in multilayer films.[7-9] Driven by the strong bonding between the organic layer and the carbon surface, and the diverse molecular structures that can be deposited, these layers are finding applications in composite materials,[10] in bioanalysis,[11,12] for the modification of nanostructures[13] and in molecular electronics.[14]

The irreversible interaction between diazonium derived aryl films and carbon has also led to the application of this method to other materials such as metals[15-17] and semiconductors.[18,19] Relevant to the present work, a growing body of literature reports on the structure and applications of these films on gold surfaces.[16,20-26] Bélanger and coworkers reported the first thorough characterization of diazonium derived films on gold.[25] This work showed that aryl multilayer films form on gold and that the structure and properties of the films depend on the functional group attached to the aryl ring. This study and others[21] have shown that prolonged ultrasonic treatment (sonication) removes a fraction of the multilayer films, but a tightly bound portion of the film remains. In addition, it has been reported that diazonium derived layers on gold electrodes have exhibited little degradation after 2 months storage in laboratory ambient.[22] Taken together, these studies show that tightly bound aryl layers can be can be deposited on gold surfaces by the reduction of the corresponding diazonium salt.

The most widely used method for the modification of gold surfaces has been the formation of self-assembled monolayers (SAM) of thiol or disulfide containing molecules.[27] It is well known that the adsorption of n-alkyl thiols produces monolayers that are highly organized, due to the energetics associated with establishing strong chain-chain interactions that is enabled by a reversible gold-thiolate linkage.[28] Aromatic thiols have also been shown to form ordered monolayers on gold.[29] Despite the many advantages of thiol derived SAMs on gold, the lability of the gold-sulfur interaction that permits self-organization is also the root of some of the limitations of this adsorbate-substrate combination. For example, studies have shown SAMs to be thermally unstable[30] and prone to displacement by other thiols[31] and ambient UV photoxidation.[32] The potential of a carbon-gold covalent bond drives the examination of diazonium derived layers as an alternative to SAMs for applications where extremely stable surface chemistry is required.

In this study we directly compare the structure and stability of diazonium salt derived nitrobenzene films and 4-nitrobenzenethiol monolayers on gold. A structural comparison of the layers formed from these precursors on ZnNi has been recently reported.[33] The structure and thickness of these layers on gold are probed with infrared reflection absorption spectroscopy (IRRAS), X-ray photoelectron spectroscopy (XPS), scanning force microscopy (SFM) and ellipsometry. A side-by-side comparison is presented for the two systems, addressing their relative stabilities towards heated solvents, prolonged ultrasonic treatment (sonication), and substitution reactions with competing thiols. The results of these studies show that diazonium derived films can

form more stable organic coatings for gold under certain conditions relative to thiol analogs.

2. Experimental

Preparation of Gold Substrates. Gold substrates were prepared via thermal evaporation using 99.99% Au shot (Goodfellow). A 6 nm layer of Cr was used in between the glass and gold film to enhance adhesion. For the IRRAS, XPS, ellipsometry, and cyclic voltammetry experiments a gold thickness of 300 nm was deposited onto glass microscope slides. For the AFM studies a 50 nm gold layer was evaporated onto 0211 grade glass diced into square substrates 1.4 cm on a side. All glass substrates and glassware in this study were cleaned using hot piranha solution (1:4 30% H_2O_2:H_2SO_4) followed by thorough rinsing with deionized (18 MΩ)/filtered H_2O (NANOpure™ water purification system, Barnstead International, Dubuque, Iowa). Substrates were blown dry using Ar gas. [*Warning: Piranha solution should be handled with extreme care; it is a strong oxidant and reacts violently with many organic materials. It also presents an explosion danger. All work should be performed under a fume hood*.]

Electrochemical Deposition of the Aryl Films. 4-nitrobenzenediazonium tetrafluoroborate (dNB) (≥97%), tetrabutylammonium tetrafluoroborate ($TBABF_4$) (≥99%) were used as received (Sigma-Aldrich Canada Ltd., Oakville, Ontario). Spectroscopic grade acetonitrile was also used as received (Caledon Laboratories Ltd., Georgetown, Ontario). Prior to surface modification, all gold substrates were subjected to a 10 min cleaning in a Model 42 UVO® commercial ozone cleaner (Jelight Company, Inc., Irvine California). Following the ozone cleaning, the substrates were stirred in

anhydrous ethanol (Commercial Alcohols Inc., Brampton, Ontario) for 10 min. Electrochemical grafting of the aryl layers to the gold substrates was achieved by cyclic voltammetry using a software controlled Model AFCBP1 bipotentiostat (Pine Instrument Company, Grove City, Pennsylvania). For all non-aqueous electrochemistry the reference electrode consisted of a silver wire submerged in a 200 mM $AgNO_3$ solution in acetonitrile with 0.1 M $TBABF_4$. A platinum wire/platinum mesh assembly with adequate surface area served as a counter electrode. Unless otherwise stated, all electrochemical depositions were carried out using two full sweeps from +100 mV to -700 mV at a sweep rate of 200 mV/s, and a diazonium salt concentration of 2.5 mM in acetonitrile with 0.1 M $TBABF_4$. These conditions were chosen because they resulted in a final film with electrochemical barrier properties similar to the 4-nitrobenzenethiol monolayer. Diazonium salt solutions were deaerated for 10 min with Ar gas prior to all depositions. Following the modification, samples were thoroughly rinsed with acetonitrile, blown dry with a gentle stream of Ar gas, and used immediately with minimum exposure to the ambient.

Preparation of Au-thiolate monolayers / ODT Displacement Reactions. 4-nitrobenzenethiol (98 %) and octadecanethiol (ODT, 98%) were used as received (Sigma-Aldrich Canada Ltd.). Cleaned gold substrates were immersed in 1 mM 4-nitrobenzenethiol (tNB) in ethanol. All solutions were deaerated with Ar gas for 10 min prior to the self-assembly process. For the ODT displacement studies, a previously modified gold slide was directly immersed into a 1mM ODT solution (ethanol) for 24 h.

IRRAS. IRRAS spectra were collected using an ATI Mattson Infinity Series Fourier transform infrared (FTIR) spectrometer equipped with a liquid nitrogen cooled mercury-

cadmium telluride (MCT) detector. The p-polarized IR beam was incident on the gold surface at an angle of 80° with respect to the surface normal. A total of 1500 scans were averaged for each experiment at a resolution of 4 cm^{-1}. The interferograms were Fourier transformed using triangular apodization. A gold slide modified with a SAM of $CD_3(CD_2)_{16}CD_2$-SH was used as a reference.

Electrochemical Blocking Studies. Potassium ferrocyanide (≥99%) (BDH Chemicals Ltd., Poole, England), and Potassium Chloride (≥99%) (Fisher Scientific International, Hampton, New Hampshire) were used as received. All aqueous solutions were prepared by dilution with 18 MΩ deionized H_2O, and bubbled with Ar for 10 min prior to the analysis. A 3-necked inverted electrochemical cell was clamped to a modified/unmodified electrode surface with a solvent resistant, Viton o-ring (6 mm diameter) in between to define the electrode area of 0.28 cm^2. Potentials were measured with respect to an Ag/AgCl (saturated KCl) reference electrode using the same counter electrode described above.

XPS Analysis. XPS analysis were performed using an AXIS Ultra Spectrometer (Kratos Analytical). A monochromated Al Kα source (hν = 1486.6 eV) was employed at a power of 210 W. Samples were placed in the analytical chamber no longer than 20 minutes following the deposition of the film of interest. The analytical chamber was evacuated to a base pressure lower than 4 x 10^{-8} Pa for all experiments. The hemispherical analyzer was operated in fixed analyzer transmission (FAT) mode with a spot size set at 700 x 400 um. Charge neutralization was not utilized during any of the scans. High resolution scans for N1s and S2p peak analysis were collected using a pass energy of 20 eV and a 0.1 eV step size. We restricted our spectral collection to 40 scans for the high-resolution data to

prevent any x-ray induced transformations of the surface. All spectra were referenced to the Au $4f_{7/2}$ electron (binding energy, BE = 84 eV).

AFM measurements. The thickness of the dNB films was determined with AFM by a method described previously.[7] A region of a freshly prepared dNB modified gold electrode was first imaged using tapping mode AFM so as not to disrupt the layer. Without changing the AFM tip, the instrument was then engaged in contact mode. Precise control over the engagement setpoint was exercised to carefully scratch through the layer as the tip was raster scanned over the surface. The surface was subsequently imaged in tapping mode to obtain height information and ultimately film thickness measurements for the modified electrodes.

A control experiment was performed to ensure that the contact forces used were insufficient to damage the gold surface, which would certainly introduce an error when making the film thickness measurements. The experiment was performed on a bare, unmodified gold substrate using the same force as for the thickness measurements. The results showed evidence that the surface was slightly perturbed, and the difference in height between the ploughed and non-ploughed region was negligible.

The AFM experiments were performed using a Nanoscope III Multimode microscope (Digital Instruments, Santa Barbara, CA). Rectangular Si cantilevers with a thin, reflective Al coating (Olympus, Tokyo, Japan) were employed for both contact mode and tapping mode experiments. The force constant of the cantilevers was 40 N/m. The oscillation frequency used for tapping mode was 300 ± 10 kHz. A contact force of 400 nN was used for all contact mode experiments which corresponded to a setpoint of 0.1 V. The normal force, F_N, was determined using the relation:

$$F_N = k \times \left[\frac{V_s - V_b}{s} \right] \quad [1]$$

where V_s is the setpoint voltage used for imaging, V_b is the voltage required to break the tip away from the surface, s is the optical sensitivity of the cantilever to bending and is equal to 0.01 V/nm, and k is the force constant of the cantilever.

Spectroscopic Ellipsometry. Films were characterized via ellipsometry on a variable angle spectroscopic ellipsometer (V-VASE, J.A. Woollam Co., Inc.). All measurements were performed in reflection mode with a spot size of a few hundred micrometers. Data collection and modeling was performed using the software provided by the instrument manufacturer (WVASE32 version 3.486, J.A. Woollam Co., Inc.). For a bare Au substrate the real, n, and imaginary, k, coefficients of the complex refractive index, Ñ, where Ñ = n + k*i*, were first determined, point by point, using a two phase parallel layer model.[34] The ellipsometric parameters Ψ and Δ were measured from 300-800 nm in 5 nm intervals and from 30°-60° every 5° to the surface normal. The measurements were then repeated for a modified gold electrode using the same intervals. Using the predetermined n and k values for the gold substrate, a 3 phase parallel layer model was employed to model the optical characteristics of the modified electrodes. A two-term Cauchy dispersion function was used to describe the film layer. The experimentally determined Ψ and Δ values were checked against the modeled values using a mean square error (MSE) merit function.

3. Results and Discussion

3.1 Characterization of NB layers on gold.

The nitrobenzene (NB) layers in this study were adsorbed to thin gold films (200 nm) thermally evaporated on glass substrates. Gold films prepared in this way can be described as polycrystalline. Thiol derived NB monolayers (tNB) were spontaneously adsorbed from ethanolic solutions. Diazonium derived films (dNB) were electrochemically deposited by cyclic voltammetry. Two sweeps at 200 mV/s were used to deposit NB films from 2.5 mM solutions of nitrobenzene diazonium salt. A typical set of deposition voltammograms is presented in Figure 3.01. During the first sweep a large, broad cathodic wave is observed associated with the reduction of the diazonium group to produce aryl radicals. Under these conditions, the second, subsequent voltammetric sweep exhibits negligible Faradaic current, due to the passivating nature of the deposited NB film. In addition, these conditions also resulted in films with similar electrochemical barrier properties as the tNB monolayers (*vide infra*). The voltammetry of nitrobenzene diazonium cations at our thin film gold substrates is qualitatively similar to that observed on both carbon[1,6] and gold[16,25] electrodes, implying the formation of a NB film on the surface.

IRRAS provides useful structural information on thin organic films on gold surfaces[28] and has been used to characterize diazonium derived layers on a variety of metal surfaces.[16,23] Figure 3.02 contains IRRAS spectra in the fingerprint region for gold substrates modified with both a tNB monolayer (bottom spectrum) and a dNB film (top spectrum). The prominent bands and their assignments are listed in Table 3.01. The top spectrum in Figure 3.02 is similar to those in a previous IRRAS study of dNB on gold[23] and confirms the formation of a diazonium derived NB film. Figure 3.03 contains

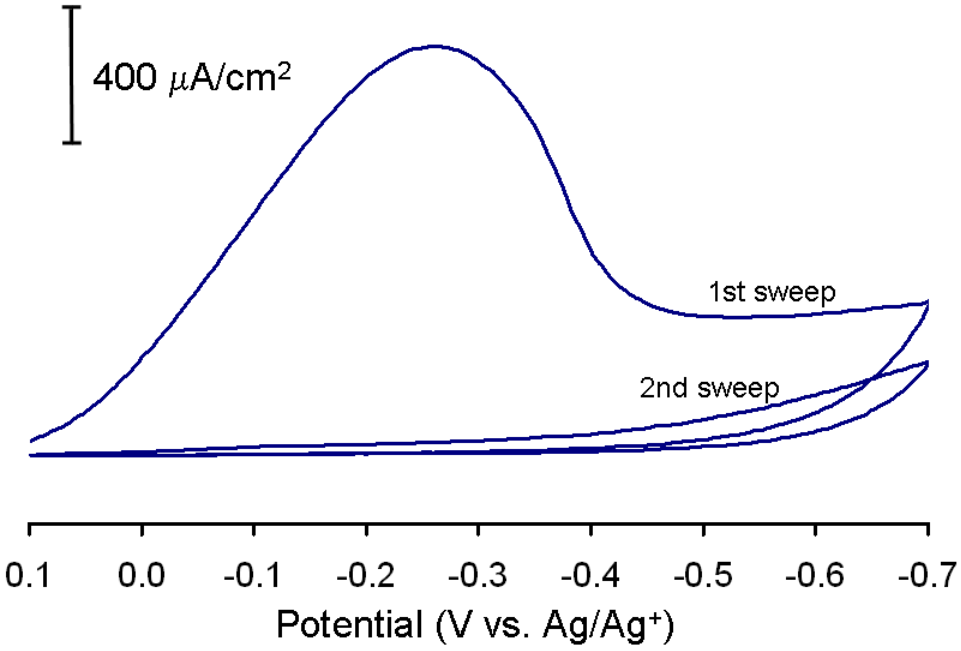

Figure 3.01. Cyclic voltammogram of 2.5 mM nitrobenzene diazonium salt in 0.1 M $TBABF_4$ in acetonitrile. The sweep rate is 200 mV/s.

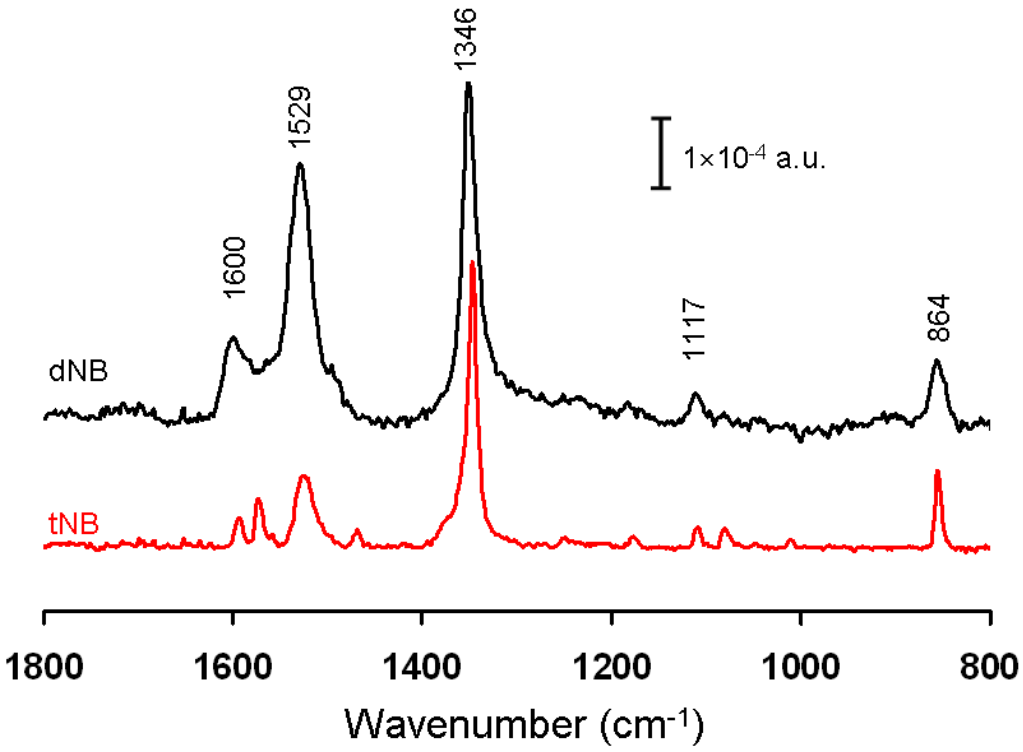

Figure 3.02. IRRAS spectra of a diazonium salt derived nitrobenzene (dNB) film and nitrobenzene thiol (tNB) monolayer on gold. Band assignments are given in Table 3.01.

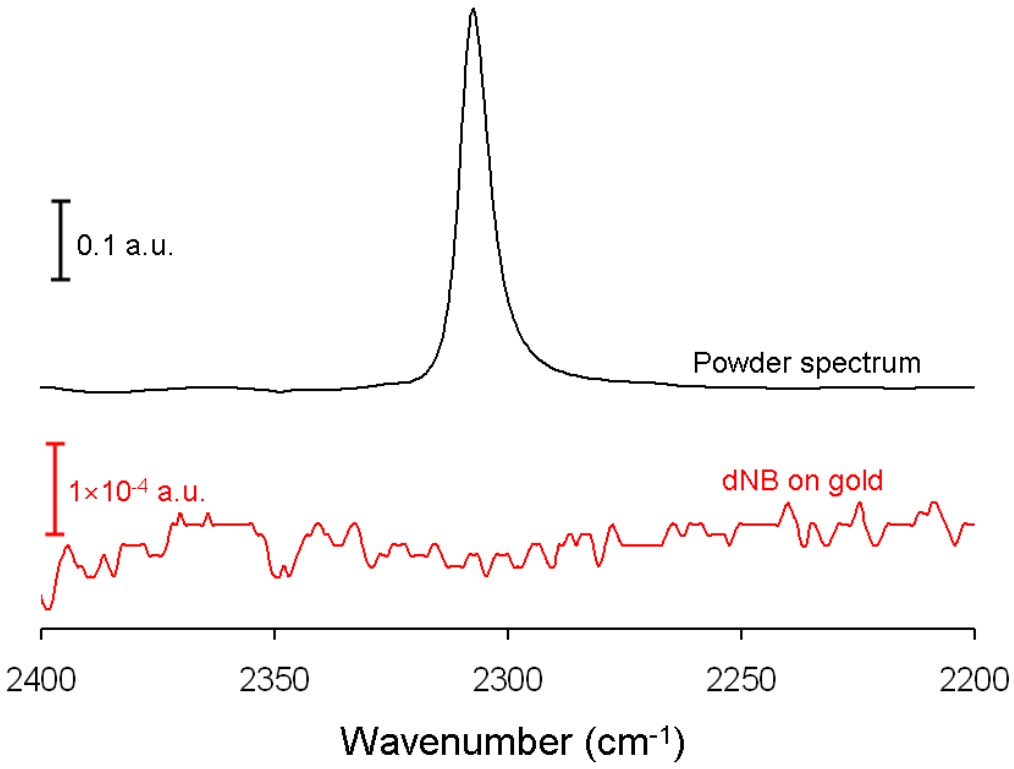

Figure 3.03. Top: IR spectrum of solid phase nitrobenzene diazonium salt. Bottom: IRRAS spectrum of a dNB film on gold.

dNB		
Position (cm^{-1})	Absorbance[1] (10^{-3} a. u.)	Assignment
1600	1.3	C=C aromatic ring stretch
1529	3.8	Asymmetric NO_2 stretch ($\nu_{a,NO2}$)
1346	5.1	Symmetric NO_2 stretch ($\nu_{s,NO2}$)
1117	0.38	Aromatic C-H in plane bending
864	1.1	C-N stretch or aromatic C-H
tNB		
1593	0.64	C=C aromatic ring stretch
1523	1.1	Asymmetric NO_2 stretch ($\nu_{a,NO2}$)
1346	4.6	Symmetric NO_2 stretch ($\nu_{s,NO2}$)
1109	0.39	Aromatic C-H in plane bending
860	1.2	C-N stretch or aromatic C-H oop

1. Absorbance values are the mean of at least two different spectra.
2. oop = out of plane

Table 3.01. Band positions, intensities and assignments for the IRRAS spectra of NB layers from Figure 3.02. All assignments are from reference,[35] unless otherwise noted.

IRRAS spectra that show the diazonium derived NB film is composed of aryl moieties and not physisorbed diazonium cations. The top spectrum in Figure 3.03 was collected from a powder sample of the nitrobenzene diazonium salt starting material. The prominent band at 2300 cm^{-1} is assigned to the N-N stretch of the diazonium functional group. The lower spectrum in Figure 3.03 was collected for a dNB film on gold. No evidence of the diazonium group is present in the IRRAS spectrum, consistent with a film comprised of molecules that underwent complete reduction to form aryl radicals during the electrochemical deposition procedure.

Qualitatively, the spectra for the dNB film and the tNB monolayer in Figure 3.02 are similar, displaying similar bands for the main observable vibrations (Table 3.01). The intensity of the most pronounced bands, specifically the asymmetric ($\nu_{a,NO2}$) and symmetric ($\nu_{s,NO2}$) NO_2 stretches, is higher for the dNB film relative to the tNB monolayer. It is well known that diazonium cation reduction at both carbon[7,9] and gold[21,25] electrodes can result in the formation of aryl multilayers. A previous IRRAS study of electrochemically deposited dNB films on gold correlated band intensity to multilayer formation.[36] Film thickness measurements confirm the formation of NB multilayers under the deposition conditions used here (*vide infra*). Thus, although the intensity of IRRAS bands are known to depend on the orientation of adsorbed molecules, due to the surface selection rule, the higher observed absorbance of bands for dNB films is attributed to multilayer formation. The variation in the absorbance of the $\nu_{a,NO2}$ bands for each film type listed in Table 3.01 is especially noteworthy. The surface selection rule for IRRAS predicts a lower absorbance for dipole moment changes that are parallel

to the surface. Assuming that the tNB monolayer is comprised of NB molecules absorbed with their C_2 axis perpendicular to the surface, the main component of the asymmetric NO_2 vibration will be parallel to the surface. In this case, the intensity of the $\nu_{a,NO2}$ band is expected to be low, which is what we (Table 3.01) and others observe.[37] A multilayer dNB structure likely contains NO_2 groups in a variety of orientations that should result in an absorbance ratio of $\nu_{s,NO2}/\nu_{a,NO2}$ similar to that of bulk NB. From the data in Table 3.01, this ratio for dNB films on gold is 1.3 and that of bulk NB is 1.2.[38] Thus, the relative absorbances of the IRRAS bands are consistent with what is known about the structure of tNB monolayers and dNB multilayer films.

The thickness of dNB films deposited under the conditions employed here was evaluated with scanning force microscopy (SFM) and ellipsometry (see the Experimental section for details). Figure 3.04 shows a tapping mode AFM image collected following the scratching step. A cross sectional profile was used to measure the thickness of the layer. The results of these characterizations are listed in Table 3.02. The SFM measurement was similar to that originally demonstrated by Anariba et al.[7] Variable angle spectroscopic ellipsometry (VASE) was also used to measure the thickness of the dNB films. In comparison to the SFM method, the size of the analysis area for the VASE measurement is roughly 2 mm diameter and can be considered an average measurement. The values from the two measurements listed in Table 3.02 are slightly different, but are statistically similar at the 95% confidence level. Also listed in Table 3.02 is the thickness of a spontaneously adsorbed tNB layer taken from a recent report.[39] This same study also employed angle resolved X-ray photoelectron spectroscopy (XPS) to measure a thickness of 0.6 ± 0.2 nm for the tNB films. It is well-known that the adsorption of aromatic thiols

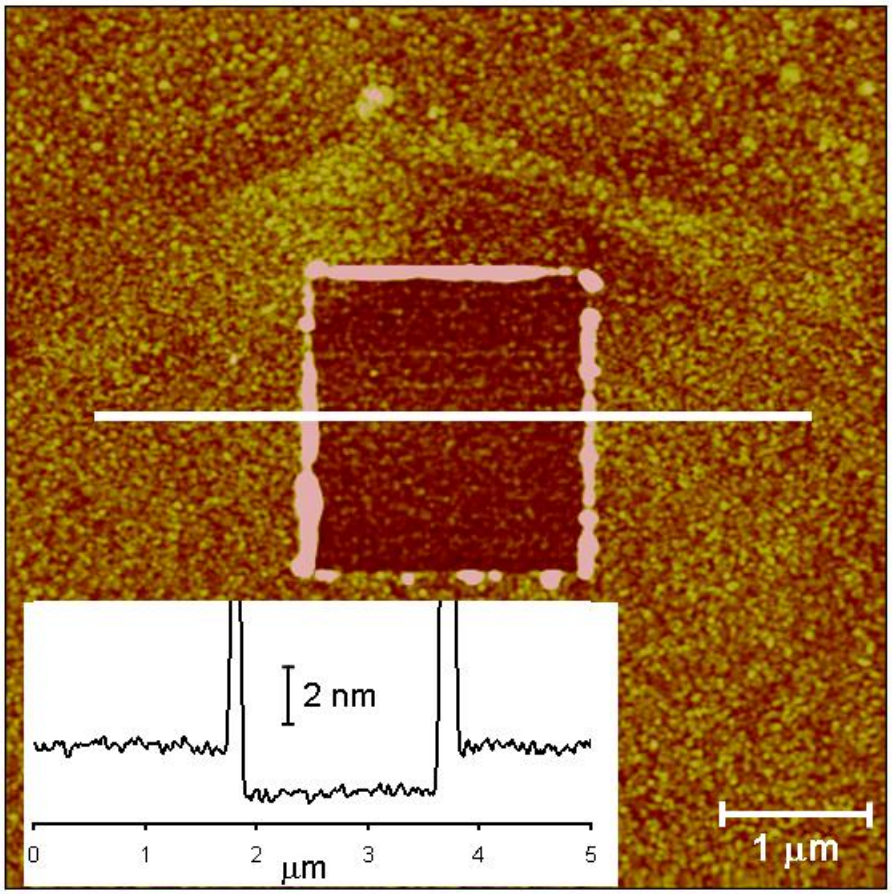

Figure 3.04. AFM image (5 × 5 μm, z-scale = 6 nm) of a region of a dNB film on gold after scratching. Inset is the cross-sectional profile through the scratched region.

Layer	SFM	Ellipsometry
dNB	1.8 ± 0.2 nm[a]	2.3 ± 0.3 nm[b]
tNB		0.9 nm[c]

a. Mean value from nine measurements on three different samples (3 per sample).
b. Mean value from three different samples
c. Value taken from reference [39]

Table 3.02. Thickness measurements of NB layers on gold.

form single, monomolecular layers on gold and thus, we take the thickness of a closely packed monolayer of NB to be in the range of 0.6 to 0.9 nm. Based on the IRRAS results discussed above and the results in Table 3.02, we conclude that the dNB layers formed on gold under our conditions are multilayers and are between 2 and 3 layers thick.

The conditions for the deposition of the dNB films were chosen based on their ability to act as an electrochemical barrier, as noted above. That is, conditions were chosen that produced a final film structure that blocked electron transfer to a similar extent as the tNB monolayers (*vide infra* and Table 3.03). It is clear from the results in Table 3.02 that these conditions produce multilayers. It has been shown that through careful control of the charge passed during deposition, a monolayer of diazonium derived aryl groups can be formed on Si(111).[40] Recently, monolayers on metal surfaces, including gold, have been demonstrated by using precursor diazonium cations functionalized to prevent multilayer formation.[41] Our attempts to deposit dNB layers under conditions that produce fewer radicals (e.g., lower concentration of nitrobenzene

diazonium cations) and thus limit the coupling reactions that form multilayers resulted in loosely packed layers that exhibited poor electron transfer blocking.

Differences in composition between dNB and tNB films on gold were assessed with XPS, which has been used extensively to study the structure of diazonium derived films, including dNB.[25,42] To our knowledge, this is the first time XPS spectra for diazonium and thiol analogs have been compared. High-resolution XPS spectra in the N 1s and S 2p regions for gold electrodes modified with dNB and tNB films were collected. The spectra of an unmodified gold substrate were also collected for comparison. The S 2p XPS results are presented in Figure 3.05. The observations for the S 2p region are as expected. The tNB samples produce a peak in the S 2p region of the spectrum, with no observable S signal for the dNB films. The spectra in the N 1s region are shown in Figure 3.06 and reveal significant differences between the two films. For the dNB films two peaks are observed in Figure 3.06; one at 405.7 eV and another at 400 eV. A single N 1s peak is observed for the tNB modified electrodes at 405.5 eV. The peaks at ~405 eV are diagnostic of the nitrogen atom of the nitro group.[42] For the dNB films a second N 1s peak is observed at a lower binding energy of 400 eV. The lower binding energy implies that the corresponding nitrogen is present in a reduced oxidation state. The origin of this reduced nitrogen peak has been previously discussed in the literature.[25,42] One study has shown evidence for X-ray radiation induced reduction of an aromatic nitro group to an amine on SiO_2 surfaces.[43] Vautrin and coworkers carried out studies to show this is a real possibility for diazonium derived aryl layers spontaneously adsorbed to zinc surfaces.[42] If the reduced nitrogen species is the result of the x-ray irradiation, we would

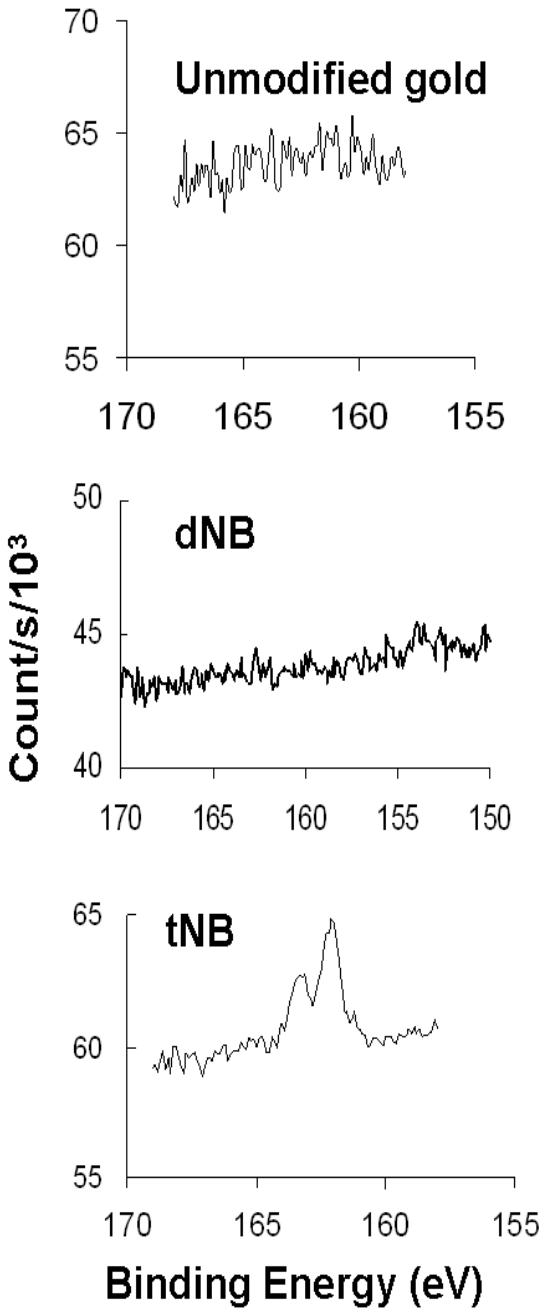

Figure 3.05. High resolution XPS spectra in the S 2p region.

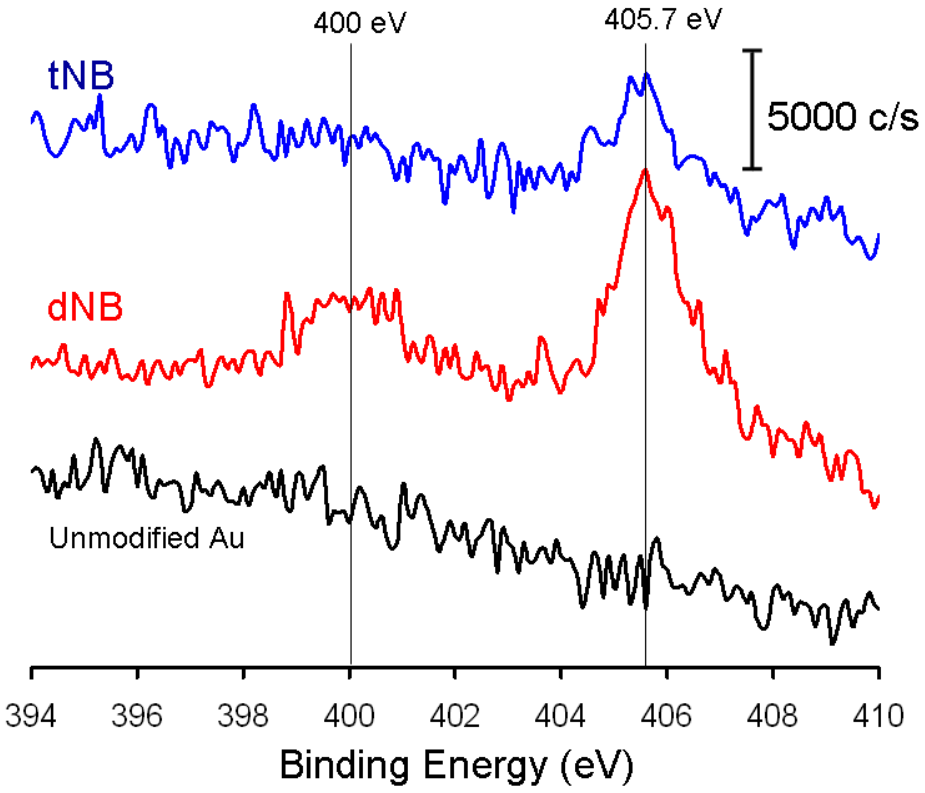

Figure 3.06. XPS spectra in the N 1s region of a tNB monolayer, a dNB film and an unmodified gold substrate.

expect to observe this reaction at both dNB and tNB layers. The lack of the signature for the reduced nitrogen in Figure 3.06 implies that under the XPS conditions employed here, there is little X-ray induced transformation of $-NO_2$ to a more reduced form.

Another proposal suggests that the reduced nitrogen arises from azo linkages throughout the multilayered network of phenyl rings comprising the film.[25,42,44,45] The initial hypothesis for the existence of this functional group was based on XPS results.[25,42,45] A recent report provides strong evidence based on secondary ion mass spectrometry experiments that azo groups exist in diazonium derived aryl layers.[44] This report proposes azo –N=N- linkages between phenyl rings in the multilayer structure and a carbon covalent bond to the surface. In Figure 3.06, the XPS signal for a reduced nitrogen species at 400 eV is only observed for the dNB film. The absence of this signal is expected for the tNB monolayer based on what is known about the adsorption of aromatic thiols. In addition, we have observed a distinct vibration for an N=N stretch in surface enhanced Raman spectra (SERS) of diazonium derived layers on gold and silver.[46] Based on the collection of these findings, we assign the observed peak at 400 eV in Figure 3.06 to a reduced nitrogen species in azo linkages within the dNB film on gold. In summary, the results above indicate that the electrochemical reduction of nitrobenzene diazonium cations at gold electrodes under the conditions used here results in a multilayer NB film that is ~3× thicker than a monolayer formed from the spontaneous adsorption of 4-nitrobenzene thiol.

3.2 Stability of dNB and tNB films on gold.

The stability of dNB films on gold was compared to that of tNB by subjecting the films to three different treatments; heating in refluxing acetonitrile (78 °C) for 1 hour, sonication for 30 min. in the solvent used to generate the film (i.e. acetonitrile for the dNB films, ethanol for the tNB films), and immersion in a 1 mM solution of ethanolic octadecanethiol (ODT) for 24 hours. Changes in the film were monitored by IRRAS and by electrochemical blocking. We used the absorbance of the $\nu_{s,NO2}$ band ($A_{s,NO2}$) at 1346 cm^{-1} (see Figure 3.02) as a semi-quantitative diagnostic of film coverage. Our assumption is that changes in $A_{s,NO2}$ are primarily due to the loss of NB groups from the surface, with some contribution due to treatment induced re-orientation of surface dipole moments, as per the IRRAS surface selection rule. The absorbance ratios of various bands (e.g., $\nu_{s,NO2}/\nu_{C=C}$ and $\nu_{a,NO2}/\nu_{C=C}$) remain unchanged before and after treatment providing support for this assumption. Brooksby and Downard have reported that the thickness of diazonium derived nitroazobenzene (NAB) multilayer films reversibly change when the film is exposed to different solvents. The NAB films swell when exposed to acetonitrile and compact when exposed to aqueous acid solutions.[47] Changes in the orientation of molecular dipole moments of an adsorbed film would be expected to accompany a swelling/de-swelling process. The diazonium-derived films in this study are exposed only to acetonitrile, which should negate solvent effects.

The uncertainty in the measurement of $A_{s,NO2}$ was evaluated for dNB and tNB films to ensure the validity of using this parameter as a quantitative diagnostic. First, the

IRRAS spectrum of the same sample was collected at three different locations. The percent relative standard deviation (%RSD) in $A_{s,NO2}$ was 3% and 1% for dNB and tNB films, respectively. The sample to sample variability in $A_{s,NO2}$ was also evaluated. The %RSD in $A_{s,NO2}$ for 6 independent samples was 5% and 7% respectively for dNB and tNB. We conclude that $A_{s,NO2}$ measurements are very reproducible within the same sample and display good reproducibility from sample to sample.

Variations in film density were evaluated by measuring the "through-film" electron transfer characteristics of the modified gold substrates. This type of measurement is used extensively for the characterization of diazonium derived layers.[21,22,25] Typically, cyclic voltammetry of a common redox probe, such as $Fe(CN)_6^{3/4-}$, is employed to evaluate the blocking properties of the diazonium derived layer. The magnitude of the cathodic-anodic peak separation (ΔE_p) is a measure of the electron transfer rate through the film with a lower value of ΔE_p and lower peak current being characteristic of facile electron transfer indicative of a disordered, defective organic film. Higher values of ΔE_p correspond to a compact, well insulating, pinhole-free overlayer.

An example of a data set illustrating the effect of refluxing a dNB sample in acetonitrile is shown in Figure 3.07. The top panel of Figure 3.07 contains the IRRAS spectra of the dNB film before and after the treatment. A significant decrease in all band intensities is observed as a result of this treatment. The bottom panel of Figure 3.07 is the cyclic voltammetric analysis of dNB films. Also shown is the voltammetry of $Fe(CN)_6^{4-}$ on an unmodified gold film electrode, which exhibits a ΔE_p of 165 mV for a

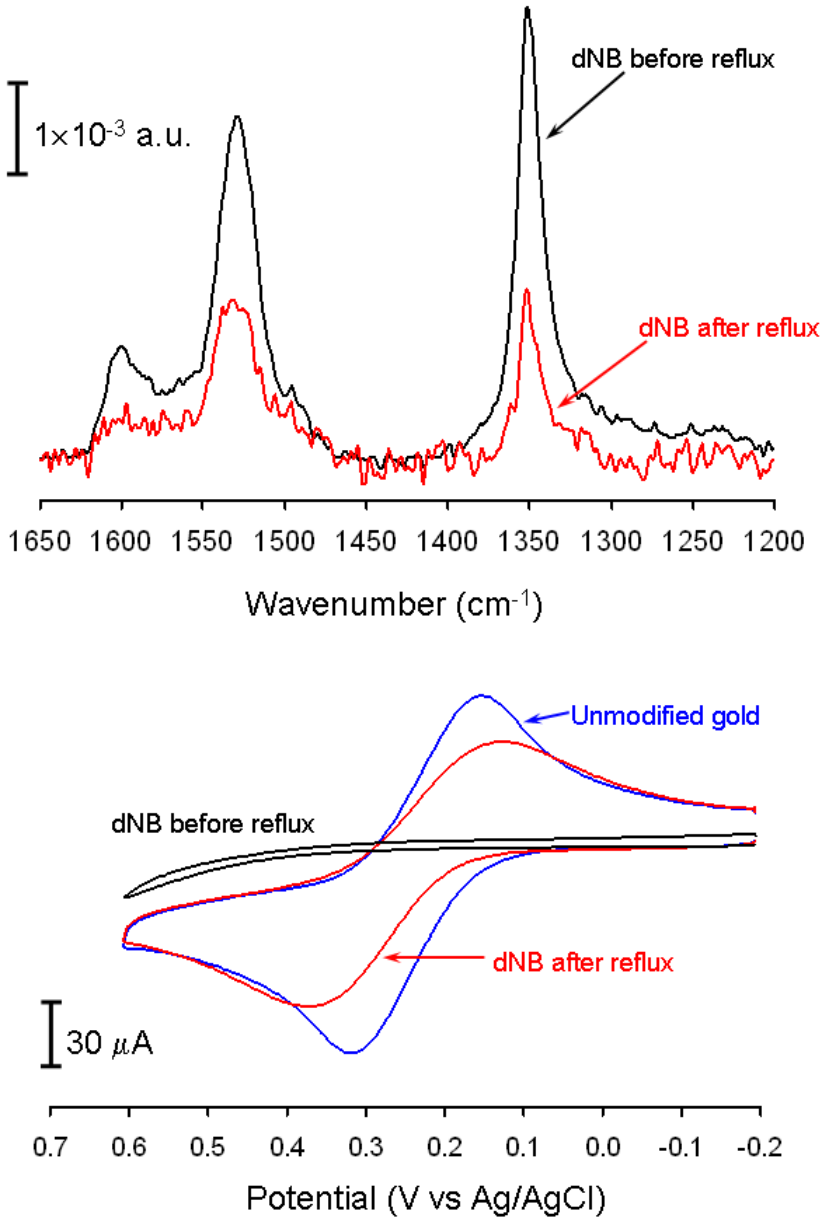

Figure 3.07. Top: IRRAS spectra of a dNB film on gold before and after exposure to refluxing acetonitrile. Bottom: Cyclic voltammetry of 1 mM $Fe(CN)_6^{4-}$ (1 M KCl) at a dNB film on gold before and after the reflux treatment and at an unmodified gold substrate. For all voltammograms, the sweep rate is 100 mV/s.

scan rate of 100 mV/s. The as-prepared, lightly rinsed dNB film completely blocks electron transfer for $Fe(CN)_6^{4-}$ in the 800 mV potential window probed, indicating that the dNB films are initially densely packed and pin-hole free. In previous studies, considerably more facile electron transfer for $Fe(CN)_6^{3/4-}$ was observed through films of carboxyphenyl (CP) [22,25] and dNB[25] on gold. In another report, films of CP and methyphenyl groups on gold blocked $Fe(CN)_6^{3-/4-}$ electron transfer completely.[21] The discrepancy in these results illustrates the lab-to-lab variability of the structure and properties of these films. The cyclic voltammetry in Figure 3.07 reveals that the dNB film is a much poorer barrier to electron transfer following refluxing in acetonitrile. Comparison to the voltammogram at unmodified Au indicates that a sufficient amount of material in the dNB layer survives the reflux treatment to block electron transfer to a moderate degree, consistent with the IRRAS results.

The results summarizing data sets such as that shown in Figure 3.07 for all the treatments are listed in Table 3.03. Values of $A_{s,NO2}$ for a single representative sample, before and after the treatment, are shown. In all cases, $A_{s,NO2}$ is lower after the treatment, which we interpret to be primarily due to the loss of NB molecules from the surface. The amount of material lost is represented by %Loss, and the values listed are the average of at least 2 samples. The ΔE_p values for $Fe(CN)_6^{3/4-}$, before and after the heating and sonication treatments are also provided. Based on the $A_{s,NO2}$ values, the initial dNB films contain 13-15% more NO_2 groups than the self-assembled tNB monolayers. This is inconsistent with the thickness measurements presented in Table 3.02 where, based on a simple multilayer model, we would expect the $A_{s,NO2}$ values of as-prepared dNB films to be 2-3 times that for tNB monolayers. The IRRAS selection rule likely accounts for a

	Absorbance $\nu_{s,\,NO2}$			ΔE_p (mV)	
	Before	After	%Loss[a]	Before	After
dNB (reflux)	0.0052	0.0021	64	> 800	242
tNB (reflux)	0.0045	0.0024	48	> 800	517
dNB (sonic)	0.0054	0.0035	35	> 800	518
tNB (sonic)	0.0046	0.0039	8	> 800	625
dNB (ODT)	0.0046	0.0016	73	NA	NA
tNB (ODT)	0.0039	0	100	NA	NA
Unmodified Au				165	

[a] %Loss = $[A_{s,NO2}(\text{before})-A_{s,NO2}(\text{after})]/A_{s,NO2}(\text{before})\times 100$. %Loss results listed are the mean for at least two independent samples. NA = not measured.

Table 3.03. IRRAS and electrochemical blocking results for NB films subjected to the various treatments.

fraction of the discrepancy. While computational analysis indicates an upright orientation is preferred for aryl groups bound to Au(111),[48] the orientation of the C_2 axis of nitrobenzene molecules in the second and third layer of the dNB film will not be perpendicular to the surface. Both as-prepared, and rinsed films completely block electron transfer to $Fe(CN)_6^{3/4-}$ in the potential window investigated. Taken together, these findings are consistent with a dNB film structure consisting of a partial monolayer of NB molecules bound to the gold with additional NB molecules either bound or adsorbed in such a way as to block access to the exposed regions of the gold.

The results in Table 3.03 show that both the reflux and sonication treatments remove more material from the dNB layer compared to the tNB monolayer. In three cases, the layers that survive these treatments contain a sufficient amount of material to provide a significant barrier to electron transfer, as indicated by ΔE_p values >500 mV. Refluxing dNB layers in acetonitrile lowers the $A_{s,NO2}$ signal by 64% and results is a layer that exhibits a ΔE_p for $Fe(CN)_6^{3/4-}$ only slightly larger than the unmodified gold electrode. Based upon the amount of material removed, it appears that the tNB monolayers are more stable to the refluxing and sonication treatments than the dNB films. However, a significant amount of the dNB film resists both treatments.

It is known that long chain alkylthiols will displace shorter chains due to the thermodynamic control of the formation of SAMs.[49,50] As another test of stability, we exposed both NB layers to an ethanolic solution to ODT for extended periods of time. The IRRAS results in Figure 3.08 show the effect of ODT displacement on dNB and tNB layers. The NO_2 stretching region reveals that while ODT displaces a significant amount

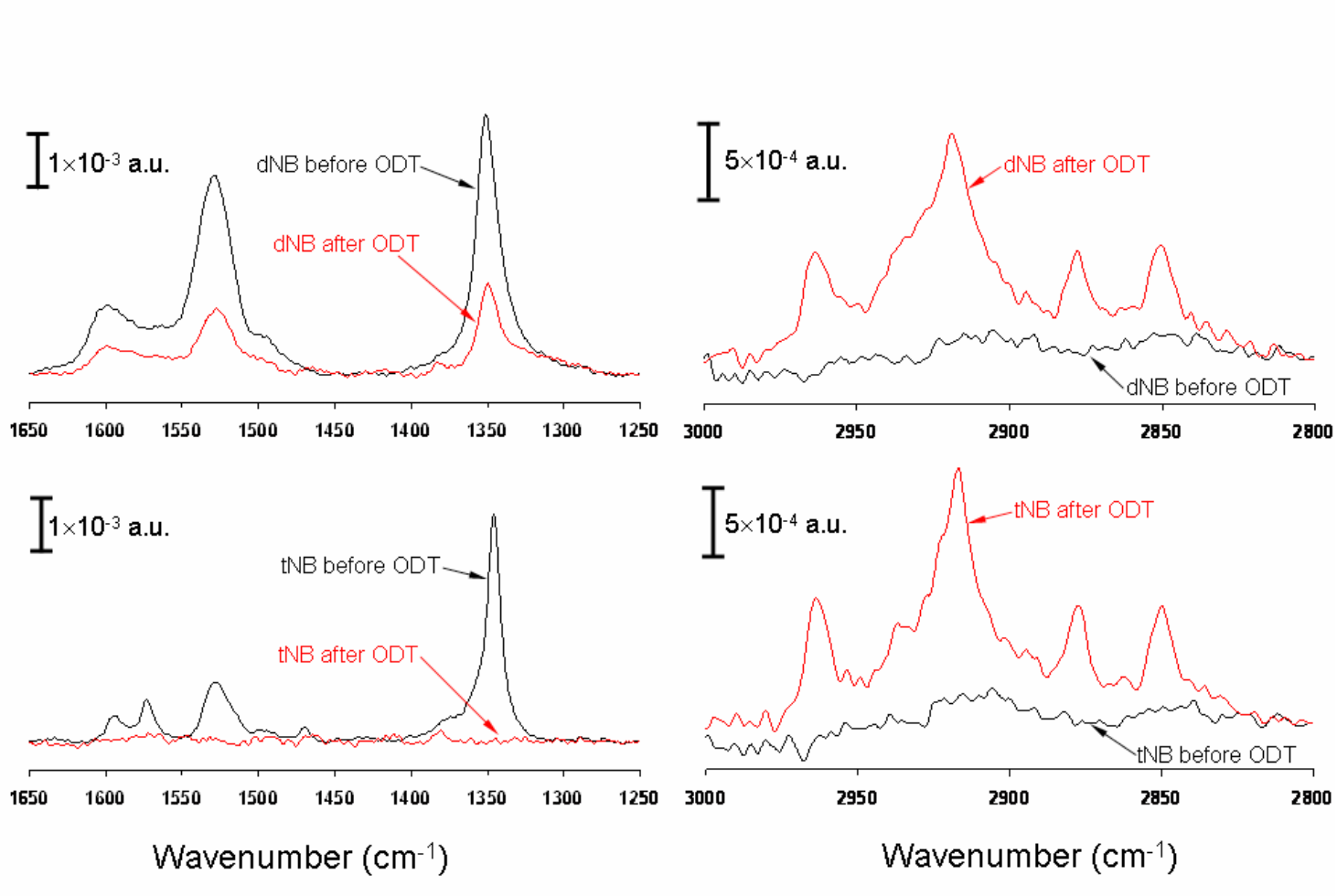

Figure 3.08. Top: IRRAS spectra of a dNB film on gold before and after exposure to a solution of ODT overnight. Bottom: IRRAS spectra of a tNB monolayer before and after ODT displacement.

of the dNB layer, the entire tNB layer is displaced by overnight exposure to ODT solution. More than 25% of the dNB layer resists displacement by ODT as shown by the results listed in Table 3.03. We have exposed dNB layers to the ODT solution for up to 1 week and found similar results. The IRRAS spectra in the high-energy, C-H stretching region provide structural information on the ODT layers following treatment, and are also shown in Figure 3.08. The width and position of the asymmetric methylene stretch ($\nu_{a,CH2}$) is sensitive to the chain structure in these monolayer systems.[28] The $\nu_{a,CH2}$ band for the ODT monolayer formed after displacing the tNB monolayer is located at 2918 cm^{-1} with a width of ~14 cm^{-1}. These values are diagnostic of a crystalline chain structure, which is expected for an ODT monolayer that fully displaces tNB. The position of the $\nu_{a,CH2}$ band at the dNB substrate is 2920 cm^{-1} and exhibits a width of ~24 cm^{-1}, which are values characteristic of a more liquid-like monolayer of ODT. In this case, a mixed layer of dNB and ODT is formed where the tightly-bound dNB molecules disrupt the packing of the ODT layer. The results of the ODT displacement study are significant because they show that a portion of the dNB layer is more strongly bound to the gold than tNB.

The findings presented in Table 3.03 are consistent with results from previous studies and provide some new information on the structure and stability of diazonium derived layers on gold. Figure 3.09 presents simplified models for the effect of the various treatments on the two types of layers compared here. It is well accepted that aromatic thiols form ordered monolayers when spontaneously adsorbed to gold.[29] Following exposure of the tNB monolayer to refluxing acetonitrile or sonication, some of the nitrobenzenthiol molecules desorb, leaving a partial monolayer. The electrochemical

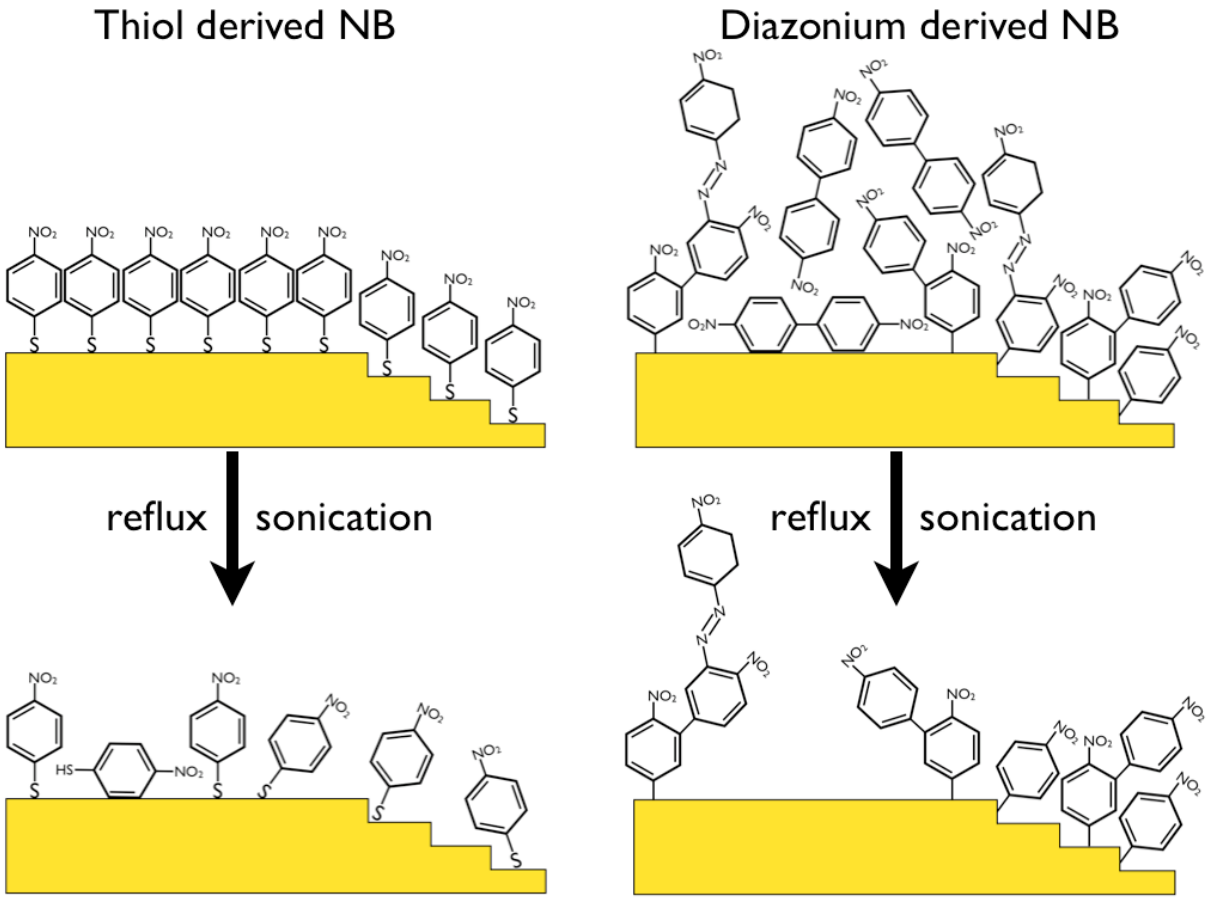

Figure 3.09. Schematic drawings of the structures of the two molecular layers studied here and the result of the treatments applied.

deposition of dNB produces a dense, yet disordered multilayer film that likely contains some strongly physisorbed material that resists thorough rinsing. This physisorbed material may be comprised of, for example, NB dimers that form via radical-radical coupling during the deposition process (Figure 3.09). Subjecting this film to the reflux or sonication treatment removes the physisorbed material and perhaps some more strongly bonded NB molecules. This is consistent with previous studies that have shown that prolonged sonication can remove material from diazonium derived films on gold.[21,25] It is unknown, at this point, whether the material removed includes gold surface atoms in the form of a NB-gold complex. There is a sufficient amount of material that survives the refluxing and sonication treatments to provide a reasonable barrier to electron transfer as evidenced by ΔE_p for $Fe(CN)_6^{3/4-}$ greater than 500 mV.

A portion of the dNB film cannot be displaced by ODT. These NB molecules are more strongly bound to the gold surface than the thiol counterpart. Computational results indicate that the bond energy between metals and diazonium derived aryl groups depends strongly on the metal and that the C-Au(111) binding energy is one of the lowest at -24 kcal/mol.[48] A more recent computational study directly compares aryl C-Au(111) bonding with aryl S-Au(111). This method predicts a maximum binding energy of 31.8 kcal/mol for C-Au(111) for bonding to a top site and 28.4 kcal/mol for S-Au(111) binding to a bridge site.[51] The gold substrates used in our study are polycrystalline that contain a fraction of (111) crystal faces as well as surface sites with other crystallographic orientations. We thus hypothesize that the strongly adsorbed NB molecules that resist ODT displacement are bound at higher energy step sites on these polycrystalline gold substrates as shown in Figure 3.09. Experiments are currently

underway to test this hypothesis and to measure the amount of gold lost from the surface by the various treatments.

4. Conclusions

The results of this work agree with previous studies in terms of the structure of diazonium-derived films on gold. Our characterizations indicate that the electrochemical reduction of nitrobenzene diazonium cations at gold electrodes under the conditions used here results in a multilayer NB film that is ~3× thicker than a monolayer formed from the spontaneous adsorption of 4-nitrobenzene thiol. Comparison of the N 1s XPS spectra of the two films provides support that a fraction of the bonds within the structure of the diazonium derived multilayer film are azo linkages. The treatments used here were shown to remove a significant amount of nitrobenzene groups from both tNB monolayers and dNB films. In terms of percentage of the number of initial NB groups, tNB monolayers are more stable towards prolonged sonication and refluxing acetonitrile. However, a significant amount of the dNB films resists both treatments. Strong bonding between dNB films and the gold surface was revealed by ODT displacement studies. While ODT is able to completely displace the tNB monolayer, approximately 25% of the dNB film cannot be displaced by ODT. This is a significant finding as it provides direct evidence for enhanced stability of diazonium-derived films over thiol monolayer analogs.

5. Acknowledgements

We thank Dr. M. Brett for use of the variable angle spectroscopic ellipsometer and James Gospodyn for useful discussions on the film modeling for VASE.

References:

(1) Pinson, J.; Podvorica, F. *Chem. Soc. Rev.* **2005**, *34*, 429-439.

(2) Saby, C.; Ortiz, B.; Champagne, G. Y.; Belanger, D. *Langmuir* **1997**, *13*, 6805-6813.

(3) Liu, Y. C.; McCreery, R. L. *Anal. Chem.* **1997**, *69*, 2091-2097.

(4) Allongue, P.; Delamar, M.; Desbat, B.; Fagebaume, O.; Hitmi, R.; Pinson, J.; Saveant, J. M. *J. Am. Chem. Soc.* **1997**, *119*, 201-207.

(5) Downard, A. J.; Roddick, A. D. *Electroanal.* **1995**, *7*, 376-378.

(6) Delamar, M.; Hitmi, R.; Pinson, J.; Saveant, J. M. *J. Am. Chem. Soc.* **1992**, *114*, 5883-5884.

(7) Anariba, F.; DuVall, S. H.; McCreery, R. L. *Anal. Chem.* **2003**, *75*, 3837-3844.

(8) Kariuki, J. K.; McDermott, M. T. *Langmuir* **2001**, *17*, 5947-5951.

(9) Kariuki, J. K.; McDermott, M. T. *Langmuir* **1999**, *15*, 6534-6540.

(10) Delamar, M.; Desarmot, G.; Fagebaume, O.; Hitmi, R.; Pinson, J.; Saveant, J. M. *Carbon* **1997**, *35*, 801-807.

(11) Corgier, B. P.; Marquette, C. A.; Blum, L. J. *J. Am. Chem. Soc.* **2005**, *127*, 18328-18332.

(12) Downard, A. J.; Roddick, A. D.; Bond, A. M. *Anal. Chim. Acta* **1995**, *317*, 303-310.

(13) Bahr, J. L.; Tour, J. M. *J. Mater. Chem.* **2002**, *12*, 1952-1958.

(14) McCreery, R. L. *Chem. Mater.* **2004**, *16*, 4477-4496.

(15) Hurley, B. L.; McCreery, R. L. *J. Electochem. Soc.* **2004**, *151*, B252-B259.

(16) Bernard, M. C.; Chausse, A.; Cabet-Deliry, E.; Chehimi, M. M.; Pinson, J.; Podvorica, F.; Vautrin-Ul, C. *Chem. Mater.* **2003**, *15*, 3450-3462.

(17) Adenier, A.; Bernard, M. C.; Chehimi, M. M.; Cabet-Deliry, E.; Desbat, B.; Fagebaume, O.; Pinson, J.; Podvorica, F. *J. Am. Chem. Soc.* **2001**, *123*, 4541-4549.

(18) deVilleneuve, C. H.; Pinson, J.; Bernard, M. C.; Allongue, P. *J. Phys Chem. B* **1997**, *101*, 2415-2420.

(19) Stewart, M. P.; Maya, F.; Kosynkin, D. V.; Dirk, S. M.; Stapleton, J. J.; McGuiness, C. L.; Allara, D. L.; Tour, J. M. *J. Am. Chem. Soc.* **2004**, *126*, 370-378.

(20) Benedetto, A.; Balog, M.; Viel, P.; Le Derf, F.; Salle, M.; Palacin, S. *Electrochim. Acta* **2008**, *53*, 7117-7122.

(21) Paulik, M. G.; Brooksby, P. A.; Abell, A. D.; Downard, A. J. *J. Phys Chem. C* **2007**, *111*, 7808-7815.

(22) Liu, G. Z.; Bocking, T.; Gooding, J. J. *J. Electroanal. Chem.* **2007**, *600*, 335-344.

(23) Ricci, A.; Bonazzola, C.; Calvo, E. J. *Phys Chem. Chem. Phys.* **2006**, *8*, 4297-4299.

(24) Lyskawa, J.; Belanger, D. *Chem Mater.* **2006**, *18*, 4755-4763.

(25) Laforgue, A.; Addou, T.; Belanger, D. *Langmuir* **2005**, *21*, 6855-6865.

(26) Gooding, J. J. *Electroanal.* **2008**, *20*, 573-582.

(27) Love, J. C.; Estroff, L. A.; Kriebel, J. K.; Nuzzo, R. G.; Whitesides, G. M. *Chem. Rev.* **2005**, *105*, 1103-1169.

(28) Porter, M. D.; Bright, T. B.; Allara, D. L.; Chidsey, C. E. D. *J. Am. Chem. Soc.* **1987**, *109*, 3559-3568.

(29) Sabatani, E.; Cohenboulakia, J.; Bruening, M.; Rubinstein, I. *Langmuir* **1993**, *9*, 2974-2981.

(30) Delamarche, E.; Michel, B.; Kang, H.; Gerber, C. *Langmuir* **1994**, *10*, 4103-4108.

(31) Bain, C. D.; Troughton, E. B.; Tao, Y. T.; Evall, J.; Whitesides, G. M.; Nuzzo, R. G. *J. Am. Chem. Soc.* **1989**, *111*, 321-335.

(32) Schoenfisch, M. H.; Pemberton, J. E. *J. Am. Chem. Soc.* **1998**, *120*, 4502-4513.

(33) Berger, F.; Delhalle, J.; Mekhalif, Z. *Electrochim Acta* **2008**, *53*, 2852-2861.

(34) H. G. Tompkins, W. A. M. *Spectroscopic ellipsometry and reflectometry: a user's guide*; John Wiley & Sons: New York, 1999.

(35) Pavia, D. L.; Lampman, G. M.; Kriz, G. S. In *Introduction to Spectroscopy*; 3rd ed.; Harcourt: Orlando, 2001, p 13-101.

(36) Ricci, A.; Rolli, C.; Rothacher, S.; Baraldo, L.; Bonazzola, C.; Calvo, E. J.; Tognalli, N.; Fainstein, A. *J. Solid State Electr.* **2007**, *11*, 1511-1520.

(37) Merklin, G. T.; He, L.-T.; Griffiths, P. R. *Appl. Spectrosc.* **1999**, *53*, 1448-1453.

(38) Lambert, J. B.; Shurvell, H. F.; Lightner, D.; Cooks, R. G. *Introduction to Organic Spectroscopy*; Macmillan: New York, 1987.

(39) Jakubowicz, A.; Jia, H.; Wallace, R. M.; Gnade, B. E. *Langmuir* **2005**, *21*, 950-955.

(40) Allongue, P.; de Villeneuve, C. H.; Cherouvrier, G.; Cortes, R.; Bernard, M. C. *J. Electroanal. Chem.* **2003**, *550*, 161-174.

(41) Combellas, C.; Kanoufi, F.; Pinson, J.; Podvorica, F. I. *J. Am. Chem. Soc.* **2008**, *130*, 8576.

(42) Adenier, A.; Cabet-Deliry, E.; Chausse, A.; Griveau, S.; Mercier, F.; Pinson, J.; Vautrin-Ul, C. *Chem Mater.* **2005**, *17*, 491-501.

(43) Mendes, P.; Belloni, M.; Ashworth, M.; Hardy, C.; Nikitin, K.; Fitzmaurice, D.; Critchley, K.; Evans, S.; Preece, J. *Chemphyschem* **2003**, *4*, 884-889.

(44) Doppelt, P.; Hallais, G.; Pinson, J.; Podvorica, F.; Verneyre, S. *Chem. Mater.* **2007**, *19*, 4570-4575.

(45) Saby, C.; Ortiz, B.; Champagne, G. Y.; Belanger, D. *Langmuir* **1997**, *13*, 6805-6813.

(46) Chisholm, R. A.; Gish, D. A.; Brett, M. J.; McDermott, M. T. *Manuscript in preparation.*

(47) Brooksby, P. A.; Downard, A. J. *J. Phys Chem. B* **2005**, *109*, 8791-8798.

(48) Jiang, D. E.; Sumpter, B. G.; Dai, S. *J. Am. Chem. Soc.* **2006**, *128*, 6030-6031.

(49) Laibinis, P. E.; Nuzzo, R. G.; Whitesides, G. M. *J. Phys. Chem.* **1992**, *96*, 5097-5105.

(50) Bain, C. D.; Evall, J.; Whitesides, G. M. *J. Am. Chem. Soc.* **1989**, *111*, 7155-7164.

(51) de la Llave, E.; Ricci, A.; Calvo, E. J.; Scherlis, D. A. *J. Phys Chem. C* **2008**, *112*, 17611-17617.

Chapter IV

Characterization of Mixed Layers Consisting of Diazonium Derived p-Nitroazobenzene Groups and Alkanethiols on Polycrystalline Gold Electrodes – Introduction to Mixed-Mode Bonded Layers

1. Introduction

The results presented in Chapters II and III showed that substituted aryl layers attached to polycrystalline gold surfaces via the electrochemical reduction of the corresponding aryldiazonium salt are comprised of two types of material: a weakly bound, presumably physisorbed material and material that binds quite strongly. We believe the tightly bound structures can be utilized to create some potentially very useful modified electrode interfaces. We envision the coexistence of the tightly bound networks of aryl groups with alkanethiolates on the same gold surface to produce a heterogeneous, mixed molecular layer. We herby refer to the phenomenon, where these two specific attachment chemistries are employed, as mixed-mode bonding.

An illustrative representation of layers formed from mixed-mode bonding is shown in Figure 4.01. The aryl component of the film is first deposited electrochemically from a solution of the corresponding aryldiazonium salt in acetonitrile. Ideally the deposition conditions are chosen such that the layer is not complete. The modified electrode is then immersed in a dilute solution of an alkanethiol, to "back-fill" any defect sites or regions where the aryl component was only loosely attached.

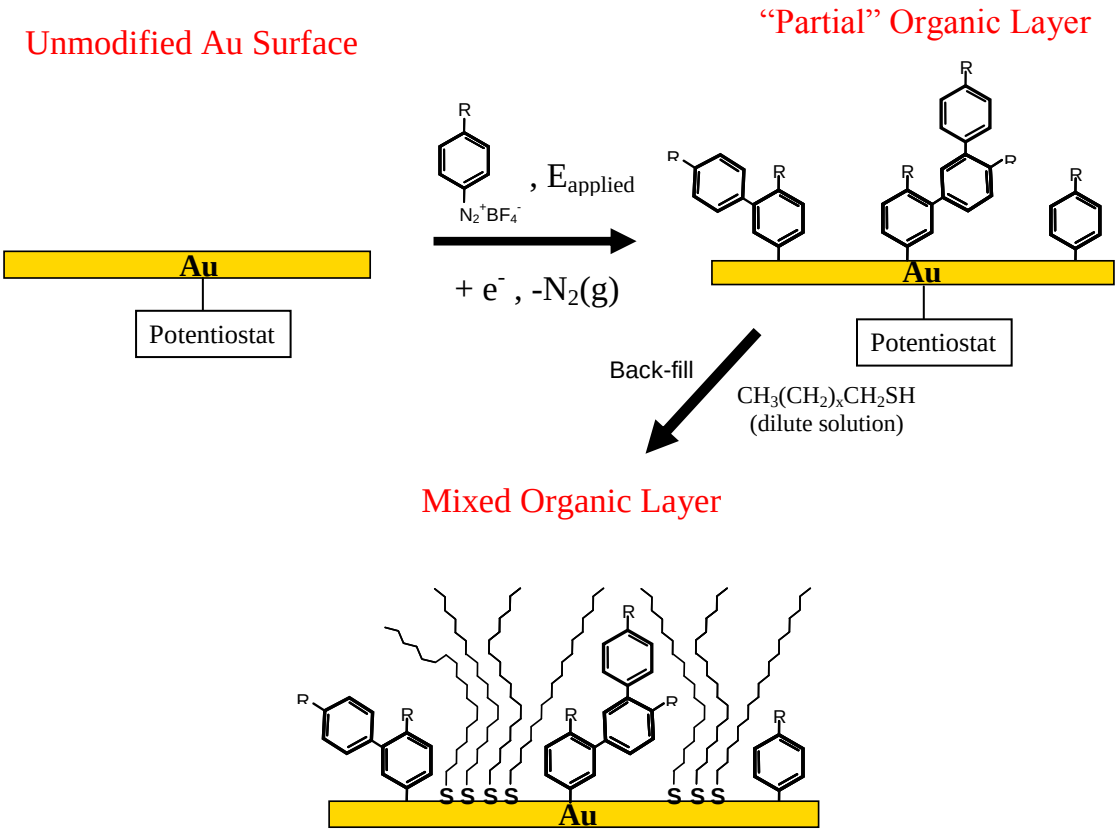

Figure 4.01. A schematic representation of a mixed-mode molecular layer. An aryl component is first deposited electrochemically from a solution containing the corresponding aryldiazonium cation. Any exposed regions are then "back-filled" upon exposure to a dilute solution of an alkanethiolate.

. Mixed-mode bonding is an extension of the concept of mixed alkanethiolate SAMs or two-component monolayers generated by the spontaneous coadsorption of two alkanethiols with different tail groups. Mixed alkanethiolate SAMs were first reported and rigorously characterized by Whitesides and coworkers.[1, 2] Their contributions resulted in several proposed applications for such films. For example, Chidsey and coworkers devised the notion of diluting a ferrocene-terminated alkanethiolate into a monolayer of an unsubstituted alkanethiolate, in order to unveil fundamental concepts behind interfacial electron transfer.[3]

More relevant to our long-term intentions with mixed-mode structures, Weiss and coworkers devised a scheme to produce isolated sites of enhanced conductivity, or molecular wires (MWs), within a SAM of non-conducting alkanethiolates.[4] Similar to the works of Chidsey, this entailed the dilution of a highly conjugated organic thiolate into a saturated alkanethiolate SAM. It was observed that these conjugated alkanethiolate MWs do not laterally diffuse during an observation period of hours.[5] However, based on the known lability of the Au-S interaction, it is expected that molecular motion on the surface would be observed for longer observation periods.

The notion that single molecules could eventually be incorporated into practical electronic devices as single electron transistors, molecular switches, or single molecule sensors provides the driving force for this area of research. With Figure 4.01 in mind, we would therefore like to emphasize the broader scope of this project. Within our multi-component films, we believe the regions with highly conjugated, branched networks of aromatic groups will produce a measurable difference in local conductivity when compared to the surrounding alkanethiolate regions. Thus, mixed-mode structures could

serve as a novel, alternative approach to the production of MWs at a gold surface. Recent investigations have shown that aryl groups grafted electrochemically to iron exhibit some degree of covalent interaction with the surface.[6] Further work in our group has explored the spontaneous adsorption of aryl diazonium salts to gold nanoparticles. Surface enhanced Raman scattering (SERS) has revealed a band at 410 cm^{-1} that is being attributed to an Au-C stretch.[7] This provides compelling evidence for a gold-carbon covalent bond. If this interaction does, in fact, exist, MWs generated from mixed-mode molecular layers would not be expected to be mobile. This property would be quite advantageous for characterizing the electrical properties of MW structures.

This chapter will focus on the characterization of mixed-mode molecular films on gold. It will be shown that the relative amounts of the aryl and thiolate components within the film can readily be controlled. Mixed-mode films will be compared to films prepared without introducing the thiol component in terms of their spectroscopic characteristics, electrochemical blocking capabilities, and atomic composition.

2. Experimental

Preparation of Gold Substrates. Gold was deposited to glass microscope slides via thermal evaporation using 99.99% Au shot (Goodfellow). A 6 nm layer of Cr was used in between the glass and gold film to enhance adhesion. For the IRRAS, XPS, and cyclic voltammetry experiments a gold thickness of 200 nm was deposited onto glass microscope slides. For the AFM studies a 50 nm gold layer was evaporated onto 0211 grade glass diced into square substrates 1.4 cm on a side. All glass substrates and glassware in this study were cleaned using hot piranha solution (1:4 30% H_2O_2:H_2SO_4)

followed by thorough rinsing with deionized (18 MΩ)/filtered H_2O (NANOpure™ water purification system, Barnstead International, Dubuque, Iowa). Substrates were blown dry using Ar gas. All gold substrates were stored under house vacuum conditions and used within 1 week of the date they were prepared. [*Warning: Piranha solution should be handled with extreme care; it is a strong oxidant and reacts violently with many organic materials. It also presents an explosion danger. All work should be performed under a fume hood.*]

Electrochemical Deposition of the Aryl Films. 4-nitroazobenzenediazonium tetrafluoroborate (NABDF) was synthesized according to procedures published by Starkey.[8] Tetrabutylammonium tetrafluoroborate ($TBABF_4$) (≥99%) was used as received (Sigma-Aldrich Canada Ltd., Oakville, Ontario). Spectroscopic grade acetonitrile was also used as received (Caledon Laboratories Ltd., Georgetown, Ontario). Prior to surface modification, all gold substrates were subjected to a 10 min cleaning in hot piranha solution. Electrochemical grafting of the aryl layers to the gold substrates was achieved by cyclic voltammetry using a software controlled Model AFCBP1 bipotentiostat (Pine Instrument Company, Grove City, Pennsylvania). Aside from a small region at one end of the electrode (to permit electrical contacts), the entire gold slide was immersed in the deposition solution. For all non-aqueous electrochemistry the reference electrode consisted of a silver wire submerged in a 200 mM $AgNO_3$ solution in acetonitrile with 0.1 M $TBABF_4$. A platinum wire/platinum mesh assembly with adequate surface area served as a counter electrode. All electrochemical depositions were carried out by sweeping the potential from +200 mV to -700 mV at a sweep rate of 200 mV/s, at the indicated diazonium salt concentrations in acetonitrile with 0.1 M $TBABF_4$. A single

voltammetric scan was used to prepare each modified electrode. Diazonium salt solutions were deaerated for 10 min with Ar gas prior to all depositions. Following the modification, samples were thoroughly rinsed with acetonitrile, blown dry with a gentle stream of Ar gas, and used immediately with minimum exposure to the ambient.

Preparation of Mixed-Mode Molecular Layers. Dodecanethiol (DDT, ≥97%) (Sigma-Aldrich Canada Ltd., Oakville, Ontario) and anhydrous ethanol (Commercial Alcohols Inc., Brampton, Ontario) were used as received. Previously modified gold substrates were immediately immersed in a solution of 1 mM DDT in ethanol for 24 h. Prior to the self-assembly process, all DDT solutions were placed in an ultrasonication bath for 5 min. to ensure the solution was homogeneous. DDT solutions were deaerated with Ar gas for 10 min prior to their use.

IRRAS. IRRAS spectra were collected using an ATI Mattson Infinity Series Fourier transform infrared (FTIR) spectrometer equipped with a liquid nitrogen cooled mercury-cadmium telluride (MCT) detector. The p-polarized IR beam was incident on the gold surface at an angle of 80° with respect to the surface normal. A total of 1500 scans were averaged for each experiment at a resolution of 4 cm^{-1}. The interferograms were Fourier transformed using triangular apodization. A gold slide modified with a SAM of $CD_3(CD_2)_{16}CD_2$-SH was used as a reference.

Electrochemical Studies. Potassium ferrocyanide (≥99%) (BDH Chemicals Ltd., Poole, England), hexaammineruthenium(III) chloride (99%) (Strem Chemicals Inc. Newburyport, Massachusetts) and potassium chloride (≥99%) (Fisher Scientific International, Hampton, New Hampshire) were used as received. All aqueous solutions were prepared by dilution with 18 MΩ deionized H_2O, and bubbled with Ar for 10 min

prior to the analysis. A 3-necked inverted electrochemical cell was clamped to a modified/unmodified electrode surface with a solvent resistant, Viton o-ring (6 mm diameter) in between to define the electrode area of 0.28 cm^2. Potentials were measured with respect to an Ag/AgCl (saturated KCl) reference electrode using the same counter electrode described above. The sweep rate was 100 mV/s.

AFM Measurements. AFM measurements were performed using a Nanoscope III Multimode™ microscope (Digital Instruments, Santa Barbara, CA). All measurements were performed under ambient conditions, using rectangular Si cantilevers with a thin, reflective Al coating (Olympus, Tokyo, Japan). The force constant of the cantilevers was 40 N/m. The oscillation frequency used for tapping mode was 300 +/- 10 kHz. A contact force of 400 nN was used for all contact mode experiments and was calculated based on a setpoint of 0.1 V. The normal force, F_N, is determined using the relation:

$$F_N = k \times \left[\frac{V_s - V_b}{s} \right] \qquad [1]$$

where V_s is the setpoint voltage used for imaging, V_b is the voltage required to break the tip away from the surface, s is the optical sensitivity of the cantilever to bending and is equal to 0.01 V/nm, and k is the force constant of the cantilever.

XPS Analyses. XPS analyses were performed using an AXIS Ultra Spectrometer (Kratos Analytical). A monochromated Al Kα source (hν = 1486.6 eV) was employed at a power of 210 W. Samples were placed in the analytical chamber no longer than 20 minutes following the deposition of the film of interest. The analytical chamber was evacuated to a base pressure lower than 4 x 10^{-8} Pa for all experiments. The

hemispherical analyzer was operated in fixed analyzer transmission (FAT) mode with a spot size set at 700 x 400 μm. Charge neutralization was not utilized during any of the scans. The high resolution data was collected with a pass energy of 20 eV and a 0.1 eV step size. For the Au 4f, C 1s, O 1s, and S 2p high resolution spectra 2, 10, 10, and 100 scans (resp.) were signal averaged. The number of scans used for the N 1s data varied according to the amount of signal observed but was typically 60-100 scans. All spectra were referenced to the Au $4f_{7/2}$ electron (binding energy, BE = 84 eV). For all measurements, the take-off angle was 0° to the surface normal.

3. Results and Discussion

3.1 Controlling Layer Composition of NAB:DDT Mixed-Mode Layers. Characterization of the NAB Component.

Mixed alkanethiolate monolayers are typically prepared by the simultaneous coadsorption of thiols of interest from solution.[1, 2, 9-11] In contrast to this, a sequential approach was employed to prepare mixed molecular films in this work. Our strategy for controlling the composition of the films is to control the amount of aryl groups deposited initially. In Chapter II it was shown that by altering certain parameters during the deposition, namely the number of voltammetric cycles, the surface density of NAB groups deposited onto the gold surface, and hence the layer quality, can be changed. Here it will be shown that layer quality can also be controlled by manipulating the concentration of the NAB diazonium cations in the deposition solution. This concept is essential to a larger goal, which is to control the composition of the mixed-mode films.

Nitroazobenzene diazonium tetrafluoroborate (NABDF) was chosen for this study because of the extensive conjugation within the nitroazobenzene group. We believe this will facilitate electron transfer through the molecule in future experiments. In Chapter II, multiple deposition waves were utilized for the purpose of creating thick, electrically insulating layers. In addition, the absence of Faradaic current after the first cycle was used as an indication that the electrode was completely modified. For the current study, however, one cycle is used to better control the amount of material deposited.

Deposition voltammograms for NABDF deposition concentrations, c_{NABDF}'s, of 1 mM, 200 μM, and 50 μM are shown in Figure 4.02. The choice of c_{NABDF} has a noticeable effect on the cathodic peak potential, $E_{p,c}$. $E_{p,c}$ shifts to more negative potentials for higher c_{NABDF}'s. We speculate that this could be a kinetic effect whereby NAB groups spontaneously graft to the electrode surface prior to the application of the external potentials. It could also be the result of NAB groups that are electrochemically grafted to the electrode near the beginning of the applied potential wave. In support of this statement, it has been shown that aryl groups spontaneously graft to gold electrodes without the need of external potentials.[12, 13] In either case, a quickly formed layer would lower the heterogeneous electron transfer rate, resulting in a more negative $E_{p,c}$.

The amount of NAB groups attached to the gold electrodes was assessed spectroscopically, using IRRAS, and using scanning probe microscopy (SPM). SPM was employed to provide film thickness, δ, measurements. Our procedures were adapted from the work of McCreery and coworkers.[14] Figure 4.03 shows an AFM image of a gold surface modified with NAB from a 1 mM NABDF solution. The 2 μm × 2 μm area in the center of the image corresponds to a region where the film has been ploughed away by

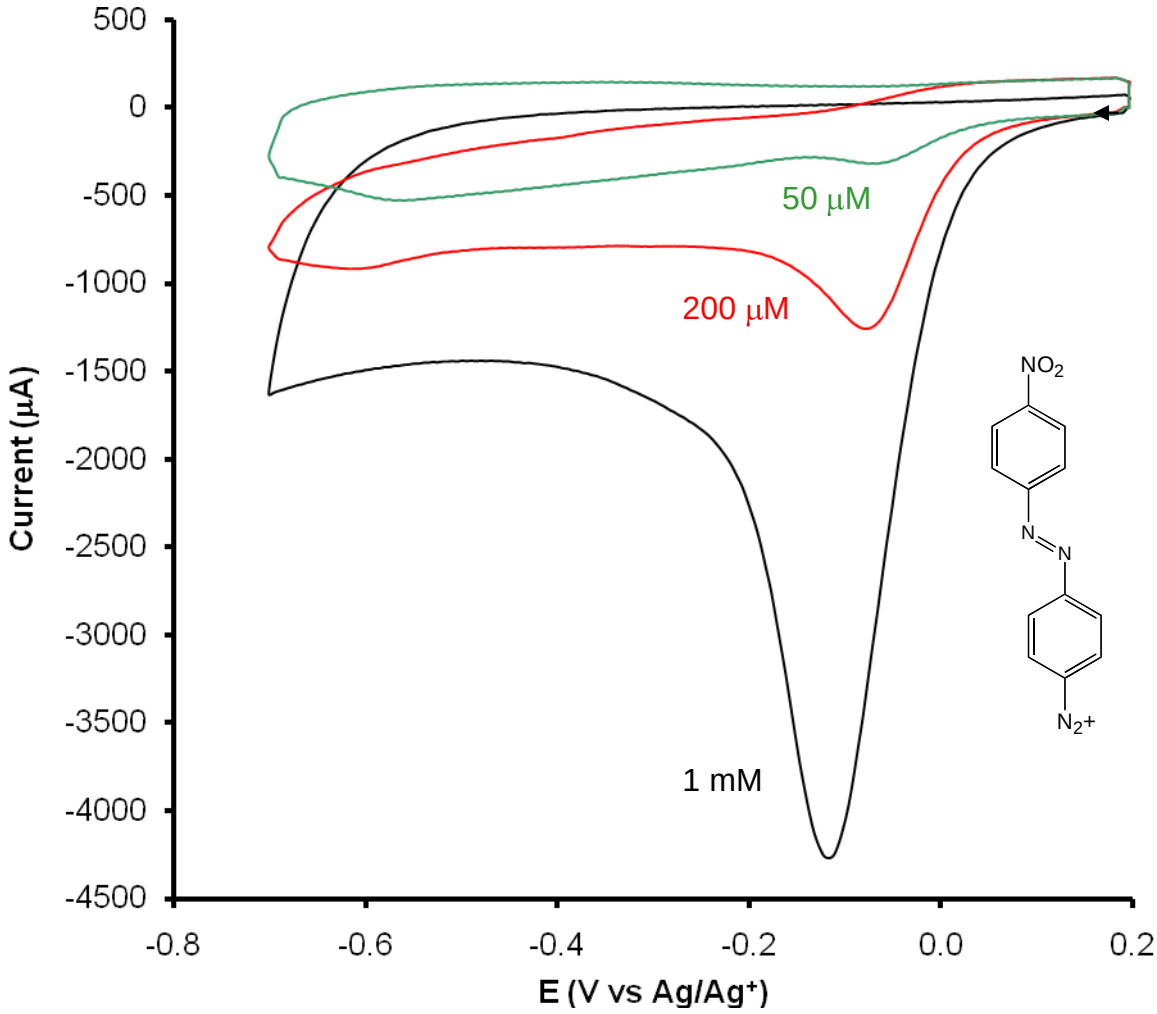

Figure 4.02. Cyclic voltammograms of a gold electrode at different NAB concentrations. The supporting electrolyte is 0.1 M $TBABF_4$ in acetonitrile. The structure of the NAB diazonium cation is shown in the bottom right. The sweep rate is 200 mV/s.

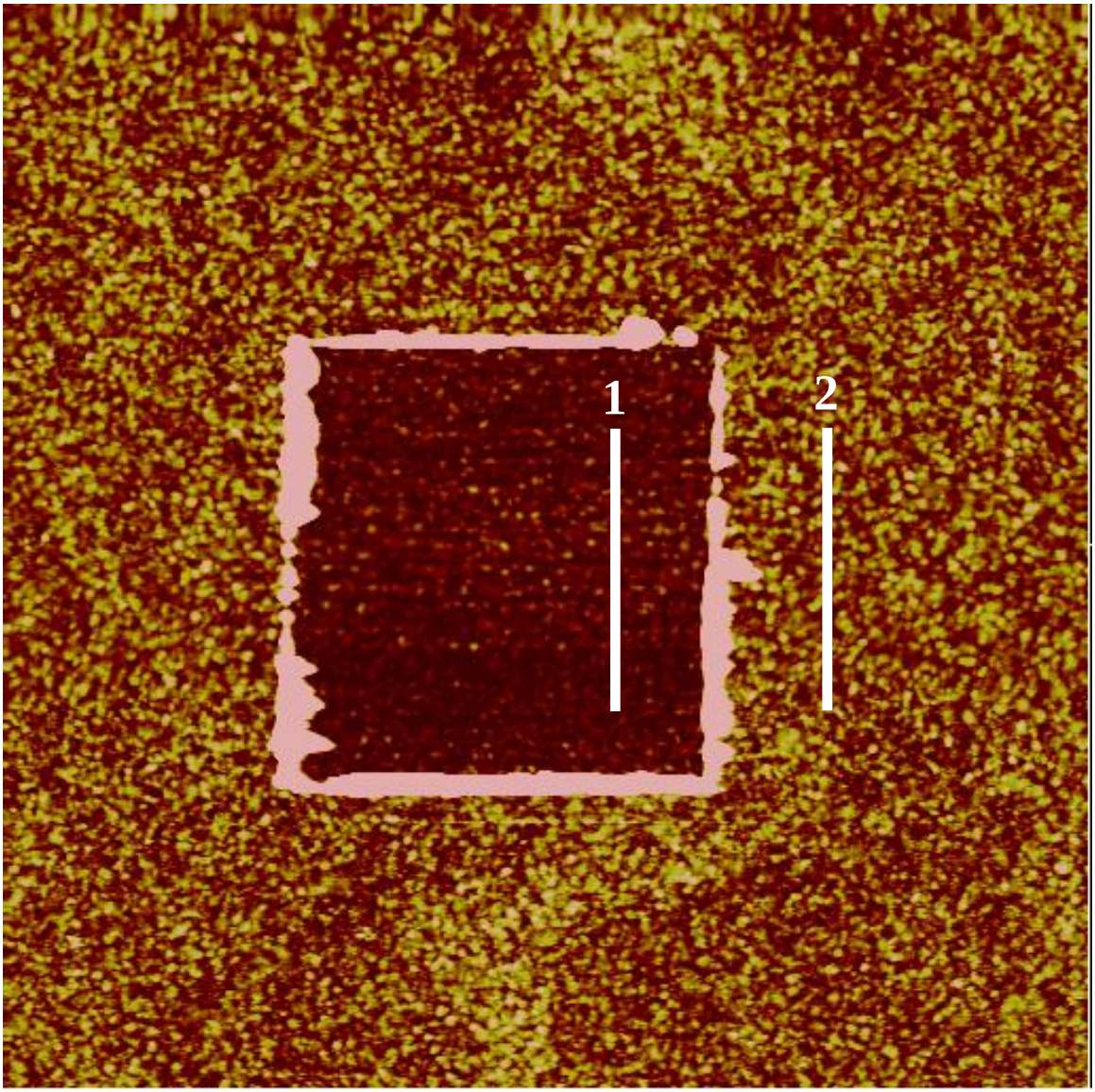

Figure 4.03. A TM-AFM image of a gold electrode modified with an NAB film formed from 1 mM NABDF. The center region has been ploughed away by the AFM tip. The AFM software is used to calculate the height difference between corresponding points on vertical lines 1 and 2. The result is then averaged along the entire line segment to yield a δ value. The image is a 5 μm × 5 μm square. The z-scale is 10 nm.

the AFM tip. δ is determined by a cross-sectional profile analysis. The large height increases observed at the edges of the center square are due to the build-up of material that has been ploughed by the AFM tip. Table 4.01 presents the height data obtained for the three concentrations of NABDF studied: 50 μM, 200 μM, and 1 mM. A sample cross-section profile for each concentration studied is also provided in Figure 4.04 to illustrate how the height information was extracted.

The theoretically predicted thickness of a monolayer of NAB is 1.43 nm.[14] The measured film thickness for a film deposited with a c_{NABDF} of 1 mM is 4.7 nm. Given this result it appears that layers deposited under these conditions are composed of networks of NAB groups that are approximately 3 monolayers thick. The measured film thickness for layers produced from both 50 μM and 200 μM NABDF is 1.1 nm +/- 0.3 nm. This result indicates that, within experimental error, relatively dilute deposition concentrations produce films that are one monolayer thick. Intuitively, one would expect differences in layers produced from these two concentrations, especially given the increased current seen in the deposition CV's. We surmise that such differences are related to film density. The density of the NAB groups is a property that would be difficult to observe from the SPM measurements alone. Both spectroscopic and electrochemical investigations were carried out in parallel to address this issue.

IRRAS was employed to semi-quantitatively assess the amount of NAB molecules attached to the gold electrode as a function of c_{NABDF}. IRRAS spectra were collected for all c_{NABDF} studied. The fingerprint regions of the spectra are shown in Figure 4.05. Similar to the methodologies discussed in Chapter II (Section 3.2), the absorbance of the symmetric nitro stretch, A_{1347}, will be used as a diagnostic for the amount of NAB

groups attached to the surface. A plot of A_{1347} vs. c_{NABDF} is shown in Figure 4.06. A_{1347} increases monotonically with c_{NABDF}. We interpret this to indicate that the amount of NAB molecules deposited increases with solution concentration.

The ratio of the absorbance of the symmetric NO_2 stretch (A_{1347}) with that of asymmetric NO_2 stretch (A_{1526}) can be used to assess structural differences between the films as was discussed in Chapter 2. The ratios are listed in Table 4.02 along with the ratio obtained from a spectrum of solid NAB diazonium salt. The values of A_{1347}/A_{1526} for films prepared from 1 mM and 200 μM concentrations are significantly higher that that for the film prepared from 50 μM. The intensity ratios for films formed from higher concentration solutions are similar, albeit lower, than that for the solid NAB diazonium salt. We interpret this to indicate that the NO_2 groups in films deposited from higher concentrations, in this case 1 mM and 200 μM, are randomly oriented, similar to what is expected in the bulk solid material. This likely reflects a disordered, multilayered structure. Films prepared from 50 μM solutions yield a lower $A_{1347/}A_{1526}$ that we believe is diagnostic of a single or partial layer of NAB groups bound to the surface. The analogous ratio for a spontaneously adsorbed monolayer of mercaptonitrobenzene is 0.24 (Table 3.01). As noted in Chapter II, the C_2 axis of mercaptonitrobenzene is oriented perpendicular to the surface. By comparison, an A_{1347}/A_{1526} value of 0.63 indicates that the NO_2 groups in films formed from 50 μM solutions are oriented near perpendicular to the surface. In summary, analysis of the intensity ratios of the NO_2 bands provides a structural description of NAB films electrochemically deposited on gold. Higher concentrations yield disordered multilayer films, while lower concentrations yield single

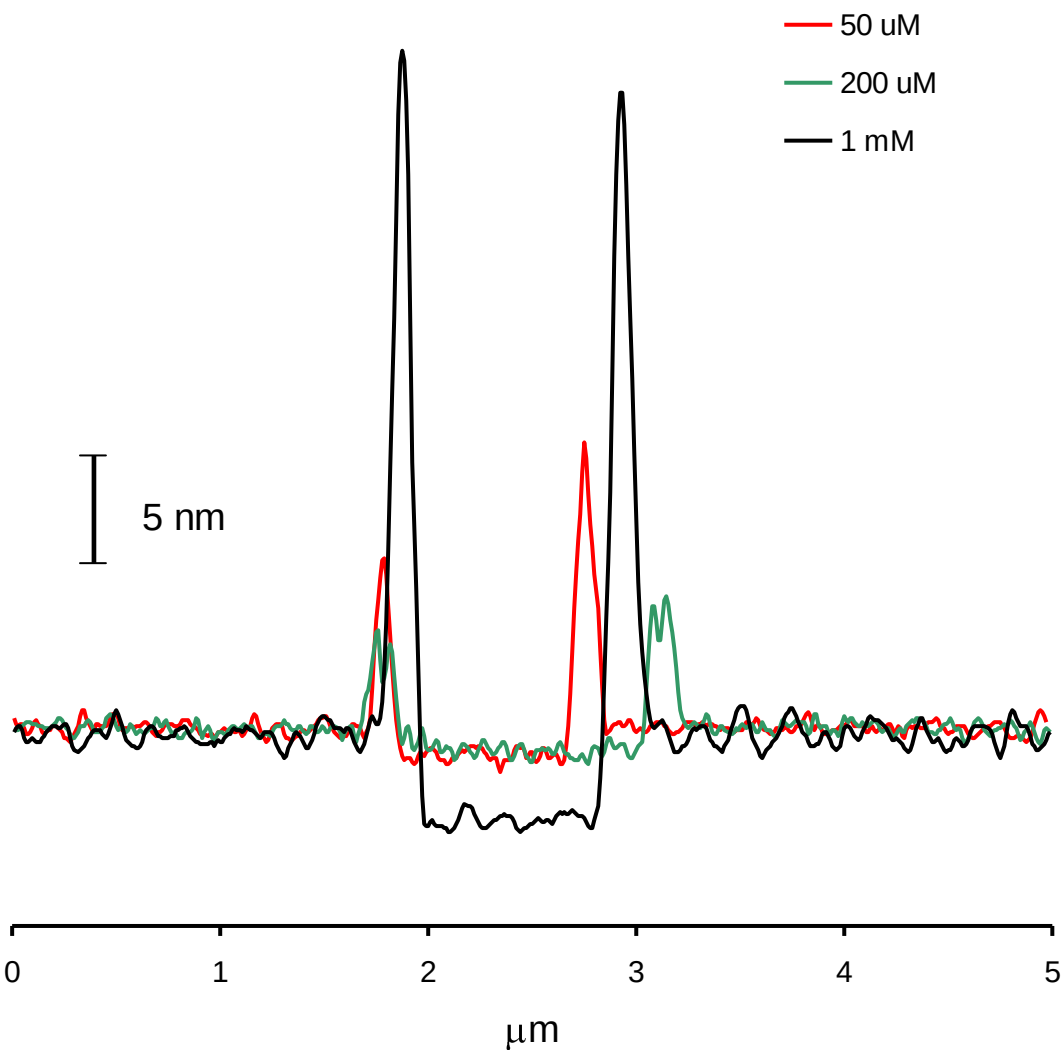

Figure 4.04. Cross-sections of AFM images after a region was ploughed away by the AFM tip. Film thickness data can be extracted by measuring the height difference between the bottom of the ploughed region and the un-ploughed regions.

c_{NABDF}	δ_{AVG} (nm)
1 mM	4.7 +/- 0.2
200 μM	1.1 +/- 0.3
50 μM	1.1 +/- 0.3

Table 4.01. Film thickness data for NAB films on gold measured by ploughing with an AFM tip. The values are averages of measurements for 3 independent samples.

or partial layers.

The structure of the NAB films was also evaluated using various electrochemical probes. These same probes will be used to explore the mixed-mode bonded films in Section 3.3. It has been shown that the amount of exposed gold at a modified electrode can be evaluated by electrochemically oxidizing and reducing the modified electrode.[15] Sweeping the potential of the electrode positively in 0.1 M H_2SO_4 oxidizes the gold surface at potentials more positive than approximately 1.0 V vs. Ag/AgCl. The return sweep typically yields a sharp, cathodic wave at 0.9 V due to the reduction of the oxidized Au surface. The integrated total charge per unit area, q, of this wave is proportional to the amount of gold surface exposed.[16] The fractional surface coverage of the gold surface by the NAB layer, θ_{NAB}, is obtained when the q value of a derivatized electrode is normalized to q_0, the integrated charge for an unmodified electrode. Thus, θ_{NAB} is calculated as,

$$\theta_{NAB} = 1 - \left(\frac{q}{q_0} \right) \qquad [2]$$

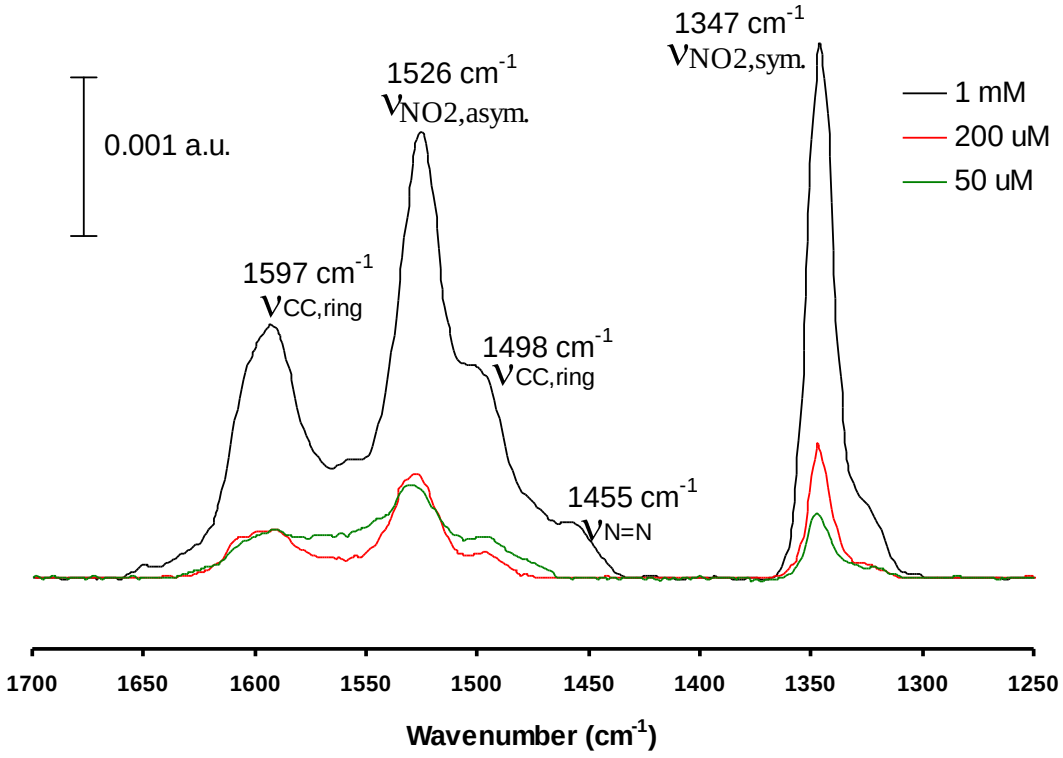

Figure 4.05. The fingerprint region of the IRRAS spectrum for gold electrodes modified with NAB as a function of c_{NABDF}.

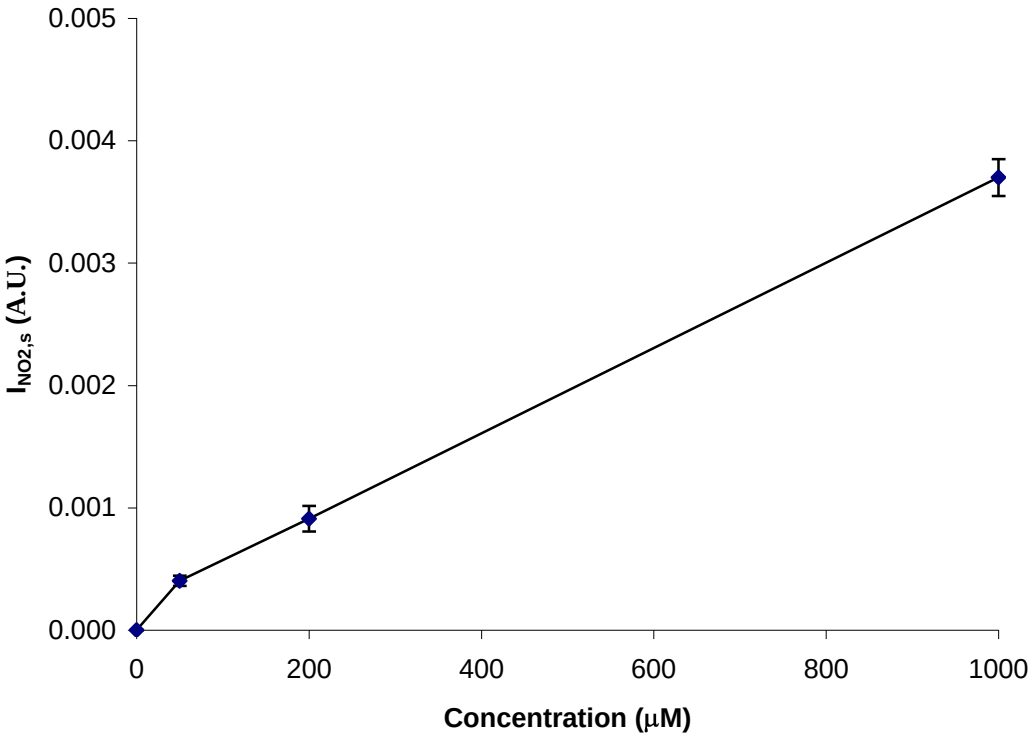

Figure 4.06. A plot of of A_{1347} vs. c_{NABDF} for NAB films on gold. The data points are connected with lines merely to guide the eye. Error bars represent the standard deviations observed for 2 independent measurements.

c_{NABDF}	A_{1347} / A_{1526}
NABDF Powder[a]	1.45
1 mM	1.21 ± 0.03
200 μM	1.28 ± 0.05
50 μM	0.63 ± 0.05

[a]Result taken from Chapter II (Table 2.02).

Table 4.02. The ratio of A_{1347} / A_{1526} as a function of c_{NABDF}. The values are averages of duplicate measurements.

Cyclic voltammograms of gold electrodes modified with different c_{NABDF}'s in 0.1 M H_2SO_4 are presented in Figure 4.07. Table 4.03 lists the q values and calculated θ_{NAB} values. The results show that NAB films deposited with c_{NABDF}'s of 50 μM and 200 μM have relatively low surface coverages with 70% and 61% of the gold surface exposed, respectively. This suggests that the NAB groups are not very densely packed and numerous defect sites are present. This is consistent with the AFM and IRRAS results which suggest that layers formed from 50 μM and 200 μM solutions are approximately a monolayer with slight differences in the density of the NAB groups. For a c_{NABDF} of 1 mM, the surface coverage is much higher, though 10 % of the gold surface is still exposed. Importantly, the Au oxidation/reduction results provide an indication of the amount of Au surface available for reaction with alkanethiols to create the mixed-mode bonding layers.

The examination of electron transfer through the layers to redox species in solution will provide further information on their permeability. Electron transfer was probed using CV in the presence of two redox probes: $Ru(NH_3)_6^{3+/2+}$ and $Fe(CN)_6^{3-/4-}$. It is generally accepted that electron transfer between $Ru(NH_3)_6^{3+/2+}$ and gold occurs via an outer-sphere pathway. There is some controversy that electron transfer between $Fe(CN)_6^{3-/4-}$ and oxygen-containing surfaces occurs via an inner-sphere mechanism.[17-20] For the sake of interest, and the possibility that this may not be an issue with the NAB-modified electrodes, we employed the $Fe(CN)_6^{3-/4-}$ probe. Cyclic voltammograms for the NAB-modified electrodes in 1 mM $Ru(NH_3)_6^{3+/2+}$ and 1 mM $Fe(CN)_6^{3-/4-}$ in 0.1 M KCl are presented in Figures 4.08 and 4.09 respectively. Table 4.04 summarizes the ΔE_p values and the peak currents from the voltammograms (*i.e.,* $I_{p,c}$ for $Ru(NH_3)_6^{3+/2+}$ and $I_{p,a}$ for $Fe(CN)_6^{3-/4-}$). The ΔE_p value measured from a cyclic voltammogram is a measure of electron transfer rate. A lower ΔE_p corresponds to a higher electron transfer rate constant, k°. The peak current, I_p, is also influenced by k° and, in addition, depends on the amount of exposed electrode area.

The ΔE_p values for the $Ru(NH_3)_6^{3+/2+}$ voltammetry at electrodes modified with c_{NABDF}'s of 50 μM and 200 μM are very similar to that of an unmodified gold electrode. This is in good agreement with the surface coverage measurements, which show that there is a significant amount of unmodified areas on these electrodes. Thus, k° for these films should be similar to that of unmodified Au. In the case of the c_{NABDF} = 50 μM electrode, gold oxidation/reduction voltammetry shows that 30 % of the surface is covered yet $I_{p,c}$ in the presence of $Ru(NH_3)_6^{3+/2+}$ only decreases by 9 %. It is therefore not

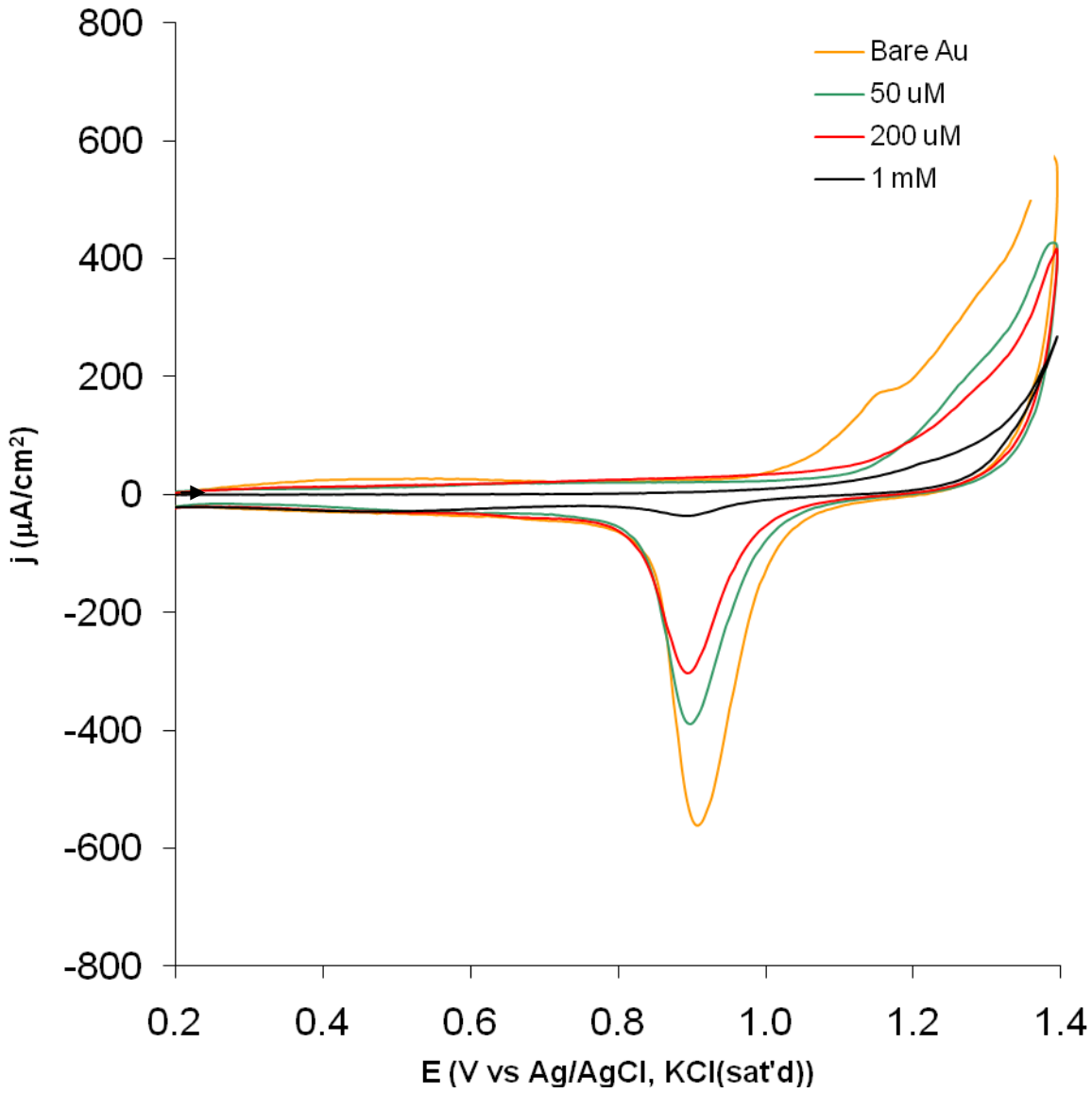

Figure 4.07. Cyclic voltammograms of NAB-modified gold in 0.1 M H_2SO_4. The sweep rate is 100 mV/s.

c_{NABDF}	q ($\mu C/cm^2$)	θ_{NAB} (%)
bare Au	12352	0
50 mM	8661	30 +/- 1
200 mM	7570	39 +/- 7
1 mM	1254	90 +/- 2

Table 4.03. Surface coverage estimations for gold electrodes modified with NAB films. Calculations are based on the total charge integrated under the gold oxide reduction wave as observed in Figure 4.07. Error estimations are based on statistics from two independent samples.

likely that the NAB exits on the surface in the form of large "patches". Rather, the data suggests that the ~60-70 % of active area on these electrodes is behaving as an array of microelectrode-sized active sites dispersed in regions modified with NAB. The observation of similar ΔE_p values and $I_{p,c}$ as bare Au implies that the size and distance between the active areas must be much smaller than the diffusion layer thickness in this experiment. Under these conditions, the diffusion layers of the individual active areas overlap. The result is that the current is controlled by planar diffusion to the entire electrode area.[21] On the time scale of these CV experiments, we estimate the size of the diffusion layer on the axis parallel to the electrode surface to be 34 μm. Our calculations indicate that, geometrically, this situation is feasible.

The observed ΔE_p for the electrode modified with a c_{NABDF} of 1 mM is significantly greater than that of an unmodified electrode. This result suggests a much lower k° and is likely the result of electron transfer according to a through-film $k°_{app}$ instead of k° of the unmodified gold. Given the measured θ_{NAB} of 90% for this electrode,

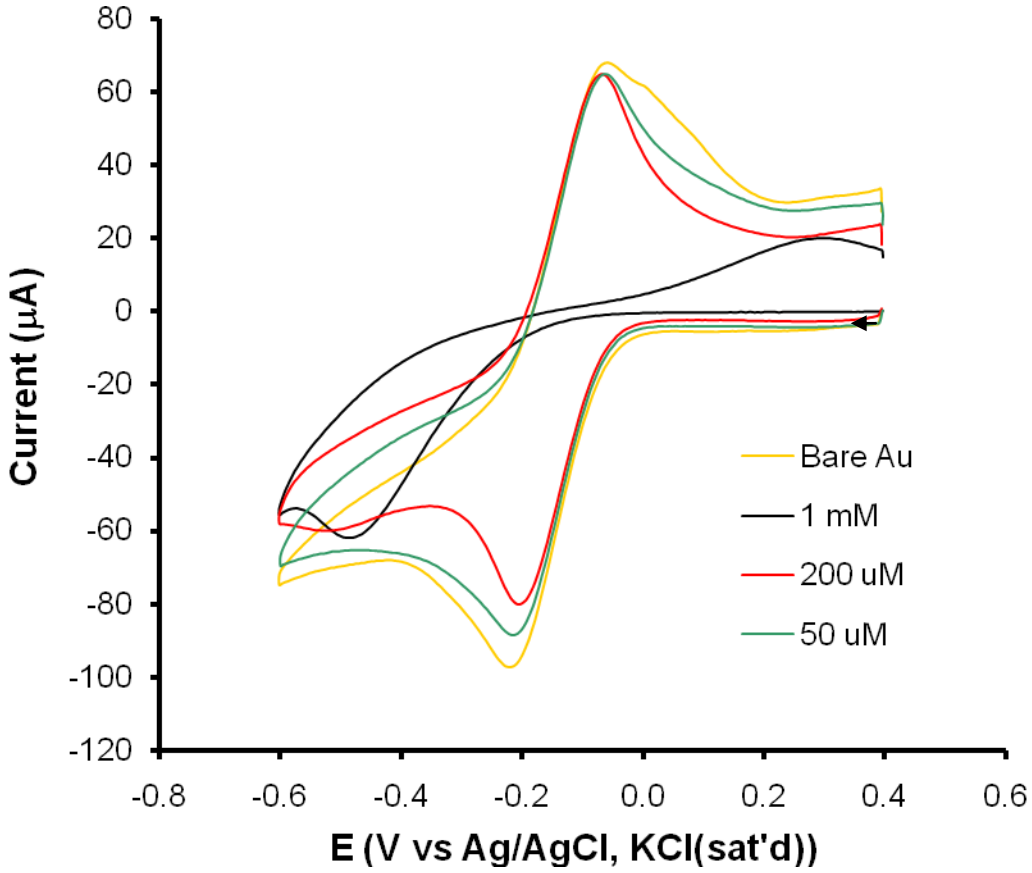

Figure 4.08. Cyclic voltammograms of NAB-modified gold electrodes in a solution of 1 mM $Ru(NH_3)_6^{3+/2+}$ in 0.1 M KCl. The sweep rate is 100 mV/s.

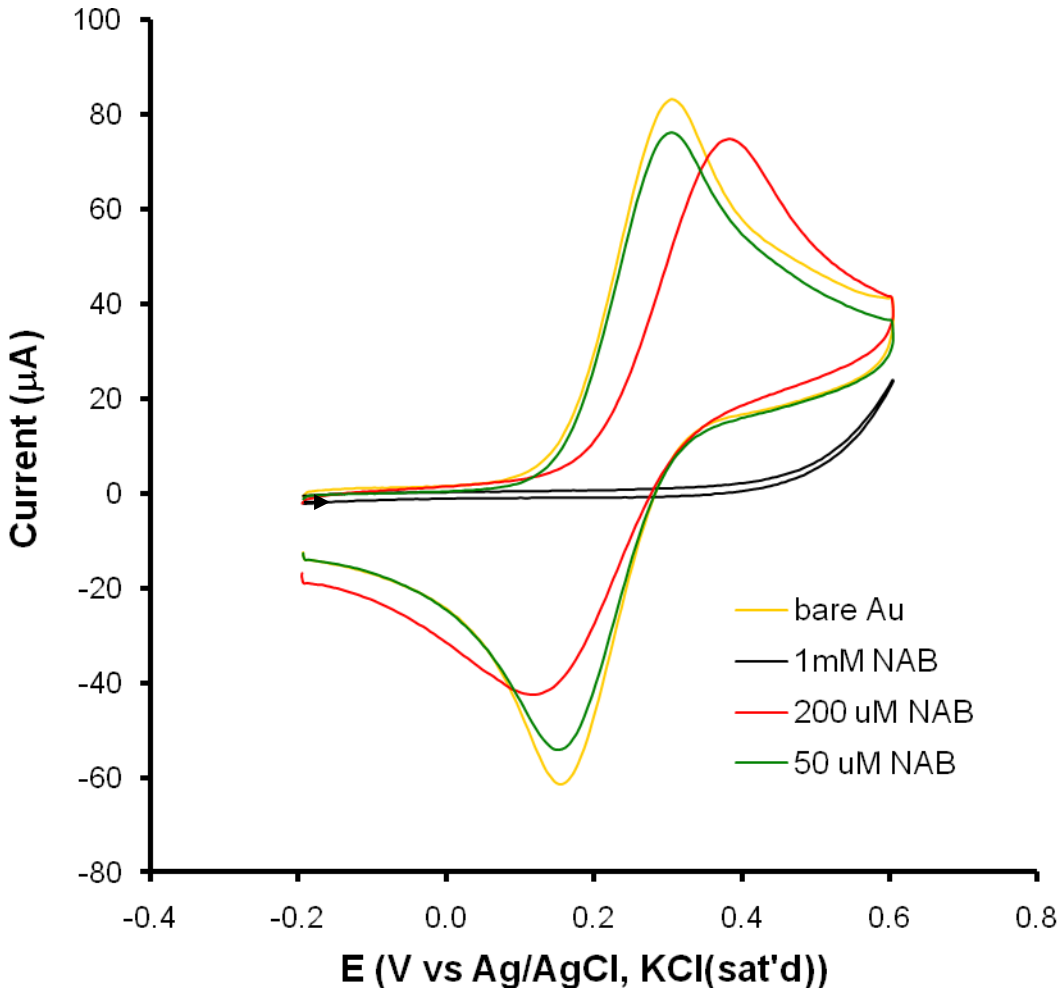

Figure 4.09. Cyclic voltammograms of NAB-modified gold electrodes in a solution of 1 mM $Fe(CN)_6^{3-/4-}$ in 0.1 M KCl. The sweep rate is 100 mV/s.

	$Ru(NH_3)_6^{3+/2+}$		$Fe(CN)_6^{3-/4-}$	
	ΔE_p (mV)	$I_{p,c}$ (μA)	ΔE_p (mV)	$I_{p,a}$ (μA)
bare Au	161	-97	158	83
50 μM NAB	155	-88	153	76
200 μM NAB	145	-80	269	75
1 mM NAB	787	-62	> 1000	NA

Table 4.04. A summary of the electrochemical blocking results for NAB-modified gold electrodes. ΔE_p, and I_p values were investigated separately for two redox probes: $Ru(NH_3)_6^{3+/2+}$ and $Fe(CN)_6^{3-/4-}$. For all experiments, the sweep rate is 100 mV/s.

it would be expected that electron transfer would take place more readily at the presumed 10 % defective regions. This is not the case, however, and it appears that the regions accessible for gold oxidation voltammetry are not accessible to $Ru(NH_3)_6^{3+/2+}$. Our interpretation of this result is that electrons transfer through the 4.7 nm thick regions of NAB groups with an apparent rate constant $k°_{appt}$ such that $k°_{appt} < k°_{Au.}$

The $Fe(CN)_6^{3-/4-}$ electrochemical blocking results largely mirror those observed with $Ru(NH_3)_6^{3+/2+}$. There are, however, some significant differences. An electrode modified with a c_{NABDF} of 200 μM displays a significantly larger ΔE_p value compared to that of an unmodified gold surface. From the $Ru(NH_3)_6^{3+/2+}$data, a change in ΔE_p was not observed for c_{NABDF}'s lower than 1 mM. Similarly, ΔE_p could not be measured for a at a film formed from a c_{NABDF} of 1 mM when $Fe(CN)_6^{3-/4-}$. These observations support the notion that $Fe(CN)_6^{3-/4-}$ is more sensitive to surface chemistry, compared to $Ru(NH_3)_6^{3+/2+}$.

In summary, the deposition conditions for the NAB component of a mixed-mode film can be altered such that the thickness, density and structure of the NAB groups are

controllable. Furthermore, the results in Chapters II and III provided evidence that a large portion of the layer is not very tightly bound to the substrate and susceptible to displacement by long-chain alkanethiols. Thus, different initial densities of the NAB layers should afford various mixed-mode structures following exposure to the alkanethiol solution. This will be explored in the next section.

3.2 Spectroscopic Characterization of Mixed-Mode NAB:DDT Layers

The first part of our strategy to characterize mixed-mode layers is to examine the effect of introducing dodecanethiol (DDT) to the pre-existing NAB layers on the gold surface. The notation that will be used to refer to a particular mixed-mode composition will be as follows: c_{NABDF}: DDT. Thus a mixed-mode layer prepared by depositing NAB with a c_{NABDF} of 1 mM will be denoted: 1 mM NAB:DDT.

Our investigation was first carried out with IRRAS, by observing changes to the NAB bands following exposure to DDT. IRRAS spectra were recorded for NAB layers deposited with c_{NABDF}'s of 1 mM, 200 μM, and 50 μM before and after immersion into a dilute, ethanolic DDT solution for 24 hours. The results are presented in Figure 4.10.

Figure 4.10a demonstrates that, for films formed from a c_{NABDF} of 1 mM, very little material is lost following exposure to DDT. This statement is based on the change in A_{1347}, which changes from 37 mAU to 34 mAu (*i.e.*, an 8% reduction). To understand these results, it is useful to consider radical-radical coupling reactions. Radical-radical coupling reactions are an important consideration in the context of the electrochemical reduction of aryldiazonium cations.[15, 22, 23] Briefly, aryl radicals can couple to form dimeric species, a process that is in competition with the direct attachment of the radical

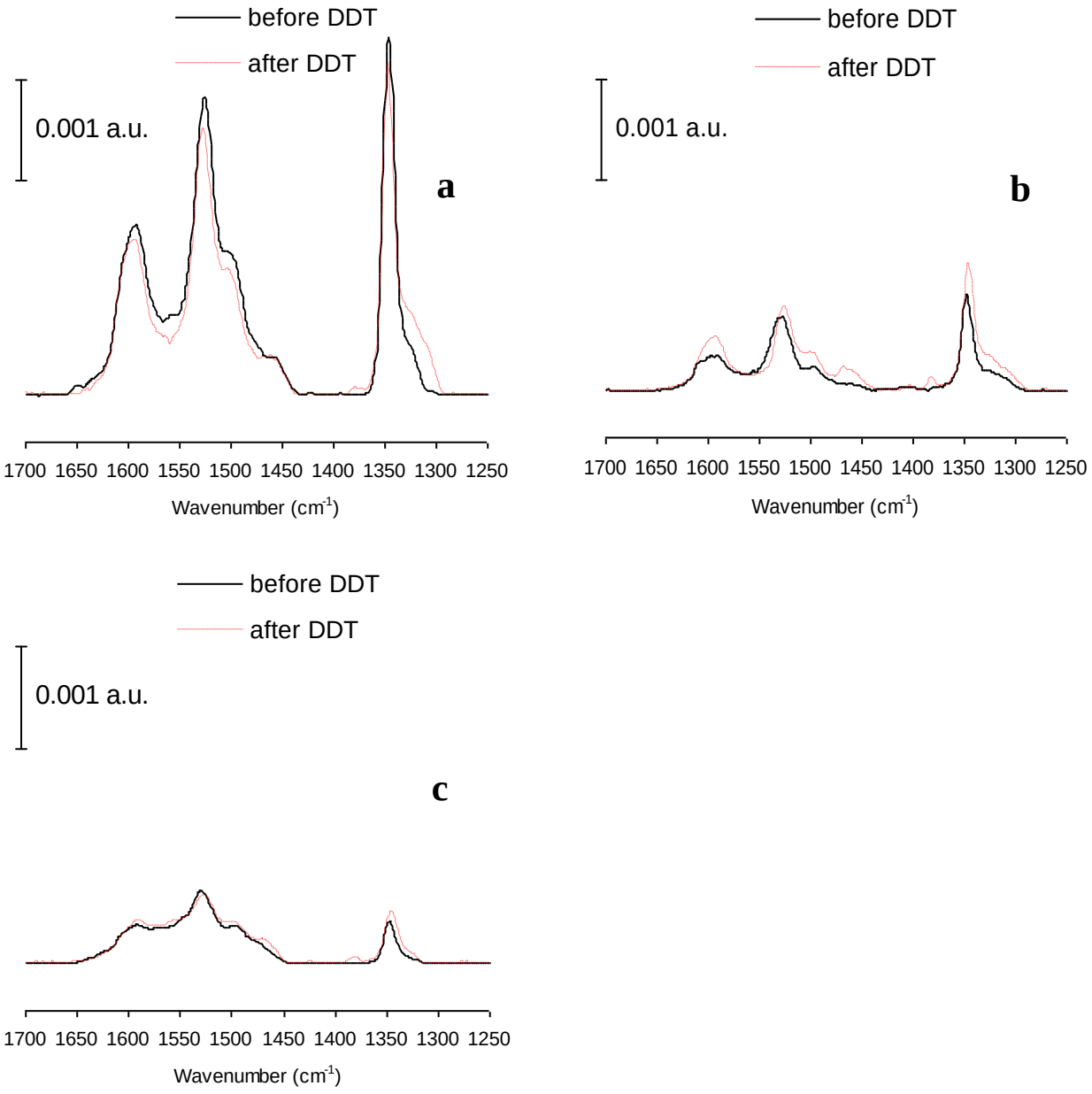

Figure 4.10. IRRAS spectra of mixed-mode molecular layers after the NAB component has been exposed to a DDT solution. a) c_{NABDF} = 1 mM, b) c_{NABDF} = 200 μM, c) c_{NABDF} = 50 μM. The black, solid traces represent spectra for which no DDT has been introduced. Red, dashed lines represent spectra for which a DDT component has been introduced.

to the surface. It is our opinion that material lost during alkanethiol displacement reactions is largely due to the loss of physisorbed NAB dimers that intercalate into the bound networks of NAB groups.[24] At high c_{NABDF}'s, the probability that two electrochemically generated aryl radicals will encounter each other will increase and therefore radical-radical coupling is expected to increase. Thus a larger portion of the film consists of weakly bound NAB dimers that are readily displaced by alkanthiolates at the surface.

The introduction of DDT to NAB layers formed from lower c_{NABDF}'s (*i.e.*, 50 μM and 200 μM) does not produce a significant change in the IR spectrum. Observe that the "before" and "after" spectra in Figures 4.10 b and 4.10c are similar within experimental error. We believe this is because the probability of a radical-radical coupling process is reduced at these low concentrations. In summary, our results demonstrate that DDT has a noticeable, although minimal effect on the pre-existing NAB films in terms of material lost.

The initial amount of NAB on the gold surface has a noticeable effect on the DDT band structure in the CH stretching region, as demonstrated in Figure 4.11. This is especially true for the asymmetric methylene C-H stretching vibration, $\upsilon_a(CH_2)$. The sensitivity of this band to the chemical environment of the alkane chain has been discussed at great length by Porter and coworkers.[25] In the case of a pure DDT monolayer, the position of $\upsilon_a(CH_2)$ at 2919 cm^{-1}, is indicative of tightly packed polymethylene chains that adopt an all-trans configuration.[26] From Figure 4.11 it is evident that as the amount of NAB initially on the surface increases, the position of $\upsilon_a(CH_2)$ shifts from 2919 cm^{-1}, the value observed for a monolayer of DDT, to 2925 cm^{-1},

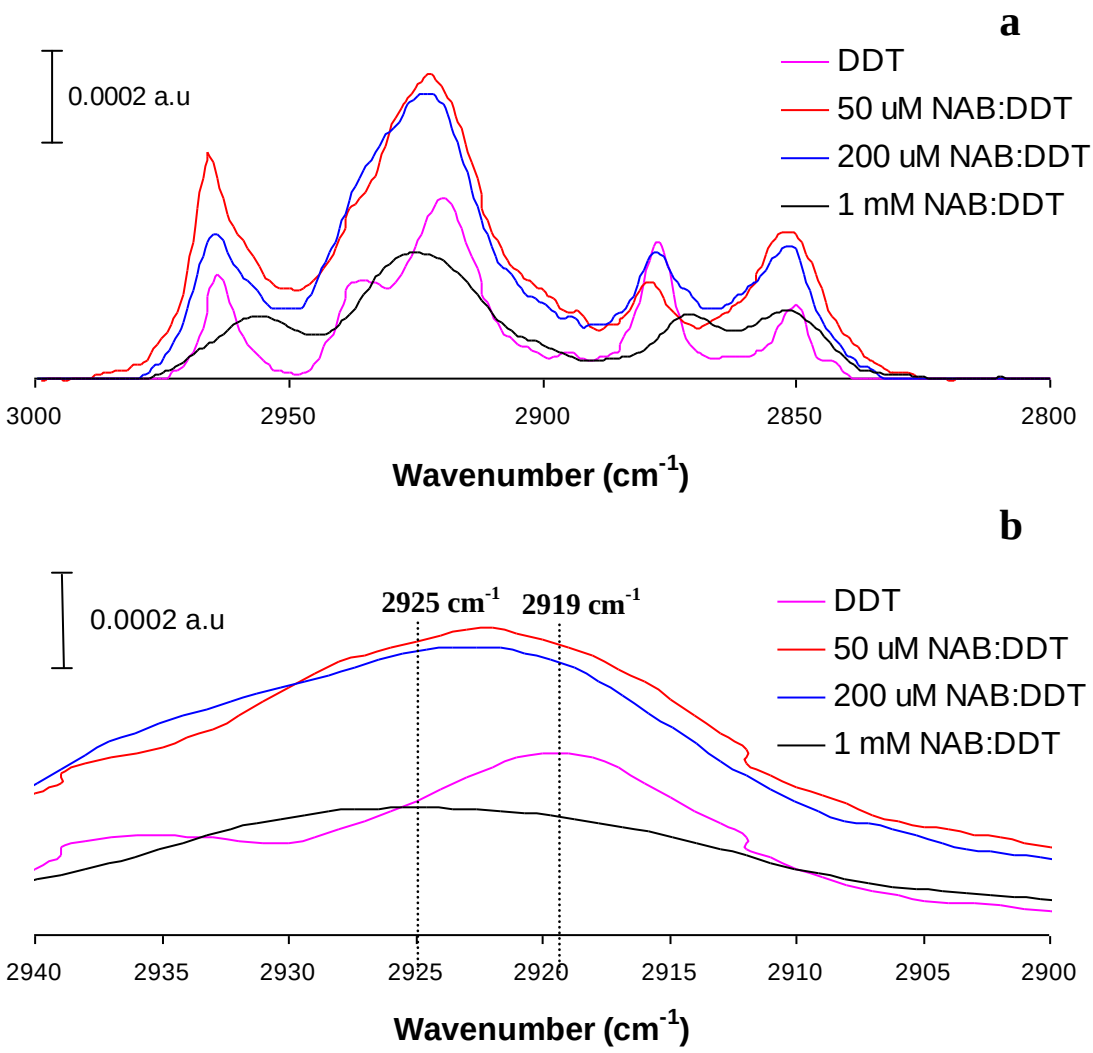

Figure 4.11. a) The CH stretching region of the IRRAS spectrum of mixed-mode molecular layers after the NAB component has been exposed to a DDT solution. b) An expansion of the region containing the $\upsilon_a(CH_2)$ mode.

the value observed for a 1 mM NAB:DDT film. The shifting of the $\upsilon_a(CH_2)$ band to higher wavenumbers with increasing c_{NABDF}'s implies that the alkyl chains become increasingly more disordered and take on a liquid-like structure when a greater amount of NAB is on the surface initially. We suspect that this is because the high density of NAB does not permit the formation of extended, crystalline DDT domains.

3.3 Characterization of NAB Layers and Mixed-Mode NAB:DDT Layers on Au by XPS.

Both the single component NAB layers and the NAB:DDT mixed-mode molecular layers were characterized by high resolution XPS (HRXPS). Core level spectra were collected for Au 4f, C 1s, O 1s, and N 1s photoelectrons. S 2p spectra were also collected for the mixed-mode layers. A table summarizing the results for all layers in terms of surface atomic composition (% at.) is presented as Table 4.05.

Core level N 1s spectra for the single component NAB films are shown in Figure 4.12. A reduced nitrogen peak is present at 400 eV and an oxidized nitrogen peak at 406 eV. The results compare well, in terms of the types of nitrogen present, with XPS studies performed on NB layers on Au.[15, 24] Qualitatively, the ratios of these peaks are reversed when compared to the NB studies. For NB layers, the intensity of the 406 eV peak is larger than the 400 eV peak. This trend is reversed here and the 400 eV peak is larger due to the presence of the azo functionality in the NAB structure. More

	Au	C	O	N	S
unmodified Au	97.2	2.1	0.71	0	0
50 μM NAB	96.6	2.5	0.5	0.5	0
50 μM NAB:DDT	94.5	4.9	0	0	0.6
200 μM NAB	92.7 +/- 0.2	5.0 +/- 0.1	1.0 +/- 0.2	1.3 +/- 0.1	0
200 μM NAB:DDT	92.2 +/- 0.8	6.7 +/- 0.6	0.22 +/- 0.01	0.3 +/- 0.2	0.61 +/- 0.01
1 mM NAB	67 +/- 3	22 +/- 3	5.0 +/- 0.4	5.8 +/- 0.2	0
1 mM NAB:DDT	62.0 +/- 0.8	26.06 +/- 0.01	5.3 +/- 0.3	6.4 +/- 0.5	0.27 +/- 0.01
DDT	93.6	5.6	0	0	0.8

Table 4.05. A table summarizing % at. for all single component NAB and NAB:DDT films investigated. Where indicated, error estimations are based on results of duplicate trials.

Sample homogeneity was also evaluated by assessing different spots on the same sample. %RSDs were typically 1-6% for any given element.

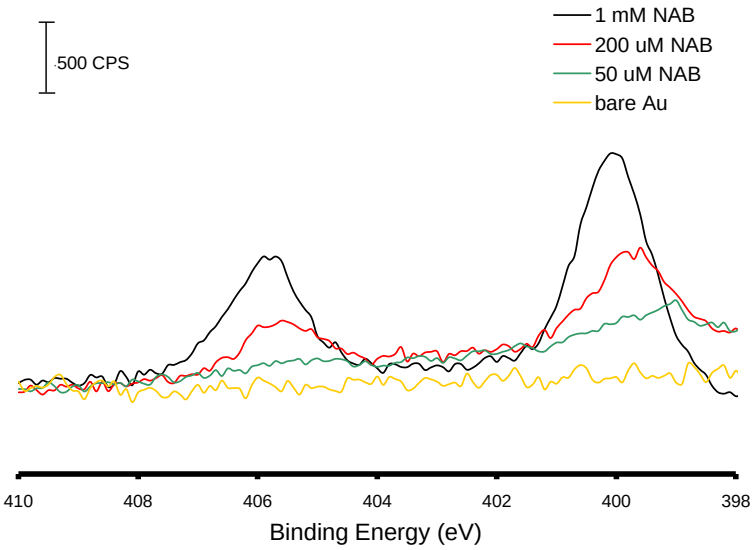

Figure 4.12. Core level N 1s HRXPS spectra for single component NAB layers.

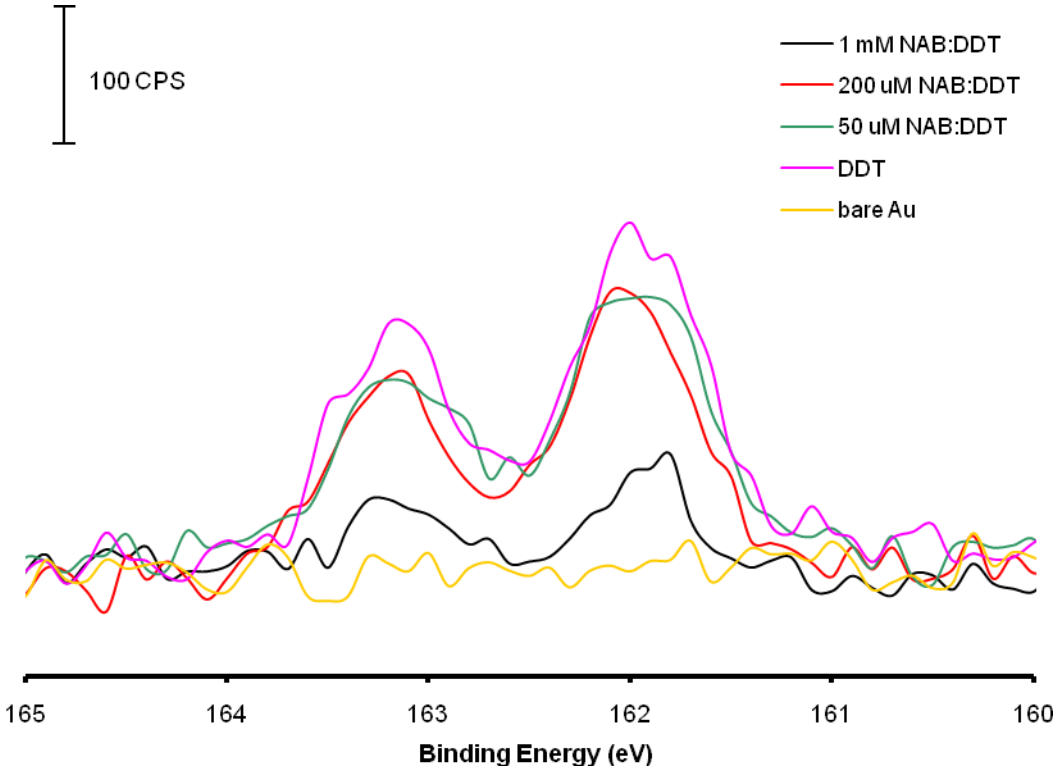

Figure 4.13. Core level S 2p HRXPS spectra for NAB:DDT mixed-mode molecular layers and a DDT monolayer.

importantly, the ratio appears to remain constant at all c_{NABDF}'s studied, indicating that the layer composition is quite consistent throughout the film growth process.

Figure 4.13 consists of S 2p core level spectra for the NAB:DDT mixed layers. The DDT monolayer produces the highest % S at the surface, 0.8 %, which is understandable since a complete monolayer can form on the entire gold surface. The 50 μM NAB:DDT and 200 μM NAB:DDT electrodes produce identical % S values of 0.6%. This result suggests that ~¾ of a DDT monolayer adsorbs to these electrodes. Recall the θ_{NAB} values calculated for the single component NAB electrodes (Table 4.03). These results are in good agreement with the %S values measured by XPS, since these electrodes displayed a relatively large amount of exposed gold. The measured %S of the 1 mM NAB:DDT electrode is 0.3 %. This is consistent with the calculated θ_{NAB} value of 90 % for this electrode because it should therefore have the smallest amount of free surface available for DDT adsorption. The intensity of the Au 4f photoelectrons is attenuated in the single component NAB layers. This can be observed in Table 4.05. The NAB layers formed from 50 μM and 200 μM solutions attenuate the Au 4f signal by only a small amount, presumably because they are approximately one monolayer thick. Films formed from 1 mM solutions cause a much larger attenuation of the Au 4f peaks, because they are much thicker. Bélanger and coworkers observed similar results where a 4.7 nm layer of 4-diethylaniline (DEA) groups caused a significant attenuation of the Au 4f signal.[15] In the same study NB layers ~10 nm thick nearly caused a complete attenuation of the Au 4f signal.

The introduction of DDT to NAB films prepared from 50 μM and 200 μM solutions results in a marked decrease in the %N. This result is inconsistent with the

IRRAS results in Figure 4.10, which show that the incorporation of DDT has minor effects on the intensities of the NAB bands. We do not believe DDT is displacing all of the NAB in these films. The %S values from the 50 μM:DDT and 200 μM:DDT films support this. That is, the 0.6 % S detected in these films is less than that observed for a monolayer of DDT. However, it is likely that some of the NAB is displaced by DDT for these lower concentration films. It is also possible that the DDT chains relax to cover NAB molecules, resulting in the attenuation of the N 1s photoelectrons.

The introduction of DDT also has the effect of increasing the %C detected in the mixed-mode layers when compared to the NAB layers. This is noticeable for NAB layers formed at low solution concentrations, but the largest change in %C is observed for layers formed from a 1 mM solution. This result disagrees with the θ_{NAB} calculated for an NAB layer formed from a 1 mM solution, which suggests that it should have the smallest amount of Au surface available for DDT adsorption compared to the other NAB-derivatized electrodes. We do not fully understand this result at this time.

3.4 Characterization of Mixed-Mode NAB:DDT Layers by Electrochemical Methods.

The mixed-mode films were investigated in terms of surface coverage and electrochemical blocking performance. The fractional surface coverages of the NAB:DDT mixed layers, $\theta_{NAB:DDT}$, were estimated by performing gold oxidation voltammetry in 0.1 M H_2SO_4. The cyclic voltammograms in 0.1 M H_2SO_4 are presented in Figure 4.14 and the $\theta_{NAB:DDT}$ calculations are summarized in Table 4.06.

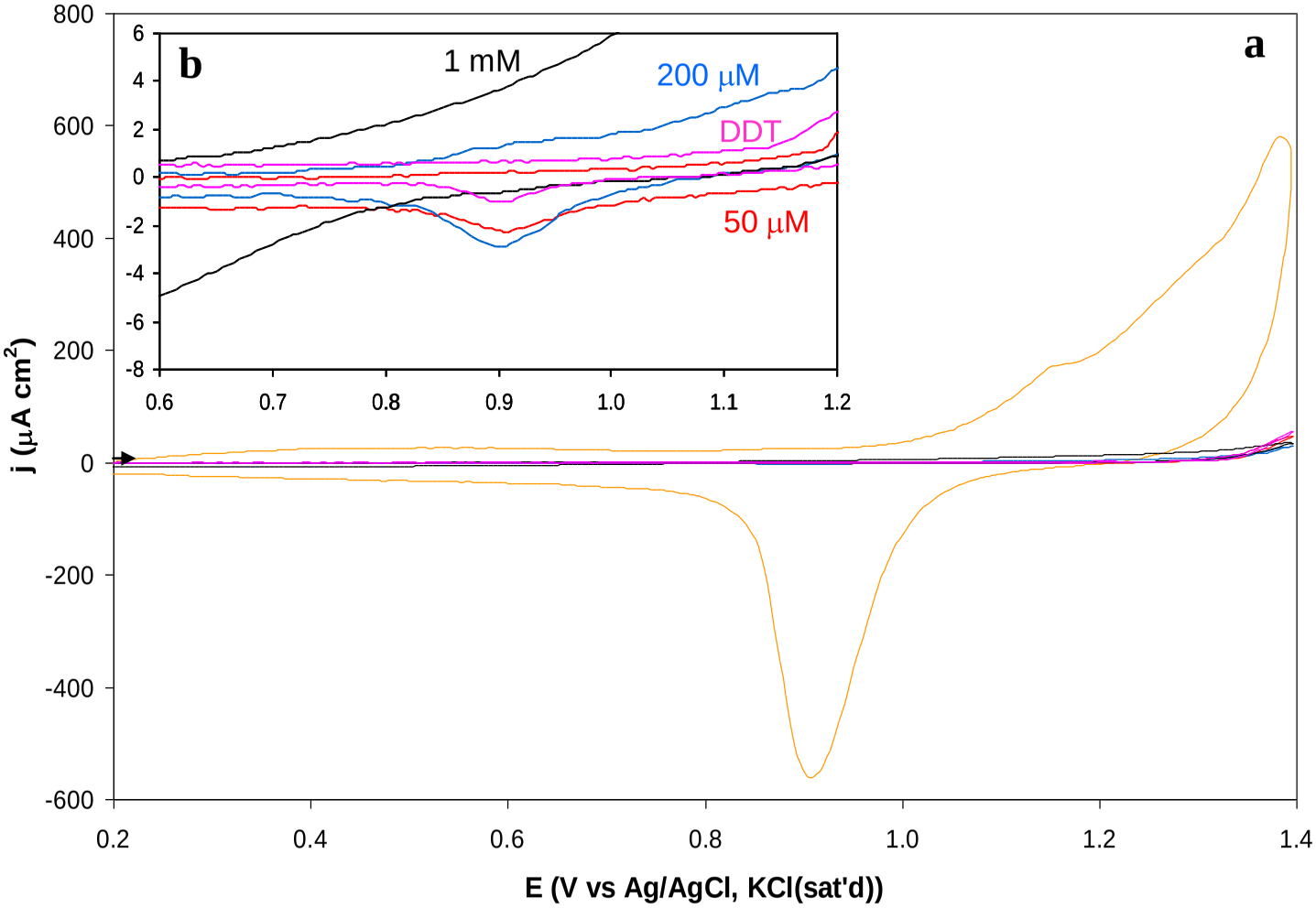

Figure 4.14. **a)** Cyclic voltammograms of NAB:DDT mixed molecular layers on gold in 0.1 M H_2SO_4. The sweep rate is 100 mV/s. **b)** Inset: An expansion of the region with the gold oxidation wave.

c_{NABDF}	q ($\mu C/cm^2$)	$\theta_{NAB:DDT}$ (%)
bare Au	12352	0
50 mM:DDT	144	99 +/- 1.0
200 mM:DDT	73	99.4 +/- 0.2
1 mM:DDT	14	99.9 +/- 0.1
DDT	32	99.7 +/- 0.1

Table 4.06. Surface coverage estimations for gold electrodes modified with NAB:DDT mixed molecular films. Error estimations are based on statistics from two independent samples.

By comparing the $\theta_{NAB:DDT}$ values obtained for the NAB:DDT mixed layers to those of the NAB layers alone (Table 4.03), we conclude that mixed-mode layers exhibit much higher surface coverages overall. Any exposed gold that is present in the initial NAB film is occupied by DDT. From Figure 4.14b it is observed that solvent (*e.g.* H_3O^+ ions) cannot reach the gold surface through a DDT monolayer. The data also suggests that when the NAB component is quite thick, as is the case with the 1 mM NAB:DDT electrode, solvent cannot efficiently reach the surface either. Further, only the 50 μM NAB:DDT and 200 μM NAB:DDT films show a measurable gold reduction peak. If we assume that this result is due to layer porosity, then it is reasonable to say that the thinner NAB regions are more porous to the solvent than thicker NAB regions. Another possibility is that solvent reaches the surface at defects near the NAB-DDT domain boundary regions. If this is the case, more defects occur at lower c_{NABDF}'s, however, defect regions account for < 1 % of the total surface.

The electrochemical blocking characteristics of the mixed-mode layers were interrogated using $Ru(NH_3)_6^{3+/2+}$ and $Fe(CN)_6^{3-/4-}$ as redox probes (Figures 4.15 and

4.16). A summary of the measured ΔE_p and, $I_{p,c}$ or $I_{p,a}$, values is presented in Table 4.07. Again, the discussion will be focused on the results for $Ru(NH_3)_6^{3+/2+}$. Recall that layers from 50 μM and 200 μM NAB solutions alone showed no change in ΔE_p when compared to an unmodified electrode. In Figure 4.15, observe that 50 μM NAB:DDT and 200 μM NAB:DDT mixed layers produce higher ΔE_p values compared to an unmodified Au surface. This result indicates that no free surface is available for direct electron transfer to $Ru(NH_3)_6^{3+/2+}$.

We feel that the mixed-mode bonded layers are excellent systems to probe through-layer electron transfer mechanisms because, as shown in Table 4.06, they are essentially defect free. For example, it is possible to measure ΔE_p for the 50 μM NAB:DDT and 200 μM NAB:DDT electrodes but not for a DDT monolayer (Figure 4.15). Further, the gold oxide reduction data suggests that this result is not attributed to increased amounts of defects in the mixed films (Figure 4.14). The observed difference in electron transfer rates for these electrodes is therefore likely attributed to two factors. Namely, these are differences in relative electron transfer rates through the NAB and DDT components and differences in the proportion of each component in the mixed layer. We propose that the overall electron transfer rate through these mixed-mode films can be expressed mathematically as a linear combination of the electron transfer rates through the respective components. For each component, the linear coefficient is equal to the fractional surface coverage of that component in the mixed layer. The equation for the overall rate of electron transfer, $k°_{film}$ is therefore:

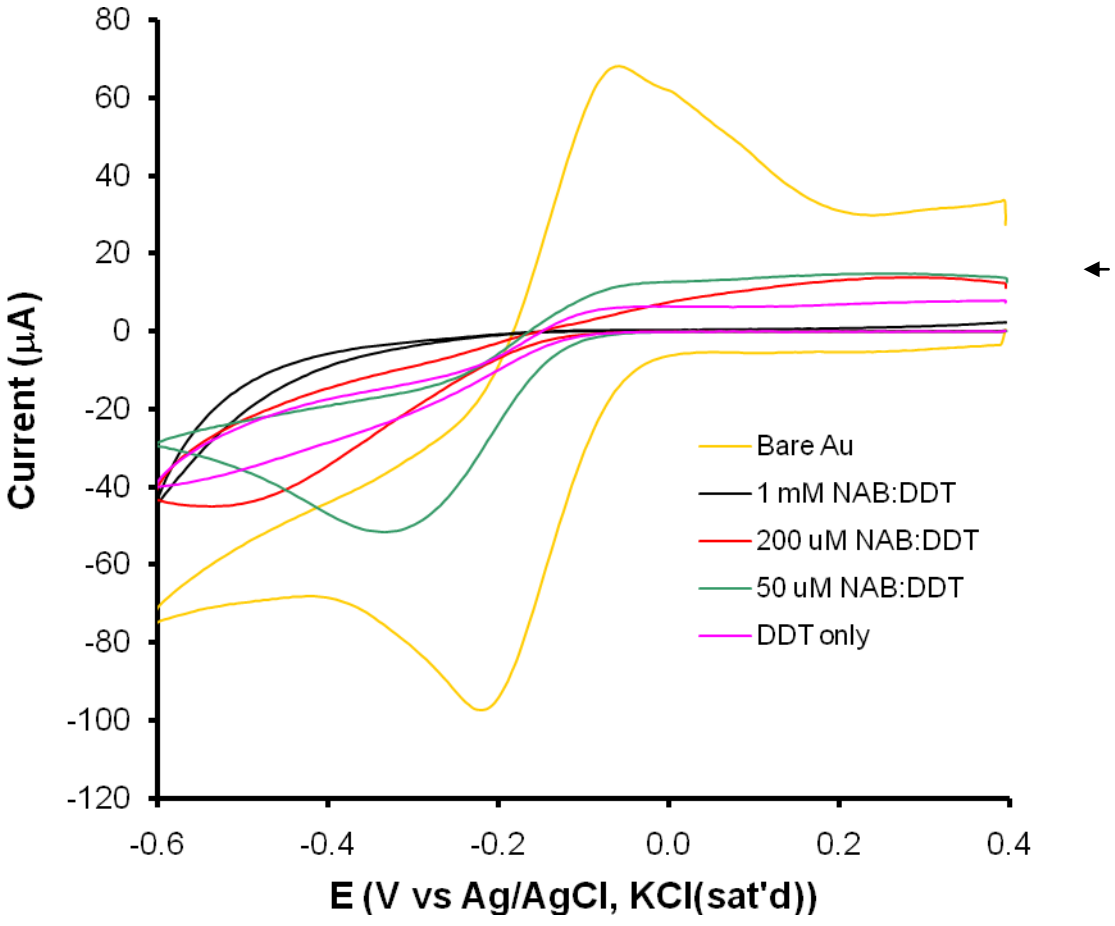

Figure 4.15. Cyclic voltammograms of gold electrodes modified with NAB:DDT in a solution of 1 mM $Ru(NH_3)_6^{3+/2+}$ in 0.1 M KCl. The sweep rate is 100 mV/s.

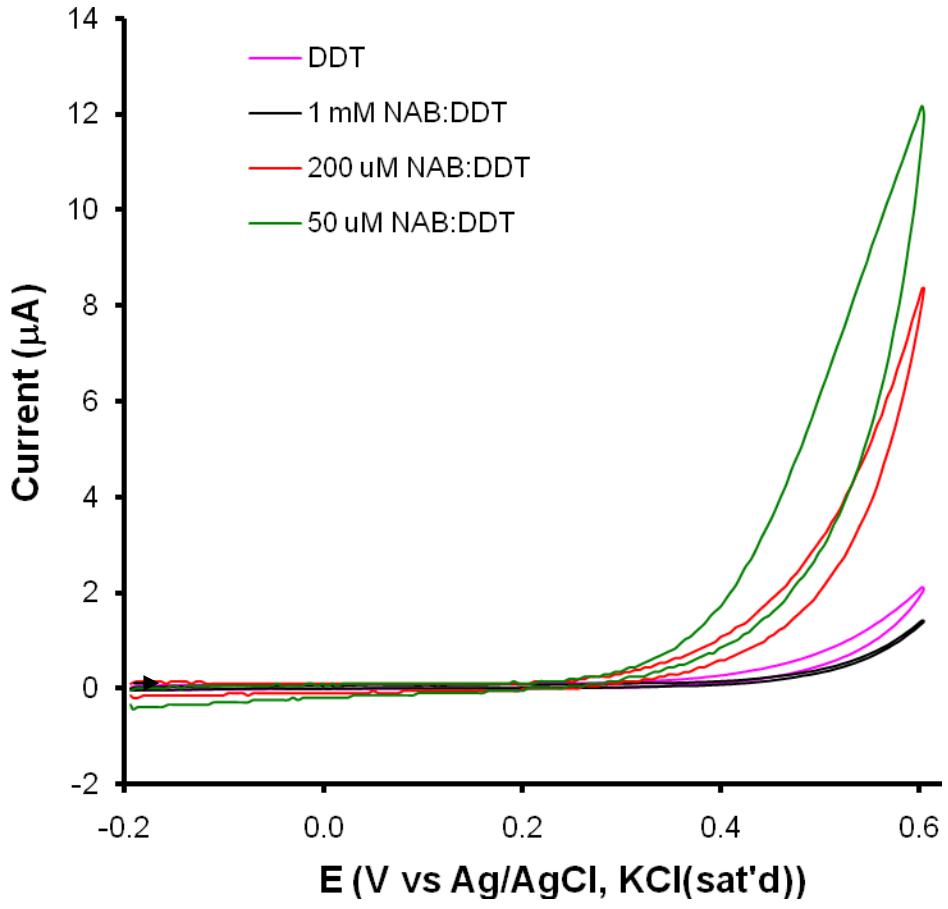

Figure 4.16. Cyclic voltammograms of gold electrodes modified with NAB:DDT in a solution of 1 mM $Fe(CN)_6^{3-/4-}$ in 0.1 M KCl. The sweep rate is 100 mV/s.This agrees with the gold oxidation data since the gold reduction peak was extremely small for these electrodes.

	$Ru(NH_3)_6^{3+/2+}$		$Fe(CN)_6^{3-/4-}$	
	ΔE_p (mV)	$I_{p,c}$ (μA)	ΔE_p (mV)	$I_{p,a}$ (μA)
bare Au	161	-97	158	83
50 μM NAB	596	-52	NA	NA
200 μM NAB	829	-45	NA	NA
1 mM NAB	NA	NA	NA	NA
DDT	NA	NA	NA	NA

Table 4.07. A summary of the electrochemical blocking results for NAB:DDT mixed layers on gold electrodes. ΔE_p, and I_p values were investigated separately for two redox probes: $Ru(NH_3)_6^{3+/2+}$ and $Fe(CN)_6^{3-/4-}$. For all experiments, the sweep rate is 100 mV/s.

$$k^\circ_{film} = \theta_{NAB} k^\circ_{NAB} + (1-\theta_{NAB}) k^\circ_{DDT} \qquad [3]$$

where θ_{NAB} is the fractional surface coverage of the NAB, k°_{DDT} is the electron transfer rate through the DDT component and k°_{NAB} is the electron transfer rate through the NAB component.

The observed ΔE_p of the 50 μM NAB:DDT electrode is smaller (and thus k°_{film} is higher) than that of a DDT monolayer. NAB is likely the minor component in this film since the amount of DDT in the film is ~75 % of that in a DDT monolayer (Table 4.05). The remaining 25 % of the surface is presumably occupied by monolayer regions of NAB (Table 4.01). Thus, the increase in k°_{film} must be attributed to the result that $k^\circ_{NAB(mono)} > k^\circ_{DDT}$, where $k^\circ_{NAB(mono)}$ is the electron transfer rate through an NAB monolayer. In contrast, less Faradaic current is produced at a 1 mM NAB:DDT electrode when

compared to a DDT monolayer. For example, at -0.4 V the anodic current for the DDT monolayer is ~29 μA while that for the 1 mM NAB:DDT layer is ~9 μA. Since, in this case, NAB multilayer regions are the majority component (Tables 4.01 and 4.05), it should follow that $k°_{NAB(multi)} < k°_{DDT}$. The quantity, $k°_{NAB(multi)}$, is the electron transfer rate through an NAB multilayer that is 4.7 nm thick. Qualitatively speaking, our overall interpretation of the mixed-mode layer data in terms of electron transfer rates is therefore as follows: $k°_{NAB(mono)} > k°_{DDT} > k°_{NAB(multi)}$.

The model described by Equation 3, cannot be used to explain why ΔE_p of the 50 μM NAB:DDT electrode is lower than the 200 μM NAB:DDT. Both of these mixed layers contain the same proportion of NAB monolayer regions (Tables 4.01 and Table 4.05). This result could be attributed to our previous assumption that NAB monolayers formed from 200 μM solutions are more compact than those formed from 50 μM solutions. To fully understand this result it is necessary to discuss the mechanisms of electron transport through the mixed-mode layers.

The mechanisms that govern electron transfer through the NAB layers are important to consider. For diazonium-derived aryl layers on glassy carbon, it was demonstrated that electron transfer does not occur at defect sites throughout the layer.[27] Further, McCreery and coworkers demonstrated a distance dependence on the electron transfer rate through these layers that is consistent with an electron tunneling mechanism.[28] It is therefore reasonable to assume that electron transfer through diazonium-derived aryl layers on gold occurs via electron tunneling. Equation 4 will be used to mathematically describe this process:

$$k^{\circ}_{app} = k^{\circ} \exp(-\beta \cdot d) \quad [4]$$

where k°_{app} is the observed rate constant at the modified electrode, k° is the heterogeneous rate constant for the unmodified surface, β is the electron tunneling coefficient, and d is the layer thickness. β is related to the chemical structure of the molecular layer. Reports have shown that, for alkanethiolate SAMs on gold, β is on the order of 1.0 $Å^{-1}$. [29] β values for diazonium-derived aryl layers were reported to be 0.2 $Å^{-1}$. [28] The thickness of a DDT monolayer, estimated by ellipsometry, is 2.1 nm.[25] Thus, compared to a DDT monolayer, an NAB molecule is shorter in length (1.4 nm). The shorter length of an NAB molecule and lower β value, compared to DDT, could account for the observed, higher rate of electron tunneling through an NAB monolayer compared to a DDT monolayer (Figure 4.15). Assuming β values of 0.2 $Å^{-1}$ and 1.0 $Å^{-1}$ for the NAB component and DDT component of the mixed-mode layers, respectively, one can predict k°_{film} using Equation 3 above. The quantity θ_{NAB} is obtained from Table 4.03. k° is obtained via the method of Nicholson.[30] Using a ΔE_p of 161 mV (Table 4.04), k° is equal to 1.61×10^{-3} cm/s. Using Equation 3, the predicted k°_{film} for a 50 μM NAB:DDT mixed layer is 5.3×10^{-5} cm/s. The most reasonable literature value to compare this to was obtained by McCreery and coworkers.[31] They examined relatively low electron transfer rates to the $Ru(NH_3)_6^{3+/2+}$probe at HOPG electrodes. In their study a ΔE_p of 285 mV corresponded to a k° of 5.6×10^{-4} cm/s. Given that the ΔE_p of a 50 μM NAB:DDT mixed layer is 596 mV (Table 4.07) it is not unreasonable to say that this corresponds to a k° that is very close to the value predicted by Equation 3 (5.3×10^{-5} cm/s). In addition, an electron tunneling mechanism may account for the observation that

ΔE_p of the 50 μM NAB:DDT electrode is lower than the 200 μM NAB:DDT. To elaborate, a more compact NAB monolayer would likely have a higher β value compared to one that is less compact. Thus, the electron transfer rate through the compact monolayer would be lower and ΔE_p would be higher, which is what is observed. In conclusion, we believe our model is a useful tool for describing electron transfer through the mixed-mode bonded layers.

Electron tunneling, however, is generally only accepted as an appropriate mechanism to describe electron transfer across layer thicknesses that are less than 2 nm. Considering the exponential relationship in Equation 4, electron tunneling would be a very slow process at larger distances. Electron tunneling alone is therefore not enough to explain electron transfer through the NAB multilayers because they are 4.7 nm thick. Recall that there was very little electron transport through the 1 mM NAB:DDT layers.

To understand this, it is useful to consider the growth process of an NAB multilayer. At some point during the growth, electrons would have to tunnel through pre-existing NAB layers > 2 nm in thickness, to further reduce additional NAB radicals. This could take place, but would proceed at a very low rate. Another possible explanation is that the external potentials applied during the derivatization process transform NAB molecules to a more conductive state. This notion has been described previously by McCreery and coworkers.[27] Whether electron transfer through the NAB multilayered regions occurs via electron tunneling or via conduction through networks of NAB molecules in a state of enhanced electrical conductivity, the overall rate is lower than that of NAB and DDT monolayers. The $k°_{film}$ for the 1 mM NAB:DDT electrode, predicted using Equation 3 and assuming a β of 0.2 $Å^{-1}$, is 1.2×10^{-7} cm/s. This value is consistent

with the extremely small currents observed at this electrode. Finally, Figure 4.17 provides a pictorial representation of electron transfer processes through the mixed-mode films.

The $Fe(CN)_6^{3-/4-}$ electrochemical blocking results again largely mirror the $Ru(NH_3)_6^{3+/2+}$ results. Compared to the $Ru(NH_3)_6^{3+/2+}$ data, Faradaic currents are generally much smaller with this probe. The $Fe(CN)_6^{3-/4-}$ CV results for a DDT monolayer are qualitatively very similar to those observed by Porter and coworkers.[25] The redox behavior of $Fe(CN)_6^{3-/4-}$ is more sensitive to the surface chemistry at the modified gold electrode than $Ru(NH_3)_6^{3+/2+}$.

4. Conclusions

This work shows that networks of NAB groups can coexist on a polycrystalline gold surface with dodecanethiolate adsorbates to produce a heterogeneous mixed molecular film. The composition of such films can readily be manipulated by controlling the concentration of NABDF during the electrochemical deposition step. At relatively dilute NABDF concentrations (*i.e.* ≤ 200 μM) it is possible to deposit monolayer regions of aryl groups.

Compared to single component NAB films, mixed-mode molecular films are less porous, contain fewer regions of exposed gold surface, and provide better electrical insulation. Their electrochemical properties largely depend on the thickness of the NAB component as well as the relative proportions of NAB and DDT present. We attribute this

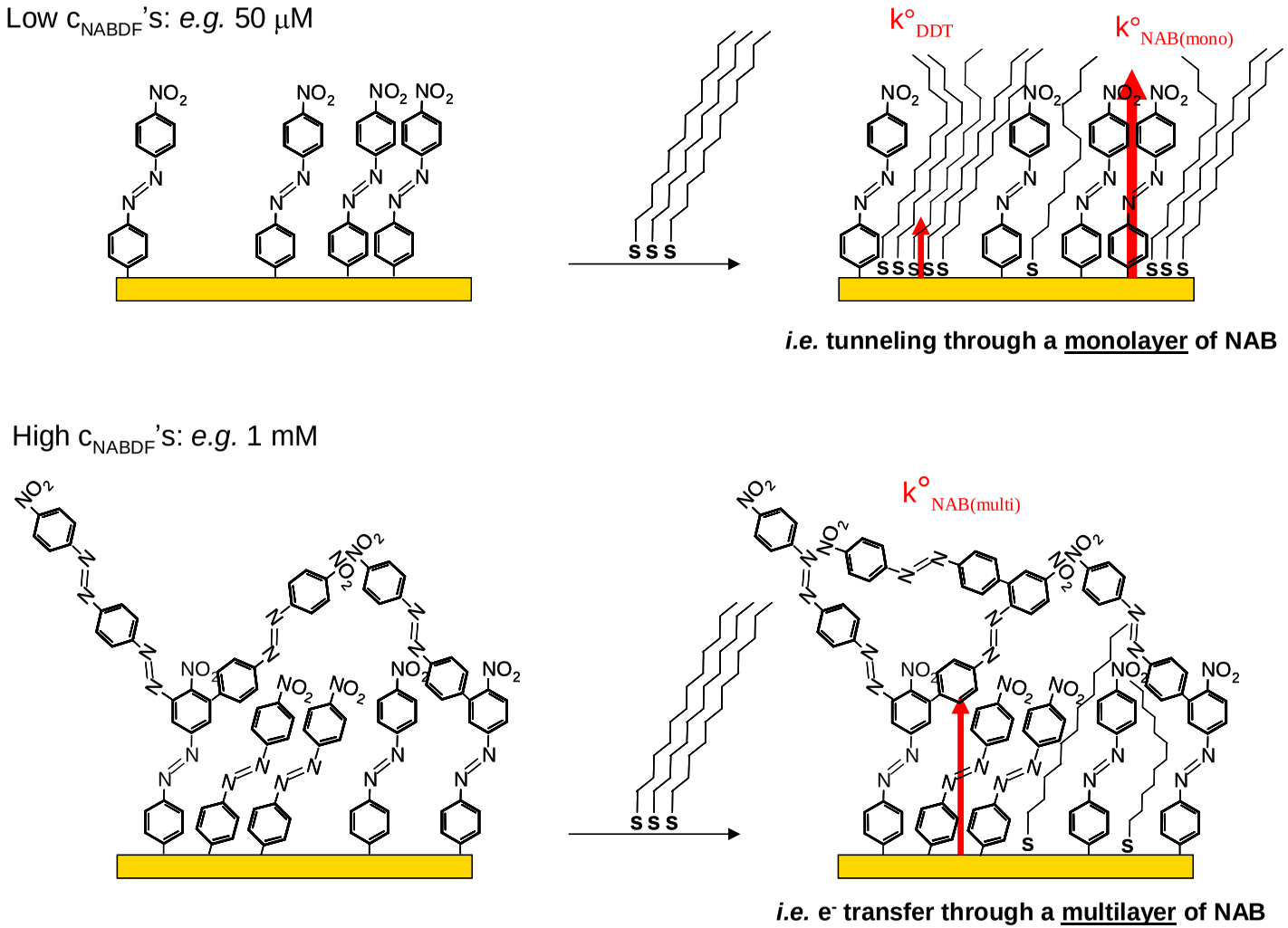

Figure 4.17. A schematic diagram illustrating electron transfer through mixed-mode layers. When low c_{NABDF}'s are used, electrons tunnel through monolayer regions of the mixed-mode layer. When higher c_{NABDF}'s are used, electrons transfer through multilayered regions of NAB.

to the different rates of electron transfer that occur through the NAB regions compared to the DDT regions.

We propose a mathematical model that describes the heterogeneous rate of electron transfer with $Ru(NH_3)_6^{3+/2+}$ (Equation 3). The rate is dependent on the proportions of NAB and DDT in the mixed film, and the magnitude of the electron transfer rate through the respective components. The individual electron transfer rates through each component can be modeled with a tunneling mechanism. From this data set, it was not possible to directly compare $k°_{film}$'s calculated from Equation 3 to those measured from ΔE_p's via the method of Nicholson.[30] This is because ΔE_p values for the mixed layers were quite large (*i.e.*, > 300 mV). $k°_{film}$ values predicted using Equation 3 do agree, within reason, to similar values cited in the literature.

The IRRAS studies show that the spectroscopic characteristics of the NAB film component are dynamic throughout the film growth process. The quantity A_{1347}/A_{1526} can be used to assess structural differences between NAB films formed from varying concentrations. Monolayer or partial NAB films that are in their early growth stages display a unique A_{1347} / A_{1526} ratio compared to films that reach more advanced stages of growth.

References:

1. Bain, C. D.; Evall, J.; Whitesides, G. M. *J. Am. Chem. Soc.* **1989,** 111, (18), 7155-7164.

2. Bain, C. D.; Troughton, E. B.; Tao, Y. T.; Evall, J.; Whitesides, G. M.; Nuzzo, R. G. *J. Am. Chem. Soc.* **1989,** 111, (1), 321-335.

3. Chidsey, C. E. D.; Bertozzi, C. R.; Putvinski, T. M.; Mujsce, A. M. *Journal of the American Chemical Society* **1990,** 112, (11), 4301-4306.

4. Bumm, L. A.; Arnold, J. J.; Cygan, M. T.; Dunbar, T. D.; Burgin, T. P.; Jones, L.; Allara, D. L.; Tour, J. M.; Weiss, P. S. *Science* **1996,** 271, (5256), 1705-1707.

5. Cygan, M. T.; Dunbar, T. D.; Arnold, J. J.; Bumm, L. A.; Shedlock, N. F.; Burgin, T. P.; Jones, L.; Allara, D. L.; Tour, J. M.; Weiss, P. S. *Journal of the American Chemical Society* **1998,** 120, (12), 2721-2732.

6. Adenier, A.; Bernard, M. C.; Chehimi, M. M.; Cabet-Deliry, E.; Desbat, B.; Fagebaume, O.; Pinson, J.; Podvorica, F. *J. Am. Chem. Soc.* **2001,** 123, (19), 4541-4549.

7. Laurentius, L., McDermott, M. T. . *Personal Communication* **2010**.

8. Dunker, M. F. W.; Starkey, E. B.; Jenkins, G. L. *Journal of the American Chemical Society* **1936,** 58, 2308-2309.

9. Bertilsson, L.; Liedberg, B. *Langmuir* **1993,** 9, (1), 141-149.

10. Folkers, J. P.; Laibinis, P. E.; Whitesides, G. M.; Deutch, J. *Journal of Physical Chemistry* **1994,** 98, (2), 563-571.

11. Stranick, S. J.; Parikh, A. N.; Tao, Y. T.; Allara, D. L.; Weiss, P. S. *Journal of Physical Chemistry* **1994,** 98, (31), 7636-7646.

12. Adenier, A.; Cabet-Deliry, E.; Chausse, A.; Griveau, S.; Mercier, F.; Pinson, J.; Vautrin-Ul, C. *Chem Mater.* **2005,** 17, (3), 491-501.

13. Lehr, J.; Williamson, B. E.; Flavel, B. S.; Downard, A. J. *Langmuir* **2009,** 25, (23), 13503-13509.

14. Anariba, F.; DuVall, S. H.; McCreery, R. L. *Anal. Chem.* **2003,** 75, (15), 3837-3844.

15. Laforgue, A.; Addou, T.; Belanger, D. *Langmuir* **2005,** 21, (15), 6855-6865.

16. Xia, S. J.; Liu, G.; Birss, V. I. *Langmuir* **2000,** 16, (3), 1379-1387.

17. Cline, K. K.; McDermott, M. T.; McCreery, R. L. *Journal of Physical Chemistry* **1994,** 98, (20), 5314-5319.

18. Deakin, M. R.; Stutts, K. J.; Wightman, R. M. *Journal of Electroanalytical Chemistry* **1985,** 182, (1), 113-122.

19. Chow, E.; Gooding, J. J. *Electroanal.* **2006,** 18, (15), 1437-1448.

20. Ji, X. B.; Banks, C. E.; Crossley, A.; Compton, R. G. *Chemphyschem* **2006,** 7, (6), 1337-1344.

21. Bard, A. J.; Faulkner, L. R., *Electrochemical Methods - Fundamentals and Applications*. 2nd ed.; John Wiley & Sons: Danvers, 2001; p 166-170.

22. Reshetnyak, O. V.; Kozlovs'ka, Z. E.; Koval'chuk, E. P.; Obushak, M. D.; Rak, J.; Blazejowski, J. *Electrochemistry Communications* **2001,** 3, (1), 1-5.

23. Allongue, P.; de Villeneuve, C. H.; Cherouvrier, G.; Cortes, R.; Bernard, M. C. *J. Electroanal. Chem.* **2003,** 550, 161-174.

24. Shewchuk, D. M.; McDermott, M. T. *Langmuir* **2009,** 25, (8), 4556-4563.

25. Porter, M. D.; Bright, T. B.; Allara, D. L.; Chidsey, C. E. D. *J. Am. Chem. Soc.* **1987,** 109, (12), 3559-3568.

26. Snyder, R. G.; Strauss, H. L.; Elliger, C. A. *Journal of Physical Chemistry* **1982,** 86, (26), 5145-5150.

27. Solak, A. O.; Eichorst, L. R.; Clark, W. J.; McCreery, R. L. *Analytical Chemistry* **2003,** 75, (2), 296-305.

28. Yang, H. H.; McCreery, R. L. *Analytical Chemistry* **1999,** 71, (18), 4081-4087.

29. Finklea, H. O.; Hanshew, D. D. *Journal of the American Chemical Society* **1992,** 114, (9), 3173-3181.

30. Nicholson, R. S. *Analytical Chemistry* **1965,** 37, (11), 1351.

31. Kneten, K. R.; McCreery, R. L. *Analytical Chemistry* **1992,** 64, (21), 2518-2524.

Chapter V

Application of Mixed-Mode Bonded Layers to Molecular Electronics Junction Devices

1. Introduction

Molecular electronics is the field of science that aims to incorporate individual molecules or groups of molecules as functional components in modern electronic devices. The origins of this idea are often credited to Aviram and Ratner, who devised a theory that describes unidirectional current transfer through a single molecule, if that molecule contains specific functional groups.[1] Since the inception of their idea, several experimental approaches have been designed to address electrical conduction through molecules. The principle challenge common to all of these experimental approaches is to cleverly devise a means to "sandwich" a molecule (or group of molecules) between two conductors such that the entire assembly can ultimately be wired to conventional, macroscale, electronic circuitry. The assembly is commonly referred to as a molecular junction (MJ).

Chemically modified electrodes (CMEs) simplify the fabrication of MJs because one end of the molecule of interest is already tethered to a conductive surface. From a design perspective, the primary concern with the fabrication of CME-based MJs is the choice of an appropriate methodology for creating the second contact. Since the majority, though not all, of the current designs for these devices are based on a bottom-up approach, we will refer to this as creating the top-contact.

Several strategies for creating top-contacts are now available. In a recent review, McCreery and Bergren categorized all of the current strategies into two categories. Namely, these are designs that are based on a single molecule approach and designs that are based on an ensemble approach.[2] As the name suggests, single molecule approaches entail electrical conduction through very small numbers of molecules, down to a single molecule. Current single molecule junction designs include devices made by bringing the tip of a conductive scanning probe instrument into contact with a CME. This has been accomplished with scanning tunneling microscopy (STM)[3] and conducting probe atomic force microscopy (cp-AFM).[4] Break junctions, where molecules are made to self-assemble at molecular-scale gaps created by stretching a thin conducting element to the point of breakage, constitute another example of a single molecule approach.[5]

Ensemble designs incorporate relatively large numbers of molecules, *i.e.* 10^3-10^{12} molecules, into MJs with macroscale dimensions. The molecules typically constitute a chemisorbed organic adlayer. The first ensemble devices date back to1971 where Mann and coworkers studied electronic tunneling through fatty-acid, Langmuir-Blodgett (LB), monolayer films "sandwiched" between two metal contacts.[6] In their devices the principle interaction between the monolayer and the metal substrate was an electrostatic interaction. Although these initial devices revealed fundamental concepts behind electron transport through MJs, the vast majority of contemporary ensemble (and single molecule) designs employ specific chemistries to link the molecular component to the bottom and top contacts. To date, this has often been achieved with the metal-S linkage produced from self-assembled monolayers (SAMs) of organothiolates at metal surfaces.[7, 8] Novel examples of this approach include devices fabricated by bringing a mercury drop

modified with a thiolate SAM into contact with another surface modified with a thiolate SAM, and "cross-wire" devices.[9-11]

A recent, novel MJ design makes use of diazonium salt attachment chemistry to covalently link the molecular layer to a conductive, carbon substrate.[12] These devices consist of molecular assemblies of diazonium-derived aryl groups covalently bound to a flat, pyrolyzed photoresist film (PPF).The top contacts are typically metals such as Hg, Cu or Ti. Alternatively, metal/metal oxide combinations have been employed as top contacts *e.g.* Al_2O_3 followed by Au, or TiO_2 followed by Au. Such devices have been extensively characterized and are now fabricated using a very streamlined "cross-bar" strategy.[12-16] Recent investigations have confirmed that the current density-voltage (J-V) responses of these junctions are highly dependent on the chemical structure of the chosen aryl substituent, the thickness of the molecular layer, and other considerations related to the junction fabrication procedures.[14, 16]

For these latter devices, the relatively strong C-C bond (bond energy ~ 100 kcal/mol) that anchors the aryl moiety to the carbon surface presents certain advantages over a weaker Au-S bond (bond energy ~ 30-40 kcal/mol).[17] Firstly, junction yields are reported to be quite high which implies good stability of the junction.[14] McCreery and coworkers report that these junctions produce stable current-voltage responses after 150 days exposure to the ambient.[16] Related to junction stability, the observed J-V characteristics are reportedly very reproducible as well. Secondly it is postulated that a C-C bond facilitates electronic coupling between the carbon substrate and the molecular layer. It is proposed that this type of coupling can induce structural arrangements in the molecular layer and enhances electron transport through the junction.[18]

We will now use the collective knowledge gained from the work presented in the previous chapters of this thesis to investigate MJs that contain diazonium-derived molecular layers within a mixed-mode bonding setting. Recall from Chapter IV that mixed-mode bonded layers consist of networks of highly conjugated nitroazobenzene (NAB) groups diluted into a self-assembled monolayer (SAM) of dodecanethiolate (DDT) at a polycrystalline gold surface. Results also showed that the surface concentration of NAB within the DDT monolayer can be controlled. Furthermore, the electrochemical properties of the mixed layers were highly dependent on the relative proportions of the NAB and DDT components. It was observed that electron transfer through the DDT regions of the mixed layers proceeded at a lower rate compared to NAB monolayer regions.These results, along with the possibility that NAB is anchored to the gold surface via a covalent linkage, have led us to believe that mixed-mode bonding could provide a means of controlling the electrical properties of molecular electronic devices.

The work presented in this chapter will describe the collaborative efforts undertaken, by Dr. A. J. Bergren and myself, to incorporate mixed-mode bonded layers into functional molecular electronic junction devices. We prepared ensemble MJs, using a bottom-up, "cross-bar" junction fabrication procedure with polycrystalline gold bottom contacts. The mixed-mode molecular layers described in Chapter IV served as the molecular assembly. Junctions fabricated without a thiolate component were prepared in parallel for the sake of comparison. We will discuss the suitability of using top contacts consisting of thin layers of Al_2O_3 and Au for these devices.

2. Experimental

Preparation of the Molecular Junctions. *Bottom Contacts:* Electron-beam (e-beam) evaporations were carried out at a base pressure < 10^{-6} Torr. Au (200 nm, 0.1 nm/s) was evaporated through a shadow mask with 0.5 mm wide line openings onto a 1.5 cm × 2.0 cm Si substrate. A thin, insulating SiO_2 layer was thermally grown on the Si substrate prior to the Au deposition. *Molecular Layer Deposition:* 4-nitroazobenzenediazonium tetrafluoroborate (NABDF) was synthesized according to procedures published by Starky.[19] Bottom contacts were derivatized with nitroazobenzene (NAB) layers by employing them as working electrodes in 50 μM, 200 μM, and 1000 μM NABDF solutions in acetonitrile with 0.1 M tetrabutylammonium tetrafluoroborate ($TBABF_4$) (≥99%, Sigma-Aldrich Canada Ltd., Oakville, Ontario) supporting electrolyte. For all depositions, a single voltammetric cycle was applied from +100 mV to -700 mV at a sweep rate of 200 mV/s. The reference electrode consisted of a silver wire submerged in a 200 mM $AgNO_3$ solution in acetonitrile with 0.1 M $TBABF_4$. A coiled platinum wire was used as a counter electrode. Diazonium salt solutions were deaerated for 10 min with Ar gas prior to all depositions. Following the modification, samples were thoroughly rinsed with acetonitrile and blown dry with a gentle stream of Ar gas. To prepare dodecanethiolate (DDT) monolayers and NAB:DDT mixed-mode molecular layers, unmodified and previously modified bottom contacts were immediately immersed in a solution of 1 mM DDT (≥97%, Sigma-Aldrich Canada Ltd., Oakville, Ontario) in anhydrous ethanol (Commercial Alcohols Inc., Brampton, Ontario) for 24 h. Prior to the self-assembly process, all DDT solutions were placed in an ultrasonication bath for 5 min. to ensure the solution was homogeneous. DDT solutions were deaerated with Ar gas

for 10 min prior to their use. *Top Contacts*: Al_2O_3 (15 nm, 0.1 nm/s) followed by Au (50 nm, 0.1 nm/s) were evaporated through a shadow mask with 0.5 mm lines oriented at 90° with respect to the bottom contact pattern.

Electrical Measurements. All J-V data was collected on a custom-built instrument consisting of a National Instruments 6210 data acquisition board run by Labview software. Electrical contacts were wired to the junctions with 3 tungsten probes controlled by three-axis micromanipulators. The software is designed to apply a voltage bias between the bottom contact probe, V^+_{drive}, and the top contact probe,V^-_{drive}, while measuring the resulting current. A third probe, V_{sense}, is also placed on the bottom contact on the opposite side of the junction. The third probe corrects for ohmic losses due to any finite resistance in the bottom contact. Current that flows between the V^+_{drive} and V^-_{drive} probes is fed into an SRS 570 current amplifier and the output is plotted as a function of the applied bias. Junction capacitances were measured by cyclic voltammetry (CV) at a sweep rate of 1000 V/s (result is obtained by dividing J at V = 0 V by the sweep rate). A photomicrograph of a typical MJ device is presented in Figure 5.01. All CVs were noise filtered with a 6-point moving average function.

3. Results and Discussion

Our notation for referring to a specific MJ composition is as follows: Au/NAB(x μM):DDT/AlO_x/Au. Read left to right, this denotes a MJ for which a 200 nm polycrystalline Au bottom contact was derivatized in a solution of x μM NABDF and then immersed in a 1 mM DDT solution for 24 hours. A top contact was then deposited by the successive evaporation of 15 nm of Al_2O_3, followed by 50 nm of Au. The nominal

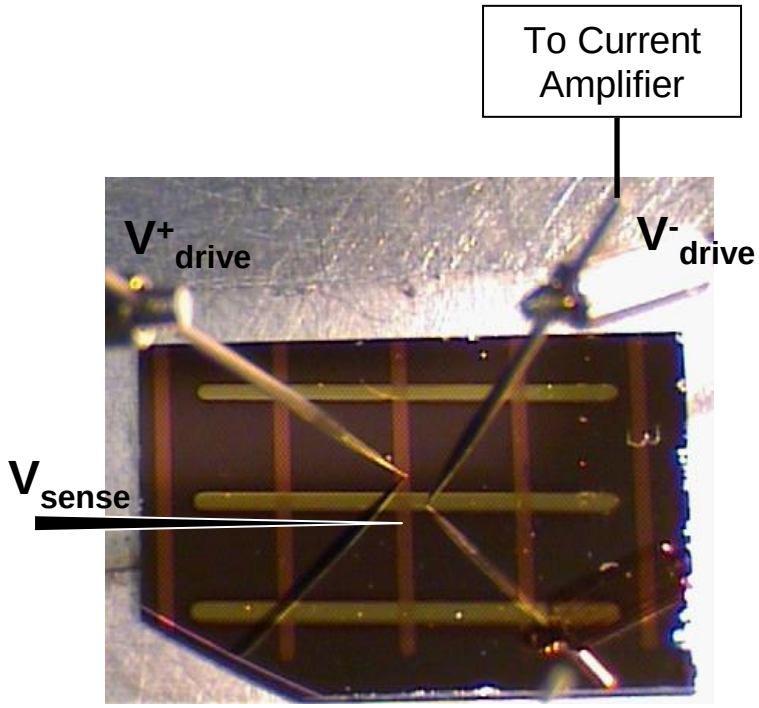

Figure 5.01. A video photograph of a Au(200 nm)/NAB/AlO_x(15 nm)/Au(50 nm) junction with a 3-point probe measurement setup. The bottom contacts are oriented vertically. A voltage bias is applied between V^+drive and V^-drive and the resulting current through the circuit is measured. The chip dimensions are 2 cm by 1 cm.

Note: The actual image is of a 2-probe measurement setup. The third probe, V_{sense} (illustrated with a cartoon), corrects for ohmic losses in the bottom contact. All measurements were performed with a 3-probe setup.

thicknesses of the top and bottom contact materials are constant for all junctions studied in this chapter, and therefore are assumed in the notations. AlO_x denotes a hydrated Al_2O_3 layer and will be further discussed in the text below.

The overall scheme for the preparation of a Au/NAB(x μM):DDT/AlO_x/Au junction is summarized in Figure 5.02. Detailed fabrication procedures are provided in the experimental section. It is known that Au evaporated on top of an alkanethiolate SAM penetrates through the SAM to form Au islands on the monolayer-supporting surface.[20] Vapor deposited Al atoms similarly penetrate thiolate SAMs on Au.[21] For gold, it is postulated that this leads to the formation of tiny, bridging Au filaments that join the underlying Au surface with the freshly deposited Au film.[22] It is argued that such metallic filaments, along with a possible structural reorganization of the molecular layer, can lead to electrical "shorts" and device failure.[23, 24] Our junctions were fabricated with an Al_2O_3 layer in between the molecular layer and the Au top contact to prevent Au penetration into the molecular layer. X-ray photoelectron spectroscopy (XPS) studies have revealed that some of the Al_2O_3 layer is hydrated by residual moisture in the evaporation chamber to form $Al(OH)_3$.[15] A layer that is comprised of both Al_2O_3 and $Al(OH)_3$ is denoted AlO_x. It has been shown that for MJs containing an AlO_x layer, the AlO_x is non-interacting with the NO_2 groups of the nitroazobenzene.[15]

MJs fabricated with an intermittent Al_2O_3 layer produce a capacitive J-V response.[15] This is in contrast to the typical ohmic response that is observed for many MJ devices.[2, 25] Figure 5.03 shows that our Au/NAB(x μM)/AlO_x/Au MJs display a capacitive J-V response. The calculated total capacitance of each junction is presented in

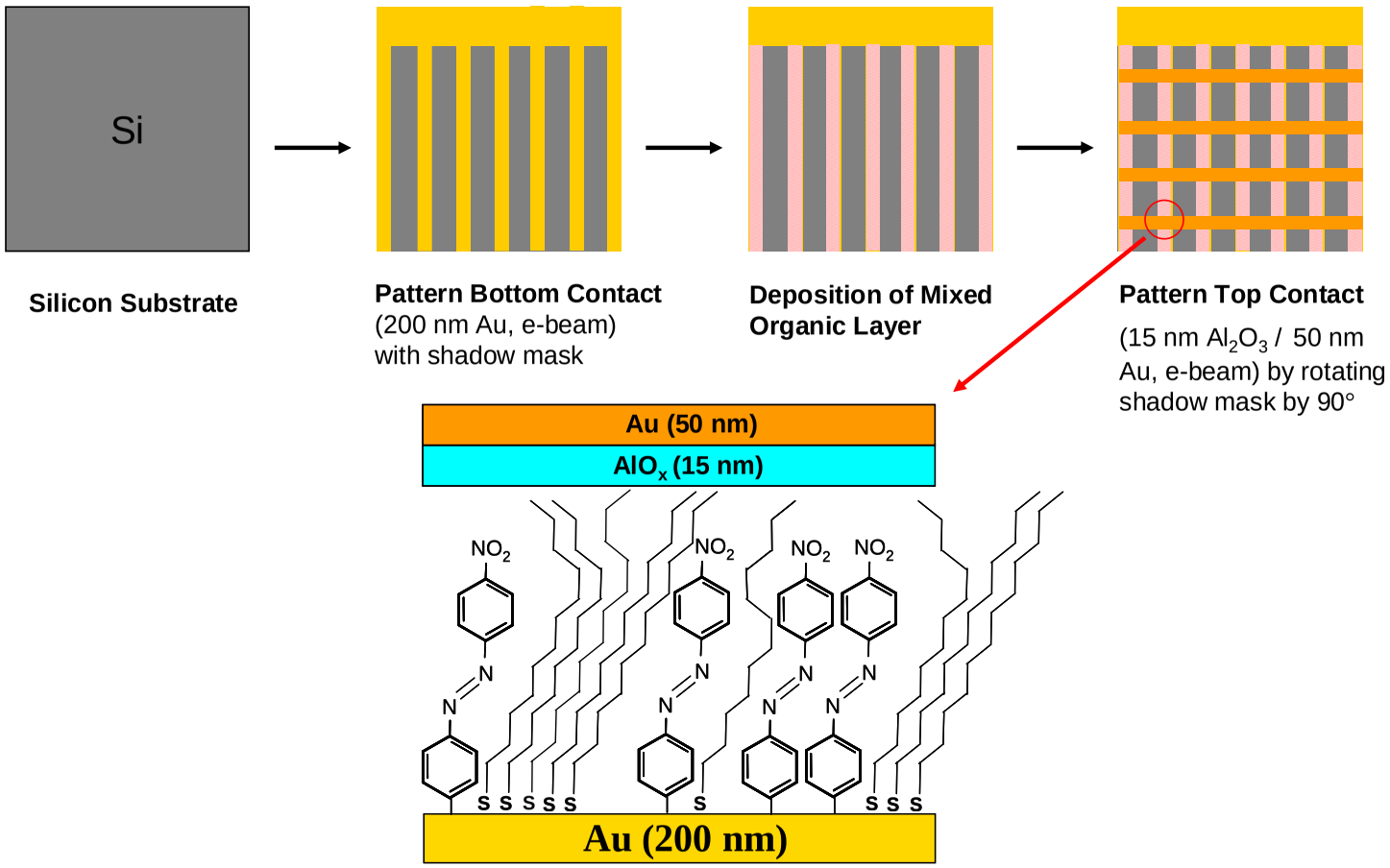

Cross-section of the mixed layer junction

Figure 5.02. Schematic diagram for the preparation of Au/NAB(x μM)/AlO_x/Au and Au/NAB (x μM):DDT/AlO_x/Au MJs.

Table 5.01. Qualitatively, the magnitudes of the capacitances follow a trend that is consistent with a classical, parallel plate model for capacitors. For a classical, parallel plate capacitor, the capacitance, C, is defined as:

$$C = \frac{\varepsilon_R \cdot \varepsilon_0 \cdot A}{d} \qquad [1]$$

where ε_R is the dielectric constant for the material between the conductors, ε_0 is the permittivity of free space, A is the area of the plates, and d is the separation of the plates. Thus, C and d are inversely rated. As such, higher capacitance values should be observed for thinner NAB layers. Although the NAB layer thicknesses were not directly measured in this study, it is not unreasonable to expect that they are very similar to the values presented in Table 4.01 of Chapter IV. It was observed that MJs with monolayer regions of NAB, *i.e.* Au/NAB(50 μM)/AlO_x/Au and Au/NAB(200 μM)/AlO_x/Au, produced higher capacitances than those with multilayered regions of NAB, *i.e.* Au/NAB(1000 μM)/AlO_x/Au. This observation gives merit to the use of a classical capacitor model to explain our results.

Experimentally measured ε_R values obtained from the literature for Al_2O_3 range from 7-11.[15] Assuming the junctions behave like classical capacitors, and the highest measured ε_R for Al_2O_3 (*i.e.* ε_R = 11), an Au/Al_2O_3(15 nm)/Au junction should produce a C value of 0.65 μF/cm^2, (Equation 1) . Further, assuming the NAB layer behaves as a dielectric material, an NAB layer in between the AlO_x layer and the bottom contact would further decrease the predicted capacitance, since d should effectively increase.

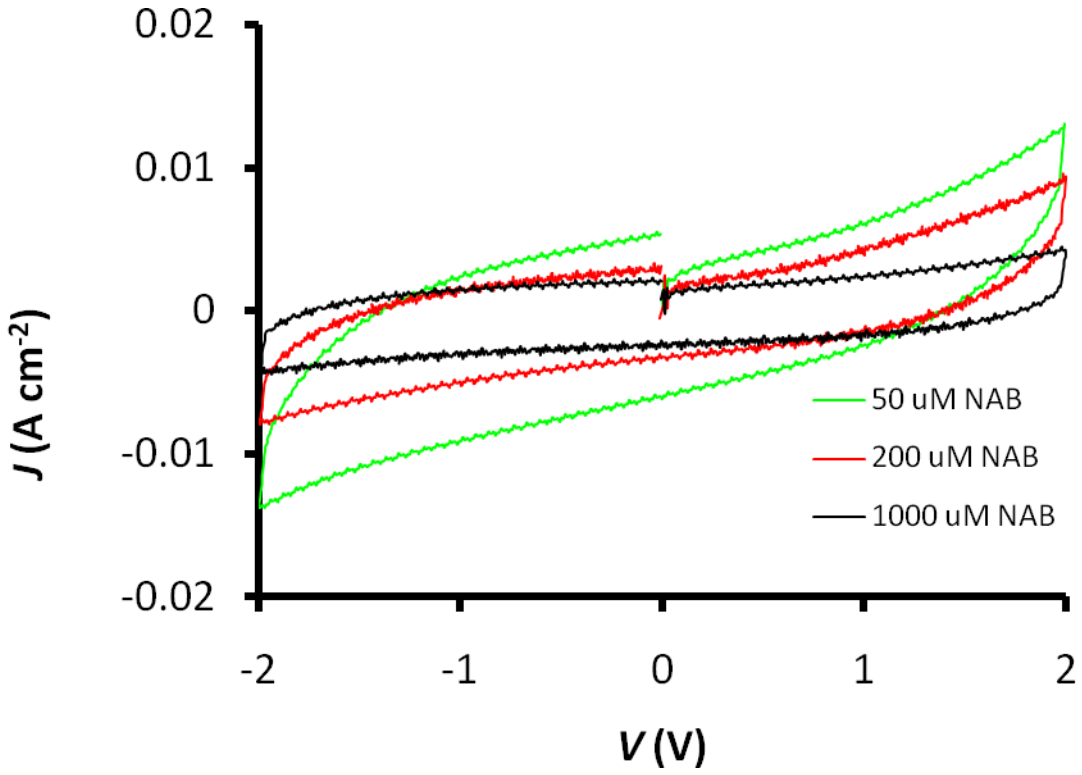

Figure 5.03. Representative J-V responses of Au/NAB(x μM)/AlO_x/Au MJs prepared from NABDF solution concentrations of 50, 200, and 1000 μM.

Thus, all of the observed C values in Table 5.02 are unexpectedly high. We prepared a Au/Al_2O_3(15 nm)/Au control chip, however, complications with the shadow mask rendered these devices visually defective. McCreery and coworkers observed unusually high capacitance values for PPF/AlO_x/Au devices.[15] It was proposed that this was the result of AlO_x having a higher ε_R than Al_2O_3. It was observed that AlO_x-containing junctions prepared with precisely the same e-beam evaporation equipment yield unusually high capacitance values.[26] We considered the implementation of a heat-drying step into our procedures, however, this idea was ultimately rejected because of the uncertain effect it could have on the molecular layer.

junction	no. of junctions	Capacitance $\mu F/cm^2$
Au/NAB(50)/AlO_x(15)/Au	5	5.4 +/- 0.3
Au/NAB(50)/AlO_x(15)/Au	4	6.2 +/- 0.3
Au/NAB(200)/AlO_x(15)/Au	6	3.6 +/- 0.4
Au/NAB(200)/AlO_x(15)/Au	5	2.5 +/- 0.3
Au/NAB(1000)/AlO_x(15)/Au	3	2.7 +/- 0.5
Au/NAB(1000)/AlO_x(15)/Au	3	2.3 +/- 0.6

Table 5.01. Experimentally measured capacitance values for Au/NAB(x μM)/AlO_x/Au junctions. Each horizontal entry of the table corresponds to a single device, each of which contains multiple junctions.

Figure 5.04 contains J-V curves for MJs with the incorporation of DDT into the molecular layer (*i.e.* Au/NAB(x μM):DDT/AlO_x/Au MJs). For these junctions, the measured capacitances are listed in Table 5.02. Figure 5.04a contains the results of the junctions that showed a capacitive response. For these junctions, the introduction of DDT to a Au/NAB(200 μM)/AlO_x/Au junction does not produce a measurable effect on the capacitance of the junction, within the limits of experimental error (Tables 5.01 and 5.02). This would suggest that neither ε_R (in this case ε_R is the combined value for the NAB and DDT components) or d change. Thus, the J-V characteristics of the junctions containing NAB deposited from 200 μM solutions are governed by the NAB component. In this case, the structure of the NAB component is not affected by the addition of DDT. It is possible that both ε_R and d change in such a way that the effects "cancel out".

Conversely, the introduction of DDT to the Au/NAB(1000 μM)/AlO_x/Au junction increases the observed junction capacitance by about a factor of 2. Recall from the results presented in Table 4.01 of Chapter IV that NAB films prepared from 1000 μM solution concentrations are ~ 3 monolayers thick (4.7 nm). Despite the larger amount of NAB contained in these films, relative to the 200 μM NAB layers, NAB films formed from 1000 μM solutions exhibit a structure that is affected by the incorporation of DDT. In light of this, one possible explanation is that free DDT becomes "entrapped" in the networks of NAB groups so as to result in a molecular layer that has a much higher ε_R. Figure 5.04b illustrates that all of the Au/NAB(50 μM):DDT/AlO_x/Au and Au/DDT/AlO_x/Au junctions produced an ohmic response characteristic of a MJ with an electrical "short." Recall from Chapter IV that mixed mode bonded molecular layers

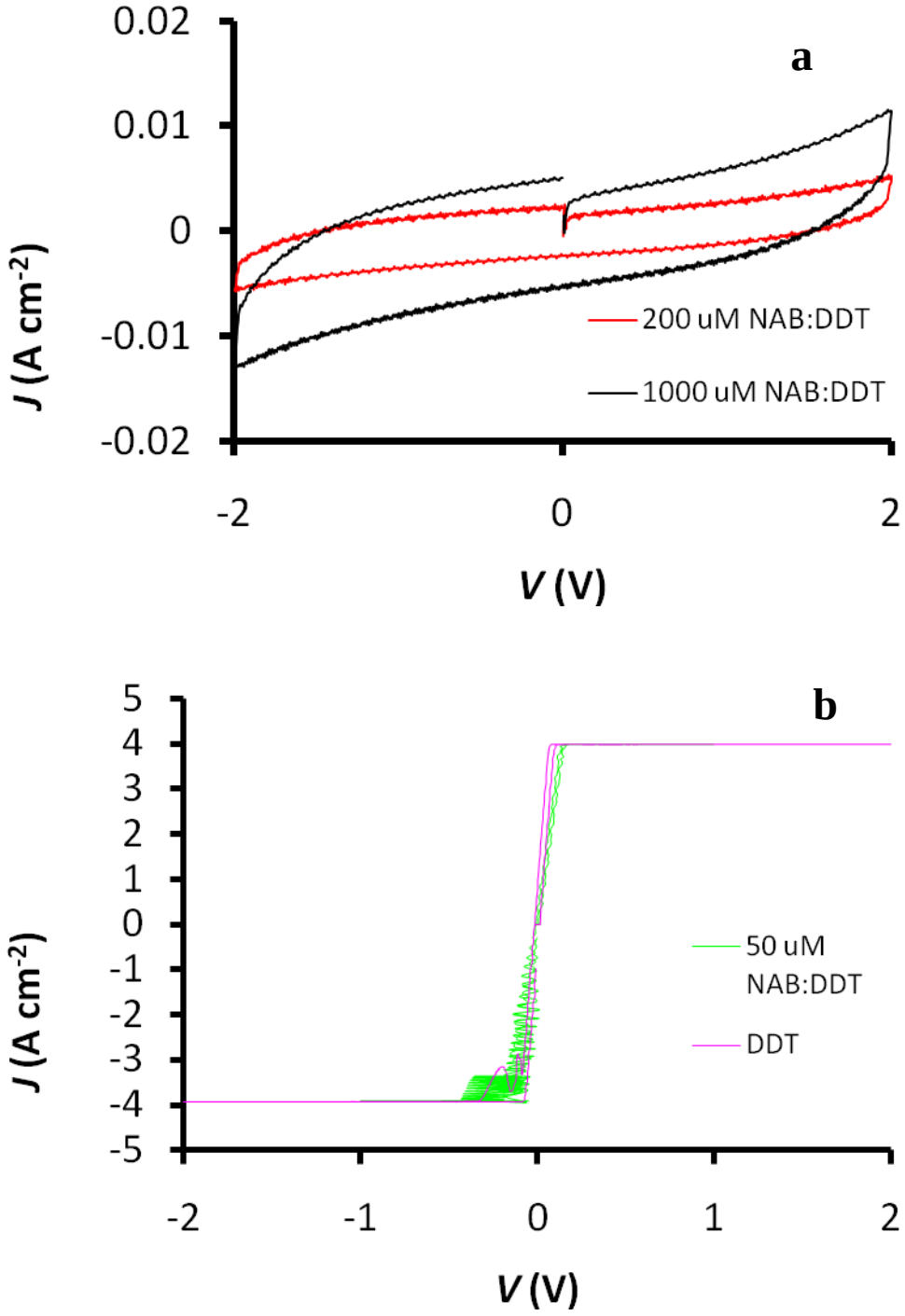

Figure 5.04. Representative J-V responses of Au/NAB(x μM):DDT/AlO_x/Au MJs prepared from NABDF solution concentrations of 50, 200, and 1000 μM.

junction	no. of junctions	Capacitance μF/cm^2
Au/NAB(50):DDT/AlO_x(15)/Au	4	short
Au/NAB(50):DDT/AlO_x(15)/Au	4	short
Au/NAB(200):DDT/AlO_x(15)/Au	3	2.0 +/- 0.3
Au/NAB(200):DDT/AlO_x(15)/Au	3	3.3 +/- 0.2
Au/NAB(1000):DDT/AlO_x(15)/Au	2	5.4 +/- 0.2
Au/DDT/AlO_x(15)/Au	2	short

Table 5.02. Experimentally measured capacitance values for Au/NAB(xμM): DDT/AlO_x/Au junctions. Each horizontal entry of the table corresponds to a single device, each of which contains multiple junctions.

formed from 50 μM solutions contain 75 % of the thiolate in a DDT monolayer in addition to monolayer regions of NAB. It therefore appears that electrical shorts are more probable in junctions for which the molecular layer is largely DDT. It is not likely that Au from the top contact deposition penetrates the AlO_x layer directly. This would have similarly caused the NAB-only devices to short, which is not what was observed. We postulate that Au may penetrate the AlO_x layer when large surface concentrations of DDT are present. Perhaps the AlO_x has limited adhesion to the DDT regions with the corollary that AlO_x aggregates at the NAB regions, exposing DDT. The Au top contact would then directly penetrate the DDT SAM regions, similar to what is reported for other MJs prepared with alkanethiolate SAMs.

4. Conclusions

Top contacts produced from the successive deposition of Al_2O_3 followed by Au are suitable for preparing MJs that contain diazonium-derived molecular layers alone, but

are perhaps not as suitable for MJs that contain mixed-mode bonded layers. We suspect that the thiolate component of the latter promotes penetration of Au atoms into the molecular assembly.

For MJs prepared with mixed-mode bonded layers, it was observed that different ratios of NAB and DDT in the molecular layer afford differences in the observed electrical responses of the junctions. This is what we initially hypothesized. However, the erroneously high capacitances observed, presumably due to the effect of residual moisture in our fabrication procedures, interfered with our ability to make any reasonable conclusions about the dielectric properties of the mixed-mode layers.

5. Acknowledgements

We gratefully acknowledge the insightful discussions with Dr. R. L. McCreery. We acknowledge the collaborative efforts by Dr. A. J. Bergren, who was responsible for the preparation of the bottom and top contacts for this work. Dr. Bergren also generously shared his expertise with respect to performing the electrical measurements.

References:

1. Aviram, A.; Ratner, M. A. *Chemical Physics Letters* **1974,** 29, (2), 277-283.

2. McCreery, R. L.; Bergren, A. J. *Advanced Materials* **2009,** 21, (43), 4303-4322.

3. Bumm, L. A.; Arnold, J. J.; Cygan, M. T.; Dunbar, T. D.; Burgin, T. P.; Jones, L.; Allara, D. L.; Tour, J. M.; Weiss, P. S. *Science* **1996,** 271, (5256), 1705-1707.

4. Kelley, T. W.; Granstrom, E. L.; Frisbie, C. D. *Advanced Materials* **1999,** 11, (3), 261-+.

5. Reed, M. A.; Zhou, C.; Muller, C. J.; Burgin, T. P.; Tour, J. M. *Science* **1997,** 278, (5336), 252-254.

6. Mann, B.; Kuhn, H. *Journal of Applied Physics* **1971,** 42, (11), 4398-&.

7. Nuzzo, R. G.; Allara, D. L. *J. Am. Chem. Soc.* **1983,** 105, (13), 4481-4483.

8. Laibinis, P. E.; Whitesides, G. M.; Allara, D. L.; Tao, Y. T.; Parikh, A. N.; Nuzzo, R. G. *Journal of the American Chemical Society* **1991,** 113, (19), 7152-7167.

9. Slowinski, K.; Fong, H. K. Y.; Majda, M. *Journal of the American Chemical Society* **1999,** 121, (31), 7257-7261.

10. Weiss, E. A.; Chiechi, R. C.; Kaufman, G. K.; Kriebel, J. K.; Li, Z. F.; Duati, M.; Rampi, M. A.; Whitesides, G. M. *Journal of the American Chemical Society* **2007,** 129, (14), 4336-4349.

11. Blum, A. S.; Kushmerick, J. G.; Long, D. P.; Patterson, C. H.; Yang, J. C.; Henderson, J. C.; Yao, Y. X.; Tour, J. M.; Shashidhar, R.; Ratna, B. R. *Nature Materials* **2005,** 4, (2), 167-172.

12. Ranganathan, S.; Steidel, I.; Anariba, F.; McCreery, R. L. *Nano Letters* **2001,** 1, (9), 491-494.

13. McCreery, R. L. *Analytical Chemistry* **2006,** 78, (11), 3490-3497.

14. Anariba, F.; Steach, J. K.; McCreery, R. L. *Journal of Physical Chemistry B* **2005,** 109, (22), 11163-11172.

15. Kalakodimi, R. P.; Nowak, A. M.; McCreery, R. L. *Chemistry of Materials* **2005,** 17, (20), 4939-4948.

16. Bergren, A. J.; Harris, K. D.; Deng, F. J.; McCreery, R. L. *Journal of Physics-Condensed Matter* **2008,** 20, (37).

17. Nuzzo, R. G.; Zegarski, B. R.; Dubois, L. H. *J. Am. Chem. Soc.* **1987,** 109, (3), 733-740.

18. McCreery, R.; Dieringer, J.; Solak, A. O.; Snyder, B.; Nowak, A. M.; McGovern, W. R.; DuVall, S. *Journal of the American Chemical Society* **2003,** 125, (35), 10748-10758.

19. Dunker, M. F. W.; Starkey, E. B.; Jenkins, G. L. *Journal of the American Chemical Society* **1936,** 58, 2308-2309.

20. Ohgi, T.; Sheng, H. Y.; Dong, Z. C.; Nejoh, H. *Surface Science* **1999,** 442, (2), 277-282.

21. Hooper, A.; Fisher, G. L.; Konstadinidis, K.; Jung, D.; Nguyen, H.; Opila, R.; Collins, R. W.; Winograd, N.; Allara, D. L. *Journal of the American Chemical Society* **1999,** 121, (35), 8052-8064.

22. de Boer, B.; Frank, M. M.; Chabal, Y. J.; Jiang, W. R.; Garfunkel, E.; Bao, Z. *Langmuir* **2004,** 20, (5), 1539-1542.

23. Chen, B.; Metzger, R. M. *Journal of Physical Chemistry B* **1999,** 103, (21), 4447-4451.

24. Fisher, G. L.; Hooper, A. E.; Opila, R. L.; Allara, D. L.; Winograd, N. *Journal of Physical Chemistry B* **2000,** 104, (14), 3267-3273.

25. Ulgut, B.; Abruna, H. D. *Chemical Reviews* **2008,** 108, (7), 2721-2736.

26. Bergren, A. J. *Personal Communication* **2009**.

Chapter VI

Conclusions and Future Work

Overall Conclusions

An important theme of this thesis was to assess the stability of diazonium-derived aryl films at polycrystalline gold surfaces. The results of this assessment are of great importance for determining whether these films are suitable for practical applications. For example, this information would be extremely valuable were these films considered for use in devices like hand-held electronics or portable chemical sensors.

First, the stability of the films must be addressed in terms of a specific application. This might depend on the typical conditions the films must endure in that application. For example, if a particular application requires that the films need only to resist slightly elevated temperatures (*i.e.* 30° C) in an aqueous environment then I believe diazonium-derived films may be suitable for that application. If the films are to be incorporated into an electronic device and need to withstand ~ 1 V of an applied voltage in an electrolyte solution, they are not likely the ideal choice.

Second, the stability of these films, as gauged by their resistance to harsh treatments, depends on the chemical structure of the aryl substituent. Compared to nitroazobenzene (NAB) layers, nitrobenzene (NB) layers appeared to be much more prone to removal by treatments such as sonication, refluxing in organic solvents, and chemical displacement by alkanethiols. There are several possible reasons why this is the

case. It is possible that the products of the reactions that govern the removal of NB layers from the surface are thermodynamically more stable than those of NAB layers. It's also possible that the reactions that govern the removal of the NB layers have a lower activation barrier than those that govern the removal of NAB layers and therefore occur more rapidly.

It is also possible that the attachment of the aryl groups does not occur via a direct, covalent Au-C bond. The film may simply be an extended, polymerized moiety that is physisorbed to the surface. It is well known that other polymer films, Nafion™ for example, can be attached to a surface without any specific type of bonding. Thus, it is possible that diazonium-derived films are extended polyphenylene chains spread across the surface. If this is the case, the strength of the attachment should strongly depend on the nature of the chemical functional groups on the phenyl ring. This uncertainty warrants further investigation into the mechanisms by which diazonium-derived aryl films are affixed to metallic surfaces such as Au.

Suggestions for Future Work

It is my belief that efforts should be focused on understanding the nature of the interaction between these films and the Au substrate before they are employed in any practical applications. I believe it is necessary to understand why these layers exhibit the two types of material I consistently observed throughout my thesis work *i.e.*, strongly bound material and weakly bound material. My colleague observed a Raman-active vibration, at 412 cm^{-1}, for NB layers on Au.[1] This peak could be attributed to a Au-C stretch. Efforts are being made to model this vibration to an Au-C stretch for a NB

molecule attached to a cluster of Au atoms. In a recent study Bélanger and coworkers observed that, for carboxyphenyl layers, the C 1s peak in the XPS spectrum could be modeled such that a contribution from a Au-carbide peak on the low binding energy side produced a good fit to the experimental data.[2] This provided some evidence that a Au-C may be present, however the result was not unambiguous because nitrobenzene and diethylaniline layers did not produce a similar peak. I believe these experiments should be followed-up in a thorough investigation that involves many different aryl layers. Nuzzo and coworkers carried out temperature-programmed thermal desorption experiments on alkanethiolate SAMs in order to gain quantitative information related to the Au-thiolate bond strength.[3] I feel that a similar strategy should be employed for diazonium-derived layers on Au.

Even though the details pertaining to the attachment chemistry have not yet been unraveled, diazonium chemistry has recently shown promise for applications related to biosensing. Harper and coworkers demonstrated that Au electrodes modified with NB groups can be used to covalently tether pyrroloquinoline quinine (PQQ) to the surface for β-nicotinamide adenine dinucleotide (NADH) detection. [4] The nitro group was electrochemically converted to an amine, allowing for subsequent EDC/NHS coupling and cross-linking to PQQ. Grant demonstrated that gold electrodes modified with carboxyphenyl groups could be used to immobilize rabbit anti-IgG antibodies for IgG detection via surface plasmon resonance imaging.[5] It is desirable that these investigations will serve as catalysts for the continued exploration of diazonium salt surface attachment chemistry on metals as a tool for biosensing applications.

References

1. Laurentius, L., McDermott, M. T. . *Personal Communication* **2010**.

2. Laforgue, A.; Addou, T.; Belanger, D. *Langmuir* **2005,** 21, (15), 6855-6865.

3. Nuzzo, R. G.; Zegarski, B. R.; Dubois, L. H. *J. Am. Chem. Soc.* **1987,** 109, (3), 733-740.

4. Harper, J. C.; Polsky, R.; Wheeler, D. R.; Dirk, S. M.; Brozik, S. M. *Langmuir* **2007,** 23, (16), 8285-8287.

5. Grant, C. F. Surface Modification for SPR Imaging Studies. University of Alberta, Edmonton, 2009.